Using poly(3,4-ethylenedioxythiophene) polystyrene sulfonate surfaces to develop an electroanalytical sensor for therapeutic monitoring of tricyclic-antidepressants

Steven Gibney

Thesis submitted to the University of Nottingham
School of Pharmacy for the degree of Philosophy

March 2022

Abstract

This project aims to develop an electroanalytical sensor capable of measuring the real-time concentration of tricyclic antidepressants (TCA) in complex biological environments. Advances in micro- and nano- scale engineering have opened new avenues of sensor development; it is now possible to design sensors which function *in vivo*. The ability to accurately measure the concentration of an analyte *in vivo* provides crucial information about the pharmacokinetic behaviour of an analyte, while avoiding the need for repeated and potentially difficult sampling procedures. The main challenges which limit the development of an *in vivo* sensing device are caused by immune response, inflammation and surface contamination, all of which can prevent a sensor from functioning. To overcome these challenges a multidisciplinary approach must be used. Through a combination of electroanalytical chemistry and biomaterial development I have attempted to design and develop a sensing platform capable of the *in vivo* detection and monitoring of tricyclic antidepressant (TCA).

Initially, I studied the electrochemical behaviour of the TCA compounds to provide electroanalytical insight that would support the development of an effective sensor. I studied the redox activity of six TCA compounds: imipramine, desipramine, trimipramine, clomipramine, nortriptyline and doxepin. An unmodified glassy carbon electrode was used to perform scan rate studies and generate diagnostics plots for each of the TCA compounds in phosphate buffer solution (versus Ag/AgCl). Comparison of voltammograms, and analysis of peak current vs scan rate, confirmed that the oxidation of the central nitrogen in the TCA structure is irreversible and diffusion-limited. This was further reinforced by plots of current function which supported previous mechanistic data. I also identified variation between

clomipramine and other members of the TCA family, in particular a shift in peak current caused by the presence of Cl- in the TCA ring structure.

Next, the conductive polymer Poly(3,4-ethylenedioxythiophene) polystyrene sulfonate (PEDOT:PSS) was selected as a potential surface for the development of a sensor; it has shown promise in both sensing and implantable bioelectronic technology. I sought to investigate how the electrical and morphological properties of PEDOT:PSS films changed when mixed or blended with additional components. In this work, I used tunnelling atomic force microscopy (TUNA AFM) paired with Peak Force mode to investigate a PEDOT:PSS polyvinyl alcohol blend. I studied how the properties of a polymer film, made from a blend of PEDOT:PSS and polyvinyl alcohol (PVA), changed with increasing PEDOT:PSS concentration. Surface analysis showed that the level of aggregation in these films increased with increasing concentration of PEDOT:PSS. Further investigation was carried out into how various additives, such as Dimethyl sulfoxide and Divinyl sulfone, changed the morphological and electrical behaviour of PEDOT:PSS films. Peak Force TUNA AFM proved to be an effective method for studying modified PEDOT:PSS films and provided insight about the electrical behaviour of PEDOT which informed the design of a PEDOT based sensor.

Finally, I attempted to design a biodegradable scaffold that could house a PEDOT:PSS formulation and be used to electrochemically detect the redox behaviour of TCA compounds. This work involved the use of 3D extrusion printing to generate a biodegradable scaffold using the commercially available RESOMER® (LR708), a biodegradable polymer. I designed scaffolds and optimised the printing parameters to produce scaffolds which could be used as biodegradable implants. Following this, I characterised the electrochemical behaviour of scaffolds loaded with PEDOT:PSS, using them to detect both an ideal electrochemical analyte and a therapeutically relevant compound, in this case TCA.

This project acts as a proof-of-concept for a biodegradable sensor for the monitoring of electrochemically active therapeutic compounds. Given further development this work could be translated to a clinical setting and contribute towards the growing fields of both bioelectronics and personalised medicine.

Acknowledgements

I would firstly like to thank the sponsors and funding bodies who have made this work possible. This includes the Engineering and Physical Sciences Research Council (EPSRC), now a part of the UK Research and Innovation (UKRI) council, which funded this work through the Centre for Doctoral training in Advance Therapeutics and Nanomedicine. I would also like to thank Evonik Operations GmbH for providing funding and research materials. Likewise, my thanks go to the members of Evonik who have provided their technical expertise and general advice during this project, in particular Christian Moers, Alexander Bernhardt and Marcel Arndt.

I would like to acknowledge all the members of my supervisory team. This includes Dr Paul Smith who inspired the idea which started this project and Dr Andrew Hook who has provided technical input and offered personal guidance throughout the project. Significant thanks must go to my primary supervisor Dr Frankie Rawson. Over the last 4 years, he has given me the freedom to follow my research interests while challenging me to become a better researcher. I am immensely grateful for the mentorship he has provided. I also wish to thank all the members of the Rawson research group, in particular Jacqueline Hicks for providing equipment training and being a soundboard for my experimental plans.

I also want to thank all the people who have supported me outside of the lab. Most importantly I could not have made it this far without my wife Maddy. She has taught me patience and kindness, any work I have done could not have been accomplished without her by my side.

Finally, I would like to acknowledge the Stoic philosopher and Roman emperor Marcus Aurelius who taught me that “The impediment to action advances action. What stands in the way becomes the way.”

Contents

Abbreviations and Symbols

The abbreviations and symbols used in this thesis are in separate tables below and are listed alphabetically.

Term	Abbreviation
(3-Glycidyloxypropyl)trimethoxysilane	GOPS
Absorption, Distribution, Metabolism and Excretion	ADME
Atomic Force Microscopy	AFM
Blood brain barrier	BBB
Carbon nanotube	CNT
Clomipramine	CLO
Conductive AFM	C-AFM
Conductive Polymer	CP
Counter Electrode	CE
Cyclic voltammogram	CV
Deoxyribonucleic acid	DNA
Desipramine	DES
Dichlorometahne	DCM
Dimethyl sulfoxide	DMSO
Dioxythophene nuclaic acid	DNA
Divinyl Sulfone	DVS
Dodecylbenzenesulfonic acid	DBSA
Doxepin	DOX
Electrochemical impedance spectroscopy	EIS
Electron transfer–chemical reaction	EC
Electron transfer–chemical reaction–electron transfer	ECE
Engineering and Physical Sciences Research Council	EPSRC
Ethylene glycol	EG
Ferricyanide	FIC
Ferrocyanide	FOC
First in Human	FIH
Food and Drug Administration	FDA
Glassy Carbon Electrode	GCE
GlaxosmithKline	GSK

Gold nano particles	AuNP
High pressure liquid chromatography	HPLC
Human epidermal growth factor receptor 2	HER2
Human equivalent dose	HED
Human immunodeficiency virus	HIV
Imipramine	IMI
Inner Helmholz Plane	IHP
International Union of Pure and Applied Chemistry	IUPAC
Molecularly imprinted polymer	MIP
Monoamine oxidase inhibitor	MAOI
National Health Service	NHS
National Institute for health and care excellence	NICE
National Institutes of Health	NIS
No observed adverse effect levels	NOAEL
Normal Hydrogen electrode	NHE
Nortriptyline	NOR
Outer Helmholz Plane	OHP
Peak Force	PF
Pharmacodynamics	PD
Pharmacokinetics	PK
Phosphate buffer saline	PBS
Point-of-care	POC
Point-of-care testing	POCT
Poly (3,4-ethylenedioxythiophene) Polystyrene sulfonate	PEDOT:PSS
Poly(ethylene glycol)diglycidyl ether	PEGDE
Polyethylene glycol	PEG
Polyvinyl alcohol	PVA
Quantum dots	QD
Reference Electrode	RE
Scanning electrochemical microscopy	SECM
Scanning Probe Microscopy	SPM
Selective serotonin reuptake inhibitors	SSRI
Silver nanoparticle	AgNP
Square wave voltammetry	SWV
Standard Hydrogen Electrode	SHE

Therapeutic drug monitoring	TDM
Therapeutic Index	TI
Time-of-Flight Secondary Ion Mass Spectrometry	ToF SIMS
Tricyclic antidepressant	TCA
Trimipramine	TRI
Tunnelling AFM	TUNA AFM
United Kingdom Research and Innovation	UKRI
United States	US
Working Electrode	WE

Term	**Symbol**
Current	i
Depth of diffusion layer	δ
Diffusion coefficient	D
Electric Potential	Φ
Faraday Constant	F
Flux	J
Gas constant	R
Number of electrons	n^{e-}
Peak Separation	ΔE_p
Position in space	x
Potential	E
Roughness	R_q
Scan rate	v
Temperature	T
Time	t
Valence	z
Voltage	V

1 Introduction

During the 20th century advances in physiology, cell biology and biochemistry led to some of the most important medical advances in human history[1,2]. In comparison, however, the developments made in the last two decades eclipse almost all of the progress made during the 100 years prior. Nanoscale engineering, biotechnology and advanced manufacturing techniques have paved the way for therapeutic and diagnostic technology which was unimaginable at the start of the millennium. Advances in nanotechnology form the foundation of nanomedicine a field which, in 2017 alone, was responsible for the development of almost 50 novel nano-pharmaceuticals - a number that grows annually[3]. Likewise, work across molecular and cellular biology has created regenerative medicine, an area that has given rise to advanced therapeutic strategies such as bioprinting, biopharmaceutics and stem cell based treatments[4].

The last decade has witnessed a growth in the field of personalised healthcare, which attempts to design treatment based on a patient's genotype, phenotype and individual pathophysiology. Research into personalised medicine is often interdisciplinary; involving a combination of physiology, pharmacology and biotechnology. The following introduction will give an overview of some of these, and related topics, to provide context for the rationale and aims of this thesis, which are summarised at the end of this introduction.

1.1 Pharmacokinetics and personalised medicine

1.1.1 The impact of pharmacokinetic variability

Historically the drug development industry has taken a one-size-fits-all approach when identifying the ideal dose of a new therapeutic compound. Initially, an approximate dose is identified using preclinical data, including early toxicology information, *in silico* modelling and *in vitro* testing (Figure 1-1). This knowledge is then used to begin animal trials which establishes crucial safety limits, in particular the no observed adverse effect level (NOAEL) and the human equivalent dose (HED)[5]. This data is further optimised through repeated animal trials, ideally across multiple species. Following this a conversion factor is applied which takes into account species variation allowing an approximate human dose to be determined, which is then used for the first in human (FIH) clinical trials. Finally, human trials are used to establish a safe human dose range, this allows the compound to reach the market. For the majority of patients the administered dose will lie within the therapeutic window allowing clinicians to use this as a guide when issuing prescriptions.

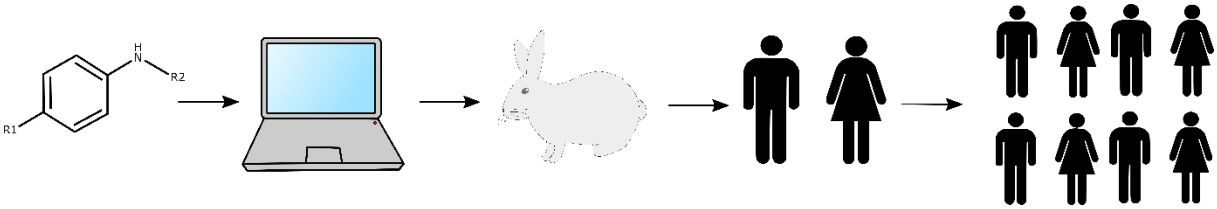

Figure 1-1 - A schematic overview of the typical drug development process, including early chemical and *in silico* data, animal and small population human trials and larger population studies

The pharmaceutical industry has developed this process with efficiency in mind; the goal is to identify the safest dose for the widest population of patients. This is a logical approach; it would be unrealistic to expect international companies to tailor their library of drugs to individual patients. For example, in 2019 GlaxosmithKline had >100 products on the European market, attempting to identify a personalised dose for all of those products would be more than a

challenge; it would be both financially and logistically unfeasible[6]. However, we now know that variation between individuals limits the success of a compound developed using the one-size-fits-all approach. This variability can be so severe that some therapies fail to reach market or display significantly reduced efficacy during clinical trials[7,8]. In some cases these problems can be addressed through modifications to treatment regimens, such as in a hospital setting where doses can be titrated to according to a patient's body weight. However, once again a combination of logistical and technical limitations make this an unfeasible approach for every clinical situation.

As our knowledge of human biology has grown the field of pharmacokinetics has developed a detailed understanding of what happens to a drug once in the body, a process roughly divided into four stages. Firstly, a drug is transported from the site of administration to the systemic circulation, a process known as absorption. The drug is then distributed throughout the tissues and organs of the body where it is either metabolised or excreted. This process is generally described as the absorption, distribution, metabolism and excretion (ADME) pathway[9]. Each step in this process is unique to the drug in question and each individual patient. Understanding a compound's ADME pathway is crucial in the drug development process; it impacts how a drug can be administered, how efficacious the drug is and any potential side effects or toxicity. For example when insulin is administered orally it is metabolised by enzymes in the stomach and intestine causing poor oral bioavailability. Previously this meant that insulin could only be administered via subcutaneous injection, until insulin formulations were developed which could overcome this physiological barrier, such as permeation enhancers, insulin conjugates or nanoparticle systems[10,11].

Each individual has a unique ADME profile influenced by a combination of physiological and genetic factors. In some cases these factors are easy to identify, such as biological sex, variation in age and weight and the presence of pre-existing health conditions; all of which have been

shown to impact how effective a drug is following administration[12–14]. Examples include differences in the half-life between male and female patients, decrease in overall bioavailability of compounds due to increased age and decreases in drug elimination due to obesity[15–17].

Genetic variation also has a significant impact on clinical outcomes and the study of this correlation, between genetics and pharmacological response, is the focus of pharmacogenomics[18]. One example is the impact of genetic polymorphisms in the cytochrome P450 family of enzymes. Genetic variations in the genes which encode cytochromes can determine which drugs can safely to be administered and, in the case of the anticoagulant warfarin, what dose can safely be given to a patient[19]. Similar examples involving cytochrome P450 include anticancer and antidiabetic drugs; variations in P450 genes have been shown to determine if a patient will respond to treatment or suffer adverse effects[20].

These examples provide a cursory glance at the role physiological and genetic differences play in determining the pharmacokinetic response of a patient. The examples highlighted above have been studied extensively, and while others have been investigated we still lack a complete understanding of how genetic and physiological variability impacts individual pharmacological response. The FDA approved 48 compounds in 2019, a number which is likely to increase annually, therefore it is unlikely we will ever develop a complete understanding of how each drug interacts with each individual; there are too many genetic and physiological variables to assess[21]. Despite the challenges personalised medicine aims to design better therapeutic strategies which can be tailored to suit a patient's unique pharmacokinetic profile.

1.1.2 Current approaches in personalised medicine

Pharmacokinetic variation limits the effectiveness of therapeutics developed using the traditional drug development process and the field of personalised medicine has attempted to counteract these limitations[22,23]. The term personalised medicine broadly describes any type of

clinical decision making which relies on available knowledge about a patient and uses it to make decisions which will maximise positive outcomes and minimise negative consequences for that individual patient[24]. Advances in technology have vastly increased the amount of "available knowledge" we can gather about an individual patient. A deeper understanding of the human genome paired with the commercialisation of genetic testing has allowed pharmacogenomics to become a viable avenue of interest for many healthcare systems. In the United Kingdom (U.K) the National Health Service (NHS) has developed a strategy that will design and implement a state-of-the-art genomic based medicine service. They plan to establish new diagnostic pathways which will carry out whole genome sequencing and use data from this service to inform clinical decision making[25]. Likewise, in the United States (U.S) the National Institutes of Health (NIH) has launched the "All of Us" research programme which is currently gathering data from >1 million citizens to investigate how a combination of biology, environment and lifestyle factors influence human health. This data will then be used to modify existing therapeutics, as well as develop new treatments based on individual healthcare[26]. These initiatives, while promising, are still in the process of being set up. In contrast, a number of smaller scale approaches have already been established and are currently in use. These examples rely on patient genotyping to identify which clinical interventions are most appropriate for the patient. Examples include some anti-cancer agents, including those used to treat melanoma or non-small cell lung cancers, as well as certain chemotherapy drugs[27,28]. The national institute for health and care excellence (NICE) has recommended the use of genotyping for these and several other treatments. For those interested in seeing a full discussion on the use of genotyping in personalised medicine I recommend the Brittain *et al* review[22].

Until recently personalised medicine has focused on the use of pharmacogenomics to guide clinical decision making and provides some of the most well-established examples currently used in practice. However, there are a growing number of additional tools that personalised

medicine can rely on, including advanced sensing technologies, such as biosensors, which can support the expansion of personalised medicine.

1.2 Latest developments in biosensing technology

1.2.1 Components of a biosensor

Prior to discussing the latest developments in biosensing technology it is necessary to understand the key components of any biosensor system. The simplest definition of a sensor is a device that detects and responds to a given input signal. In a healthcare setting, the term biosensor is more commonly used; as recommended by IUPAC a biosensor is a device which contains a sensing component which is biological in nature such as an enzyme, immune component or whole cell[29,30]. Likewise, the biological component can also refer to the analyte being detected, the environment where the sensor functions, or the method by which an analyte is detected.

The concept of a biosensor has existed since the mid-1950's when the "father of biosensors" Leland Clark developed the earliest known biosensor for oxygen detection[31]. Since this point the field of biosensing has grown considerably and is multidisciplinary, spanning biology, chemistry and physics. While the number of commercial biosensors continues to grow, the core principles that define a biosensor have remained relatively unchanged for the last few decades. An overview of the key components which make up a biosensor is provided in Figure 1-2.

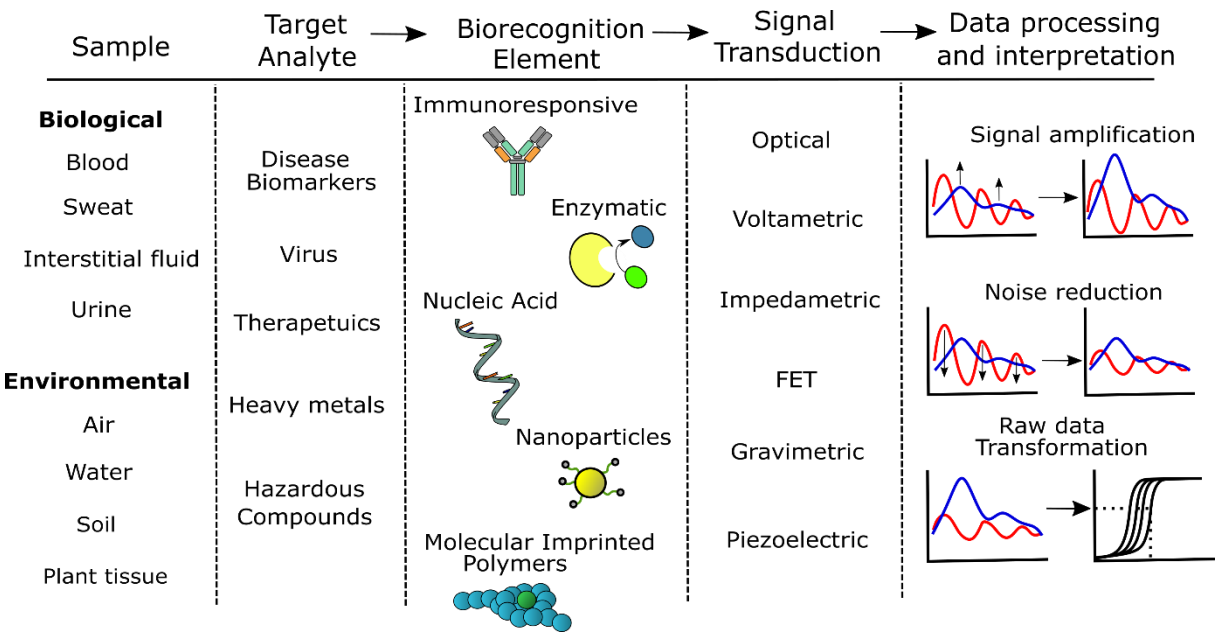

Figure 1-2 - Components of a biosensor - adapted from Bhalla et al[32].

Firstly, a biosensor requires a sample that will be tested, the source of which is dependent on the location of the target analyte. Biological fluids such as blood, sweat or urine all provide a range of analytes, such as biomarkers related to specific diseases, therapeutic drugs or bacteria, all of which can be detected in biological fluids[33–35]. Likewise, environmental samples can be used, such as air, water or plant tissue, which can be provide a range of analytes which relate to pesticide toxicity, pollution and pathogen identification[36].

Once a target analyte has been selected the next component of a biosensor is the biorecognition element which interacts with the target analyte. This interaction must be specific; any interference can lead to error which will make the sensor inaccurate. The signal produced by the interaction between the analyte and the recognition element is then transduced to a produce a measurable signal. The most common examples of transduction mechanisms involve optical or electrical signals; both of which can be proportional to the interaction occurring between analyte and recognition element.

Finally, the signal which has been produced is processed to maximise the signal-to-noise ratio and additional data transformation is performed to produce a relevant read-out.

These core components provide a road map for developing a biosensor. The ability to modify and select components based on a desired target has made the biosensor one of the most flexible and effective diagnostic tools, especially for in a personalised healthcare setting.

1.2.2 Biosensors for point-of-care analysis and personalised medicine

The miniaturisation of electronic circuitry paired with biochemical engineering has opened up new analytical strategies for biosensor development. The first biosensor was the glucose biosensor developed by Clark and Lyons which was able to monitor glucose levels during cardiovascular surgery[37]. Early glucose biosensors such as this relied on glucose oxidase and glucose dehydrogenase, enzymes that catalyse the oxidation of glucose[38]. The specificity of this reaction, due to enzyme kinetics, made it ideally suited for use in a biosensor. Glucose biosensing has now progressed into its third generation; forming a sub-field within the biosensing community. Glucose biosensors are potentially the most well-known example of a successful point of care testing (POCT) device; they are rapid, sensitive and easy to use. It is unsurprising therefore that POCT for glucose has seen incredible clinical and commercial success[39,40].

As demonstrated by the glucose biosensor a diagnostic device that can carry out rapid and reliable POCT can be of immense clinical value and represents an important tool in personalised healthcare. Under normal circumstances when a patient requires clinical intervention or needs to adjust current treatment the first step is to acquire a sample for testing (Figure 1-3).

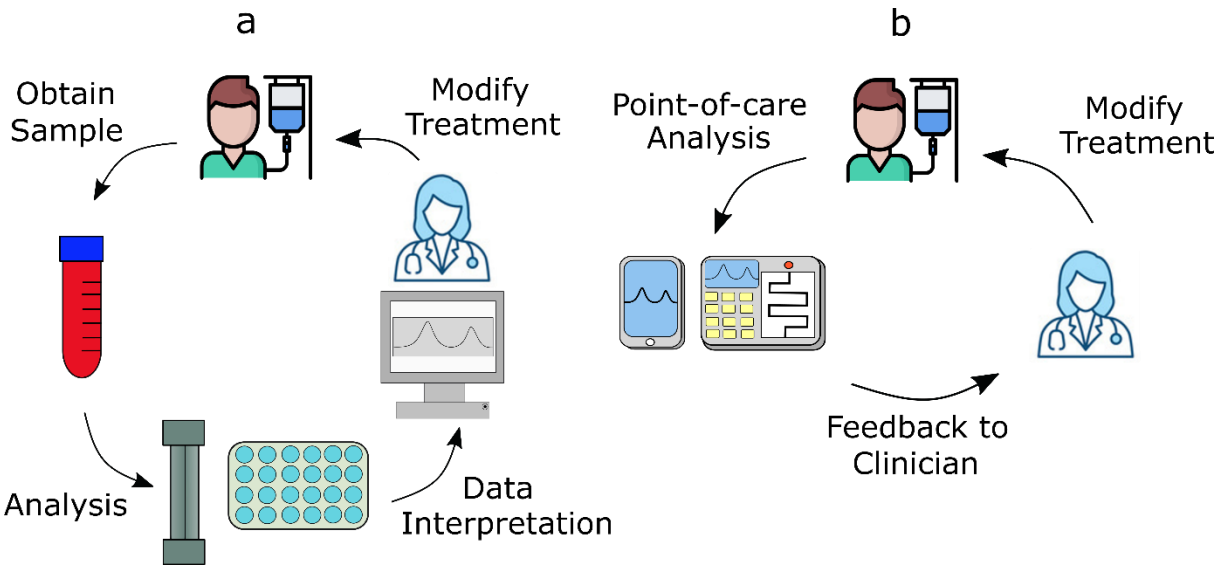

Figure 1-3 – Schematic highlighting the difference between traditional diagnostics and a point of care device.

Following this the sample will be tested and depending on the tests required this may involve specialised equipment or procedures. These may be as simple as a chemical screening via mass spectrometry or more complex such as high pressure liquid chromatography (HPLC). Once results are obtained the data can then be analysed and the results fed back to the clinician, who can then decide what the next step is for the patient. In contrast, a POCT device can be used to test a patient's sample almost immediately, depending on the speed of the test, bypassing the need for complex testing, allowing data to be obtained within minutes rather than hours or days. This situation demonstrates the major advantage of POCT in a healthcare setting; rapid testing can inform real-time decision-making to improve treatment. This approach offers several benefits; firstly for patients. Whether using antibiotics to treat an infection or chemotherapy to combat cancer, it is well documented that the earlier a treatment begins the more likely a beneficial outcome will be achieved[41,42]. Secondly, the therapeutic index for some drugs is extremely narrow; examples include lithium, phenobarbital and aminoglycoside antibiotics[43,44]. Rapidly determining how a treatment is affecting a patient can prevent unnecessary and potentially risky side effects.

POCT can provide a simple means to improve compliance; clinicians can monitor the patient and determine if they are completing the recommended dosage regimen, this can also help the clinician decide if that regime is effective or if it needs to be adjusted. POCT also provides an effective means to improve healthcare in difficult scenarios where there are technical or financial restraints. This can include low- and middle- income countries which lack access to the resources needed to perform expensive and complex analysis; POCT provides a cost effective alternative.

Finally, in certain situations there is an external pressure to optimise treatment. For instance, in the case of antibiotic treatments POCT can ensure that the right treatment is given at the right dose, preventing overuse. This is becoming increasingly important due to the rise in antimicrobial resistance[45]. Likewise, with the cost of healthcare rising there is a need to reduce equipment costs and ensure that patients are receiving cost-effective treatment, an outcome POCT can help achieve[46].

POCT is an opportunity to maximise the clinical benefit for both the patient and healthcare system. Based on this promise it is unsurprising that the number of POCT devices that are being developed continues to grow. Growth which has been accelerated by the development of novel recognition elements and signal transduction mechanisms. This includes the development of nucleic acid sensors, which rely on the interaction between target nucleotides and surface immobilised oligonucleotides, and have proven to be an effective strategy for a number of applications, including diagnosis of tuberculosis, measuring the viral load of human immunodeficiency viruses (HIV) and detection of pathogenic micro-organisms[47,48]. Likewise, advances in nanoscale engineering have led to novel biosensing technologies; some of the most notable developments include nanoparticles, quantum dots and carbon nanostructures. For instance, gold nanoparticles (AuNP) possess properties which make them ideal components of a sensing device; they have a high surface-to-volume ratio, fast electron transfer and they can

be readily modified with biomolecules for analyte detection[49]. AuNP can also be used with a variety of transduction mechanisms; allowing them to be designed according to a desired application. Examples include AuNP which rely on optical, electrochemical and piezoelectrical siganls[50]. Alongside metal nanoparticles, semiconducting nanoparticles such as quantum dots (QD) have also been a major development[51]. QD resist photobleaching and, as they rely on rapid fluorescence change, can provide real-time data. Functionalised QD have already been used in diagnostics for the detection of lung and prostate cancer biomarkers[52,53]. Finally, carbon-based nanostructures, such as carbon nanotubes (CNTs), are rapidly becoming an area of interest in biosensor development[54]. One advantage of CNTs is the range of transduction mechanisms currently available, including the use of field effect transistors, capacitive and impedimetric sensing systems for the detection of both biological and chemical targets[55–59]. CNTs have been used in the fabrication of ultrasensitive devices for the detection of several clinically relevant analytes, including cardiac biomarkers and the human epidermal growth factor receptor 2 biomarker for breast cancer[60,61]. These examples represent just some of the developments in biosensor and POCT technology in recent years, progress which has led to technologies which are continually being used to develop novel sensing strategies.

Novel approaches have also been used to overcome some of the technical barriers which have previously limited the success of biosensors systems. Depending on the type of system components present in the bloodstream can reduce the selectivity of the sensor. For instance, when developing an electrochemical sensor dopamine and ascorbic acid can be present which will interfere with the resulting signal, depending on the voltage window being used. Likewise, caffeine and nicotine are electrochemically active and may cause a significant decrease in the selectivity of the sensor which his being designed. The range of methods available for the development of a biosensor allows flexibility when attempting to overcome this problem.

This flexibility has led to unique sensor designs which have been applied to a range of fields, including environmental monitoring, food safety and a large number have seen success in healthcare applications. Table 1-1 summarises some of these recent designs, in particular nanoparticles systems are very popular, with a focus on AuNP. Furthermore, thanks to our ability to manufacture or isolate biological components there has also been an increase in the number of possible targets, from simple therapeutic biomarkers such as glucose to specific viral DNA.

Biosensor System	**Signal – Method of detection**	**Target**	**Application**	**Ref**
Nanoparticle	Electrochemical (Impedimetric) – AuNP	Bacterial DNA	Food quality Control	Izadi et al. [62]
	Electrochemical (Amperometric) - AgNP	Cholesterol	Healthcare	Nantaphol et al[63]
	Electrochemical (Differential Pulse Voltammetry) – magnetic AuNP	*Escherichia coli*	Food quality Control	Wang et al[64]
	Electrochemical (Differential Pulse Voltammetry) - AgNP	Mycobacterium tuberculosis	Health care	Ng et al[65]
	Optical (Lateral flow – fluorescence) - AgNP	*Staphylococcus aureus*	Healthcare	Wang et al[66]
	Optical (Lateral flow – fluorescence) - upconversion NP	Hg^{2+}, salmonella, hepatitis B	Health care, Environmental monitoring	Gong et al[67]
Hydrogel	Electrochemical (Amperometric) – Agarose gel (Temporary tattoo)	Glucose	Healthcare	Bandodkar et al[68]
	Optical (colorimetric) – Agarose gel (portable testing kit)	Acetylcholine	Healthcare	Kong et al[69]
	Optical (Visual) - DNA responsive hydrogel	Lead	Environmental and food monitoring	Jiang et al[70]
	Electrochemical (Differential Pulse Voltammetry) – DNA responsive Hydrogel	Lung cancer micro RNA	Healthcare	Liu et al[71]
Microfluidic	Optical microarray (Plasmonic)	*Chlamydia trachomatis* and *Neisseria gonorrhoeae*	Healthcare	Soler et al[72]
	Paper-based microfluidic optical (colorimetric) and electrochemical (amperometric)	Salmonella typhimurium and glucose	Healthcare	Li et al[73]
	Electrocehmical microfluidic array (impedametric)	D-dimer	Healthcare	Lakey et al[74]

	Field effect transistor	Prostate specific antigen	Healthcare	Mandal et al[75]
Quantum dot	Optical (immunofluorescence) - Surface plasmon resonance (AgNP)	H1N1 virus	Healthcare	Takemura et al[76]
	Optical/magnetic (fluorescence) – Fe3O4 NP	botulinum and staphylococcal toxins	Food quality Control	Wang et al[77]
	Electrochemical (Impedimetric) - QD-Ag hybrid NP	Vitamin D_3	Healthcare	Wadhwa[78]
	Optical (fluorescence) – magnetic quantum dot nanobeads	Prostate specific antigen	Healthcare	Rong et al[79]

Table 1-1 - summary of recent developments in POCT

An increase in the number of recognition elements and transduction mechanisms that are available has made biosensor development a flexible process; it is now possible to choose components based on a desired application. Despite the promise however the commercial success and clinical uptake of biosensors remain limited, especially in a personalised healthcare setting. Before biosensors can become an integral component of personalised healthcare a number of challenges remain to be addressed, including the development of biosensors that can maintain their sensitivity in increasingly complex environments, in particular biological matrices.

1.3 Clinically relevant analytes for therapeutic monitoring

1.3.1 Importance of therapeutic drug monitoring

As the range of available analytical tools has grown so has the number of sensing applications in personalised medicine. Early diagnostic applications focused on the identification and measurement of disease relevant biomarkers. As highlighted previously the most successful example is the measurement of glucose for the optimisation of diabetes treatment. However, our understanding of disease biomarkers has developed and a large portion of diseases now

have some form of associated biomarker. Examples includes the use of DNA biomarkers to determine the level of breast cancer metastasis, proteomics to determine optimal treatment regimens for kidney disease and the concentration of dopamine in the brain can be guide Parkinson's Disease treatment[80–82].

The principles behind personalised medicine have also been used to design novel therapeutic strategies, creating the field of targeted therapeutics. This approach focuses on developing treatments which will only be applicable to a very small number patients, if not one specific individual. To successfully develop a targeted therapeutic a detailed understanding of a patient's individual pharmacokinetic and physiological profile is required. There is also a need to investigate how a patient's pharmacokinetic profile changes once a drug has been administered and is processed by the body. This can be achieved using therapeutic drug monitoring (TDM).

TDM is the process by which, once a treatment has been started, a therapeutic target is measured and the data which is generated is used to influence subsequent treatment. TDM is a type of personalised medicine; it uses analytics to inform clinical decision making and aims to optimise treatment for maximum clinical benefit. While personalised medicine describes any approach which involves tailoring a treatment to a patient, TDM specifically refers to the monitoring of a drug treatment to determine an optimal dose.

In the late 1990's and early 2000's it was unclear whether TDM would become a routine healthcare procedure[83]. The advantages TDM offered were obvious; improved patient care, more cost-effective treatments and the opportunity to gain valuable insight into individual pharmacokinetic variability. For TDM to be effective however it must be; widely accessible, provide rapid sample testing (within a clinically relevant time frame), and minimise the amount of technical and specialist knowledge required[46]. Ideally this would all be carried out within 12 - 72 hours from when a sample is taken; to ensure that the data collected is accurate. In some

cases prefabricated assay kits can be used to determine the concentration of a drug in biological samples within that time frame. However not every compound has a prefabricated detection kit available, especially compounds which are less frequently prescribed. For those compounds a more technical method can be used, such as chromatographic measurement using HPLC[84]. However, these procedures require sample preparation, processing and analysis by a skilled technical staff, a procedure that can be expensive and time-consuming.

TDM has yet to become a routine procedure and is rarely used by clinicians. The two main reasons for this are time and cost effectiveness. As mentioned, to test patient samples the samples need to be processed, handled, and analysed by fully qualified technicians. Establishing this system would require not only a significant monetary cost but could take several years before it could be fully operational. Furthermore, as novel therapeutics are developed novel analytical methods are needed which can accurately detect those therapeutics. This, once again, would require a significant time and monetary and investment; new methods of analysis would themselves require development and optimisation before they could be used.

If successfully used TDM has the potential to be a powerful tool for personalised medicine, however TDM has yet to become a common practice in the clinic. Advances in POCT and biosensor development offer an opportunity to develop new drug monitoring tools which could drive the use of TDM forward.

1.3.2 Clinically relevant analytes which are currently monitored

TDM can, theoretically, be used for any compound which is given therapeutically; it only requires a sufficiently powerful analytical method so that it can be detected in a patient sample. However, realistically not every drug can, or needs to be, monitored. For instance some compounds are significantly more toxic than others, some have external pressures like cost and societal impact to consider, and some therapeutics are more easily monitored than others

because of their chemical properties. As such there are certain drug families which are more commonly measured using TDM than others.

A general criteria has been designed to determine when TDM can be used to guide a patient's treatment. This guide aims to determine if a drug would benefit from being monitored and if doing so is an achievable goal for that particular drug or class of drugs. Devised by a number of authors over the course of several years, the criteria can be summarised as follows[83–86]:

1. Does the compounds have a level of pharmacokinetic variability between patients that cannot easily be predicted?
2. Is there a relationship between the concentration and the clinical response or toxicity?
3. Is treatment duration for an extended period? (To allow for dosage modifications to occur)
4. Are there any other markers to determine the relationship between dose and response?
5. Is the target consistently stable? (To allow for accurate testing)

Of the library of drugs that are given therapeutically a surprising number do not meet these criteria; hence why uptake of TDM has been limited. A range of chemotherapeutic drugs are among those most commonly used as TDM targets. This includes the compound methotrexate which is extremely cytotoxic against several forms of cancer; it inhibits the synthesis of DNA precursors and limits cell replication[87]. While effective against cancer cells methotrexate also has significant off target effects; it can be toxic to healthy cells. However, if too low a dose is administered it will not slow the progression of cancer cells, thus making treatment ineffective and allowing cancerous cells to spread. This balance between cytotoxicity and ineffective treatment is why methotrexate is the target of TDM - to ensure maximum benefit with minimum side effects[88,89]. To improve the monitoring of methotrexate a number of biosensors have been developed. An example is the use of nanoparticles functionalised with folic acid; this system relies on surface plasmon resonance to detect methotrexate in patient samples at the nanomolar

level[90]. Nanoparticles functionalised with the human dihydrofolate reductase enzyme have also been developed which are capable of detecting similarly low concentrations of methotrexate within 10 minutes[91]. Alongside methotrexate other anticancer agents have been of interest for TDM, this includes electrochemical sensors for Irinotecan, 5-fluorouracil and cyclophosphamide[92–94]. Anticancer agents represent a prime example of a therapeutic that has benefited from TDM; due to their inherently toxic mechanism of action. However they are not the only class of compound that benefits from the development of TDM biosensors.

Antimicrobial compounds are increasingly become a target for drug monitoring die to societal pressure to optimise any treatment involving antimicrobials; the rise of antimicrobial resistance (AMR) has become a global healthcare crisis[95]. Furthermore, antimicrobial drugs can also be severely toxic and therefore, as with chemotherapeutics, TDM can be used to improve individual patient care. Work has focused on developing biosensors which accurately measure a wide range of antibiotic compounds, such as a microfluidic amperometric sensor capable of detecting ß-lactam antibiotics, including penicillin and cephalosporin, at a nanomolar range using extremely small volumes of sample, down to 1 µL[96]. Likewise, a platform has been developed which relies on dual enzyme-linked assays to provide accurate measurement of multiple analytes within 15 minutes of sample collection[97]. These examples demonstrate how technological developments, in particular microfluidics, can be used to create point-of-care devices capable of measuring analytes rapidly with nanomolar accuracy.

Recently, there has been significant progress improving the sensitivity of antibiotic TDM biosensors, in particular with regard to *in vivo* functionality. For instance, by using gold nanorods Zhu *et al* were able to design an optical biosensor for Gentamicin that had ng/ml sensitivity[98]. A microneedle system has been used to measure the concentration of Vancomycin at <100 nM using sub-nanoliter volumes[99]. A similar approach has been tested for real-time

monitoring of phenoxymethylpenicillin, with results from early clinical trials showing promising results[100].

The final family of compounds that are commonly the target of TDM are those which show psychopharmacology activity, a category which includes antiepileptics, antipsychotics and antidepressants. These compounds are a target for several reasons. Firstly, it has been suggested TDM can significantly reduce the rate of failure during treatment, this is particularly important for antiepileptic compounds which have a high rate of failure[101,102]. Likewise, for both antidepressant and antipsychotic compounds TDM could reduce the risk of toxicity as well as increase compliance, a common difficulty in patients with neuropsychological symptoms[103,104]. Evidence indicates that for almost all of these psychopharmacological compounds significant improvements could be made if TDM was used[104]. However, these compounds lack the same level of development as previous examples. For instance, only a limited number of drug monitoring sensors can be found for antiepileptic compounds, such as a fibre optic immunosensor developed in 1994 and a microcantilever sensor which, while functional, can only detect a single antiepileptic, phenytoin, in foetal bovine serum[105,106]. Likewise, portable sensing devices for TDM of antipsychotics and antidepressants are currently limited. Until recently immunoassays and HPLC have been the primary methods for TDM of these compounds[104]. Several electrochemical sensors have been developed for the detection of monoamine oxidase inhibitors, a class of antidepressants, however these examples have only been used to detect a single antidepressant target such as imipramine or only function in phosphate buffer saline (PBS)[107,108].

The lack of progress concerning TDM of psychopharmacological compounds is caused by two major limitations. Firstly, these compounds must cross the blood-brain barrier; that is where they mainly act. This means that the concentration within the brain is of interest, compared to the concentration found in systemic circulation. To accurately measure the concentration of an

analyte that has penetrate the blood brain barrier would involve taking samples from either cerebral spinal fluid or tissue from the brain, both of which can be impractical. While some data suggest that the concentration within the plasma correlates with observed clinical outcome, there remains debate over how accurate blood or urine sampling is when monitoring compounds whose primary site of action is the brain[109]. Secondly, many neuroactive therapeutics display complex non-linear pharmacokinetics. One of the most well documented characteristics of antidepressant therapeutics is a delay in the onset of action, the mechanism of which is still under debate[110,111]. This makes it difficult to associate observed clinical improvement with the concentration of a therapeutic in the patient's blood stream. This could mean that a patient will have a high systemic concentration of antidepressant but show no sign of improvement. These challenges explain why the monitoring of psychopharmacologics in the clinic has been low, as well as why developments in POC devices for TDM has lagged behind the developments seen for other compounds.

Advances in TDM biosensors have the potential to change how certain groups of therapeutics are prescribed. The examples discussed here represent the majority of TDM biosensor technology; as shown antibiotic and anticancer agents have been the primary focus. Additional TDM biosensors exist for compounds other than those discussed here, however, as with neuropharmaceutics current progress is limited. Recent examples include a nanoplasmonic device constructed from gold nanodisks for detection of the anticoagulant Acenocoumarol and the use of surface plasmon resonance (SPR) for detection of the monoclonal antibody Infliximab, a therapeutic antibody treatment used to treat autoimmune conditions[112,113].

For further discussion on TDM biosensors, with a focus on those targeted towards anticancer and antibiotic compounds, I recommend the 2016 review by McKeating *et al*[114].

1.3.3 Therapeutic monitoring of Tricyclic antidepressants

As discussed psychopharmaceutical compounds would benefit from TDM, however challenges in the field remain. Sensors for antiepileptics are currently being developed and antipsychotics can have a wide therapeutic window compared to antidepressants. As such TDM of antidepressant compounds remains an unexplored area of interest and thus far there has yet to be a commercially successful rapid point-of-care device capable of measuring antidepressant concentrations in biological samples.

All antidepressants display a level of toxicity and therefore could be of interest to TDM, however the modern variations, such the monoamine oxidase inhibitors (MAOI) and the selective serotonin reuptake inhibitors (SSRI), have a wider therapeutic window and less toxic side effects compared to their predecessors - the tricyclic antidepressants (TCAs). The TCAs were first developed in the late 1950's when they were first used as treatment for patients with schizophrenia[115]. They had little to no effect as antipsychotics they grew to become one of the earliest therapeutic treatments for mood disorders, such as clinical depression. From that point onward they were used as either a first line treatment or in combination with additional compounds. However, their use declined as they were replaced by less toxic alternatives such as MAOIs and SSRIs. This was particularly appealing as TCAs have severe side effects including sedation, confusion and disruption to motor coordination during the first few weeks of treatment[9]. Likewise, TCAs have an acute risk of toxicity; they exhibit cardiotoxic effects which increase the likelihood of cardiac dysthymia[116]. As such they were commonly used during suicide attempts; due to their narrow therapeutic window they were easy to overdose. Because of these risks TCAs moved from a first line treatment to, now, being used only in severe cases of mood disorder, particularly those which are resistant to other types of treatment. These factors make TCAs an ideal target for TDM; they have clinical benefits but due to a

narrow therapeutic window can be severely toxic. TDM is an opportunity to tailor a dose regime to a patient and reduce the risk of those toxic side effects.

Monitoring of TCAs has been limited to either HPLC or fluorescence based immunoassays[117–119]. These methods, while accurate, have high equipment and labour costs; hence they are not used for the majority of cases. Furthermore, the TCAs are rapidly metabolised, with a half-life of approximately 24 hours; this means that by the time testing is complete and results are given to the clinician the concentration in a patients system has already changed[120]. These factors have thus far limited the use of TDM for tricyclic compounds.

Attempts to overcome these limitations have focused on the design of POC sensors which can measure TCA; this can offer some obvious benefits. Firstly, sensors which detect TCA concentration in real-time could mitigate some of the risk associated with TCA toxicity. If patients were at risk of overdosing, due to individual pharmacokinetic variability or accidental overdose, the ability to measure the actual concentration of TCA in a patient's blood would allow more effective treatment of overdose and the ability to prevent future overdose by tailoring the dose to the individual patient. Secondly, POC sensing of TCAs could provide a means to improve patient compliance; treatment of clinical depression often relies on patient feedback and while patients may report that they are completing their regimen, there is little way for the clinician to confirm this fact. This can be particularly problematic with any therapeutic that has uncomfortable side effects, such as the TCA which can cause constipation, weight gain and blurry vision. A POC sensor for TCA would therefore allow both the clinician and patient to monitor adherence to the prescribed treatment regimen.

Previous attempts to develop POC testing for TCA has included electrochemical sensors using screen-printed electrodes or glassy carbon electrodes modified with carbon nanotubes have been developed for detection of either Desipramine or Doxepin, respectively[121,122]. Likewise, an optical biosensor that made use of reflectometric interference spectroscopy to detect

amitriptyline has also been developed[123]. These examples demonstrate the ability to detect some of the TCAs, however some of these sensors have not been able to achieve the resolution needed monitor clinically relevant concentrations of TCA; current estimates suggest that the concentration of TCA in blood stream following oral administration is between 0.5 and 1.25 mM. Likewise, many of the sensors discussed above only have the ability to detect a single TCA compound. Given that there are six commonly prescribed TCA compounds an ideal sensor would be able to detect all of these analytes, otherwise it is of limited use[124].

TDM of the TCAs would clearly be an effective tool; it would allow a personalised approach to treatment which would reduce the toxicity and improve clinical outcome. However, the development of tools for this application have thus far been limited and currently there are no clinical examples of POC-TDM devices for tricyclic compounds.

1.4 Growing application of Bioelectronic medicine

Within the field of personalised medicine certain topics dominate the therapeutic landscape; including CRISPR, gene therapy, and the use of artificial intelligence. However, these are not the only advanced therapeutic options available when developing personalised medicine. Another growing area of interest is the field of bioelectronic medicine; which aims to understand the role bioelectricity plays in disease and one day modulate those electrical signals for therapeutic benefit.

1.4.1 Establishing bioelectronic healthcare

The concept of bioelectronics has existed since the days of the Roman Empire, when ancient physicians used the electrical properties of the Torpedo fish to relieve pain[125]. The modern concept of bioelectronics focuses on interfacing electronic and biological systems more directly. The first bioelectronic devices of the early 1900's were able to measure the electrical currents of the body, the most notable example was the development of electrocardiograms which are still used to measure the electrical currents of the heart[126]. This then led to the first

example of bioelectronic medicine - the cardiac pacemaker. The first generation of pacemakers were limited by the size of the electrical equipment available at the time. Miniaturisation of electrical components then led to the first portable, wearable cardiac pacemaker in the 1950's[127]. The field of bioelectronics has since expanded, fuelled by developments in electronic engineering, chemistry and human biology. As such the term bioelectronics can be used to describe a range of technologies. One of the most recent advances is the field of electroceuticals, which are specific examples of bioelectronic technology which are used to develop novel therapeutic stratergies. This has been of particular interest for cardiac rhythm treatments, epilepsy and several central nervous system disorders[128–130]. The field of electroceuticals is a recent development and as such the term will not be used frequently here; instead the broader term bioelectronic medicine will be used.

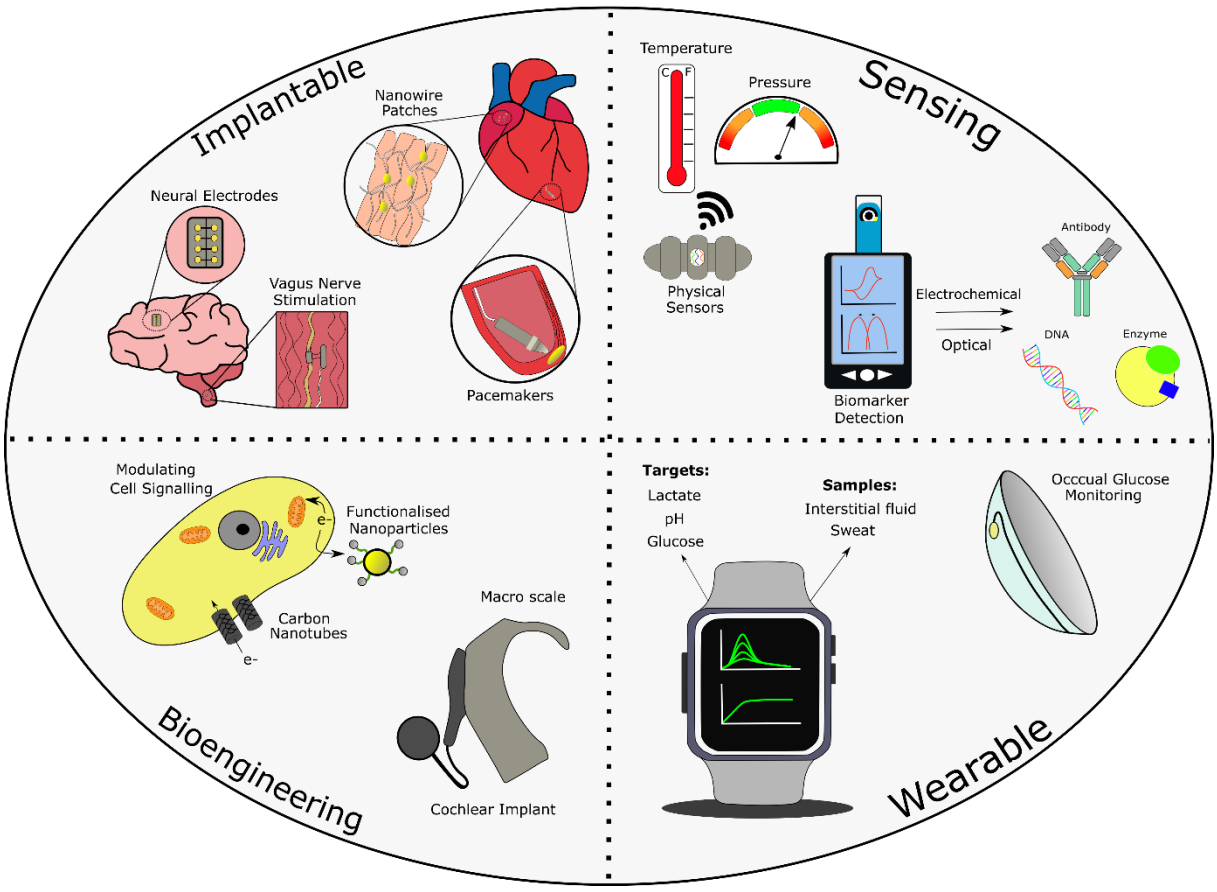

Figure 1-4 - Overview of current bioelectronic therapeutic and diagnostic technologies. Adapted from Gibney *et al*[131].

The question at the core of bioelectronic medicine is "how do you interface an electronic system with a biological one for therapeutic benefit?" Put simply, how do you merge two systems which are not designed to interact? There are a number of solutions to this problem, Figure 1-4 provides an overview of some of the key advances and technologies within bioelectronics which are trying to address this challenge.

Following the first cardiac pacemaker development of more implantable devices became an attractive goal. Many of the first bioelectronic devices were on the macro scale and focused on engineering solutions. Examples include retinal and cochlear implants which are still commonly used today and, thanks to technological advances, display significantly improved resolution compared to their predecessors[132–134]. As electrical components have become smaller and our understanding of the body's electrical circuitry has grown, new approaches can use electrical signals to modulate physiology. One of the earliest examples of such a technology was the use of electrical stimulation to improve bladder control in paraplegic patients[135]. Likewise, it has been shown that electronic stimulation can be used to activate anti-inflammatory pathways and reduce localised inflammation; a possible treatment for rheumatoid arthritis[136].

Alongside attempts to control whole organs developments in micro and nano scale technology have made it possible to target specific tissues and cellular processes[137]. For instance, nanoscale scaffolds have been developed which interact with both cardiac and neuronal cells[138]. Likewise, it has been suggested that electric fields could be used to modulate cell signalling which can be used to treat cancer[139,140].

Currently, the majority of bioelectronic medicines which are available operate at a macro scale e.g. cochlear and retinal implants. These devices have existed for longer and have had more time to develop. Furthermore, it is easier to assess the safety of these devices, allowing them to achieve regulatory approval more easily compared to devices at the micro or nano scale.

However, clinical trials are currently underway to prove the safety and efficacy of a number of bioelectronic medicines. This includes the use of micro currents for relief of sinus pain as well as vagus nerve stimulation for the treatment of Crohns disease[141,142]. Recently, the FDA has also approved the ActiPatch, a device which uses electrical stimulation to treat musculoskeletal pain[143]. While bioelectronic medicine has the potential to become a new healthcare strategy many of the devices and technologies are still in the development phase.

1.4.2 Implantable and wearable sensors for personalised medicine

During the early days of bioelectronic medicine the scale of electronic equipment combined with the lack of biologically compatible materials limited what could be developed. Advances in microelectronics and biomaterials have overcome these challenges and brought about a new wave of bioelectronic technologies.

Of particular interest has been the development of wearable and implantable bioelectronic devices; they offer a number of practical benefits. Firstly, they can perform real-time clinical intervention; the treatment no longer needs to be distributed throughout the body, reducing the time between administration and action. This is important for conditions which require rapid treatment, such as movement disorders, epilepsy and arthritis[136,144]. Secondly, a device which can be implanted or carried by the patient is an ideal tool for personalised medicine; there is no need to give the patient an approximate dose because the device will determine an appropriate dose based on an internal feedback mechanism. Any treatment they receive will therefore be tailored to suit their specific needs - the epitome of personalised medicine.

To function accurately an implantable or wearable must detect and respond to a given input. A common example would be automatic insulin injection; when blood glucose begins to fall this is detected by a glucose sensor which then triggers the automatic injection of insulin. Blood glucose levels will then be monitored to create a feedback loop between blood glucose levels

and insulin delivery[145]. Without this feedback loop implantable and wearable devices would not be able to function independently; they would require constant monitoring.

The most recent advances in both implantable and wearable sensing has been in the field of material science. The development of soft and flexible electronics has been crucial; it has allowed researchers to overcome many of the previous challenges in the field. The first electronic materials were made from hard, coarse materials, mainly metals. These materials do not easily interface with biology due to the difference between the materials properties. Likewise, many of the early devices were bulky and were not portable. Combining biological systems with electrical systems was therefore difficult. The latest soft materials, such as textiles and polymers overcome many of these limitations; they are soft, flexible and trigger a minimal immune response, making them ideal for developing novel implantable and wearable electronic devices.

The development of flexible electronics has had a large impact on bioelectronic sensing, some examples are summarised in the sensing segment of Figure 1-4. Firstly, flexible electronics have been used to create wearable sensors which do not require sample extraction and preparation; reducing the labour and equipment cost of traditional diagnostic methods[146]. Early development in the field of wearable sensors focused on external devices for glucose sensing, such as watches which, while functional and still used, have been replaced by more advanced technologies. This includes tattoo based glucose monitoring which use a tattoo paired with a flexible patch to create an amperometric enzyme-based sensor[68]. Likewise, contact lens capable of measuring ocular glucose levels have been developed using a polymer substrate patterned photolithographically[147]. These devices provide a simple and relatively non-invasive method to measure patient glucose levels and they offer a personalised approach to diabetes management. Similarly, graphene based sensors have been designed which are able to detect glucose in sweat using microneedles, which maximise the surface area of the sensor and enhance signal

detection[148]. The use of sweat as an electrolyte has also been used to develop wrist and head band sensors, alongside devices which can measure multiple analytes in sweat, including glucose, lactate and ions such as sodium and potassium[149]. Similar devices are currently in development which can detect not only specific analytes but also pH[150].

Alongside wearable devices the development of implantable sensors has seen significant development thanks to advances in material science. The development of biocompatible and nanoscale materials has opened the door to many novel devices. For instance, nanowire surfaces constructed from a composite of silver and gold have been developed which display strong biocompatibility and electrical conductivity[151]. These nanowires have the potential to monitor electrical signals both externally and internally, and early *in vivo* data suggests they could be used as a cardiac monitoring patch.

Several implantable sensors have been developed which are also able to respond to physical signals. One example is an ingestible sensor which functions as a galvanic cell and measures internal body temperature and, once ingested, can transmit data wirelessly[152]. Likewise, a minimally invasive optical sensor has been developed and initial *in vivo* work has shown that the device would be an effective tool for measuring blood pressure in high risk patients[153].

Currently, the field of implantable and wearable sensing is undergoing a period of significant development. This can be seen by examining the products which have successfully made it to market, with the greatest success being wearable technology. Firstly, there is the BlueSpark temperature tracker, which is designed to monitor an infant's temperature using a patch which transmits data to a mobile app[154]. Similarly, Proteus Digital Health developed an ingestible sensor which monitors when a patient takes medication and tracks their level of activity to help design personalised treatment regimens and improve compliance[155]. However, while this device was approved in late 2017 the product never made it to market; in 2020 the company filed for

bankruptcy[156]. Finally, heart rate monitors are also now commercially available and are a component in many Smart Watches[157].

Where wearable technologies have seen consistent growth the development of implantable sensors has lagged behind. Currently, the leaders in the market are glucose sensors. Specifically, the company EverSense sell a fully implantable glucose sensor[158,159]. Their fluorescence based micro sensor can be injected into a patients arm and continuously monitor glucose for up to 90 days.

The field of bioelectronic implantable and wearable technology is becoming of greater interest for those wishing to develop a personalised healthcare system. We already have heart rate monitors included in smart watches, and the idea of wearing diagnostic technology is becoming more common place. Based on this it is not difficult to imagine a situation where other forms of bioelectronic interfaces could become more mainstream. This is reinforced by the fact that the market for bioelectronics is predicted to grow over the coming years[160]. While bioelectronic technology has seen a boom, a number of challenges remain, especially for implantable devices. An implantable device must overcome one major difficulty - how does a device maintain function in the complex biological environment that is the human body? This question highlights the main difference between implantable and wearable technology. Wearable devices have fewer hurdles from both a regulatory and developmental stand point; they do not come into direct contact internal biological systems - challenges that will always make the development of an implantable bioelectronic device difficult.

1.4.3 Biodegradable Implantable devices

To overcome some of the challenges associated with implantable bioelectronic devices attempts have been made to design devices which will degrade over time. This approach offers a number of advantages. The device will be broken down *in vivo* removing the need to extract the implant

once it is no longer required. This avoids the disadvantages associated with the extraction of a medical implant, such as the need for invasive medical procedures, or the risk of local infections and inflammation[161,162]. Furthermore, biodegradable materials often have properties more closely resembling that of biological tissue, such as a low Young's modulus and high flexibility[163]. These properties can minimise the risk of adverse reactions when the device is implanted, as well as reduce the likelihood of an inflammatory or immune response that could prevent the device from functioning. Based on these advantages it is unsurprising that there is growing interest in the design of biodegradable implantable devices.

One of the early challenges associated with any implantable bioelectronic device is providing sufficient power; batteries are often produced from hard, rigid, toxic, materials that will not degrade. A wide range of strategies have been developed to address this challenge. This includes the development of batteries, super capacitors, bio fuel cells and energy harvesters; all of which have been created using biocompatible and biodegradable materials and can be used to power implantable devices[164,165].

Another significant challenge associated with the development of a biodegradable implant, and any implantable device, is ensuring the device maintains function in a complex biological environment. This often requires the material have a high level of conductivity, to maximise any signal that is generated by the device. A range of materials have been designed that possess both a high level of conductivity and the necessary properties to survive in a biological environment. Some of these materials are biological, such as silk, hyaluronic acid and naturally occurring polymers[161,166,167]. In contrast, other approaches rely on synthetic materials, such as conductive polymers, which have in recent years proven to be an essential tool when developing degradable implantable devices. The range of conductive polymers available paired with their ability to be modified and functionalised makes them ideally suited to the design of a bioelectronic device.

1.5 Conductive polymers as biomaterials

1.5.1 The origin of conductive polymers

Polymer manufacturing experienced a boom in the wake of World War II. During the war polymer based materials were needed for the war effort but after the war production levels were kept high, allowing polymers to become a common component of many household items, from Teflon coated kitchenware to polyvinyl chloride (PVC) construction materials[168,169]. The availability of polymer-based materials spilled over into research and polymers are now used in the automotive industry, aerospace engineering and are a crucial component in the development of new environmental technologies[170,171]. Polymers have also become an important tool in the development of biomedical devices; including as surgical tools, drug delivery formulations and a range of biocompatible devices[172,173].

Of growing interest has been the use of conductive polymers. The widespread study and application of conductive polymers is a relativity recent development; the noble prize for the discovery of conductive polymers was only awarded two decades ago. Early work during 1950–60's began with investigations into organic aromatic compounds which displayed electrical conductivity[174]. However, the most significant development occurred in the late 1970s when semiconducting films were synthesised using halogen doped polyacetylene[175]. It was this work which led to the Nobel Prize and put a spotlight on the significance of conductive polymers.

Once conductive polymers could easily be manufactured and processed the number of applications grew, with a particular focus on engineering developments. This included the development of flexible conductive fabrics, such as antistatic surfaces[176]. Electronic engineering research also focused on making conductive polymers a component of rechargeable batteries, such as electrodes batteries or as components of integrated circuitry[177,178]. There was

also interest in how conductive polymers could be used as energy storage devices, such as solar cells[179].

Conductive polymers are able to transport charge through the combination of two mechanisms. If the polymer has a conjugated double bond backbone the π electrons can become delocalised to create a conduction band that will allow charge carriers to move throughout the polymer backbone[180,181]. This mechanism produces what is known as intrinsically conductive polymers; their intrinsic structure is responsible for their conductivity. However, in many cases this produces an unstable electron structure and therefore a dopant is required to add stability. This produces the second class of conductive polymers - extrinsically conductive polymers. The dopant, which serves to stabilise the polymer backbone, can be either an electron donor or an electron acceptor, producing n- and p- type semiconductors, respectively. In n-type polymers the majority of charge carriers are negative electrons, while in contrast in p-type positive holes are responsible[182,183].

In recent years the properties of conductive polymers have also made them an avenue of interest for engineering applications. However, because they are soft, flexible and can easily be modified they are also ideal materials when designing an electronic-biological interface.

1.5.2 Conductive polymers as a biomaterial

The first implantable electronic devices were made using hard materials, mainly metal such as steel, nickel and copper. One of the earliest examples is the cardiac pacemaker which was made of nickel-cadmium batteries, stainless steel and epoxy resin[127]. The device was small, 55 × 16 mm, easily implantable and caused minimal immune response, at least not sufficient enough to prevent the device functioning. Since then the materials used in implantable devices have moved away from hard materials and focused on soft materials; they reduce the discontinuity between device and tissue. Conductive polymers are ideal materials for implantable electronics

as they are sufficiently conductive; with the conductivity of an unmodified conductive polymer reaching up to 10 kS/cm[184]. Secondly, they also possess positive mechanical properties, including flexibility, stability and a low Young's modulus, all of which mean their surfaces more closely match the physical properties of biological tissue[185–188]. Conductive polymers can also be easily modified allowing new formulations to be developed depending on the properties that are required. This includes covalent modifications of the conductive back bone, addition of conductivity enhancers, such as DMSO or ethylene glycol, and the use of nanomaterials like graphene and carbon nanotubes to increase conductivity[148,180,189–191].

Finally, conductive polymers also display biocompatibility, making them ideal for use in biological electronic interfaces. In some cases conductive polymers have no inherent toxicity towards biological tissue[192]. However, when this is not possible chemical conjugation can be used to improve biocompatibility by combining the conductive polymer with a biocompatible molecule, such as fibronectin or bovine serum albumin (REFERENCE). Likewise, conductive polymers can easily be blended with other, more biocompatible polymers such as polyvinyl alcohol or silk, to improve their interaction with biological tissue[180,193–195].

The mechanical properties of CPs can also be adjusted through the addition of chemical components, which improve the interaction between the polymer and biological tissue[196]. For instance, the creation of self-assembled monolayers using conductive polymers or the use of conductive cryogel formulations reduces the adverse biological responses, such as cytotoxicity, improving biocompatibility[197,198].

Conductive polymers can easily be processed and modified to suit the desired application and they are relativity cheap to manufacture and can be made to be biocompatible. These properties make them an ideal tool for overcoming the challenges associated with implantable bioelectronics.

1.6 Summary

A deeper understanding of human biology and genetics has fuelled developments in personalised medicine. Likewise, progress in electronic engineering and biotechnology has been responsible for some of the most recent advances in sensing technology. Finally, work in the field of biomaterials and nanotechnology now represents a key component of bioelectronic medicine, particularly for the design of novel therapeutic and diagnostic approaches. This introduction has given the reader a broad overview of all of these fields. The following work lies at the interface of all of these fields and will demonstrate how principles from these disciplines can be used to design and develop state of the art healthcare technology.

1.6.1 Rationale

To support the approaches taken in the following work several key rationale must be highlighted. These points are generally discussed in the introduction but are outlined here in an attempt to better support the multidisciplinary approach which was taken. These key rationale are:

1. Tailoring a therapeutic dose to a patient's individual pharmacokinetic profile is a key component in personalised healthcare. This approach aims to maximise clinical benefit while minimising the risk of toxicity. To effectively tailor a therapeutic dose it must be possible to monitor the concentration of the drug. Ideally this would be done rapidly at a low cost and using minimal technical equipment.
2. Development of biosensors for personalised medicine has focused on diagnostics, particularly the detection of disease relevant biomarkers. Biosensors could be an effective tool for monitoring not only biomarkers but for the monitoring of therapeutic compounds.

3. Materials which have improved properties, such as biocompatibility and conductivity, have led to the development of new bioelectronic materials. These bioelectronic materials can be used for therapeutic benefit, and potentially for the development of wearable and implantable bioelectronic devices.

These rationale provide a road map for addressing a number of healthcare challenges. Firstly, when a clinician wishes to carry out therapeutic monitoring there are a limited number of analytical tools available, mainly chromatographic and fluorescent based techniques. For certain compounds, such as the tricyclic antidepressants, this is particularly detrimental as the methods are slow and due to their extremely narrow therapeutic window TCAs would benefit from real time data acquisition. Secondly, while the development of wearable and implantable biosensors shows promise, many are still in the development phase and have yet to make it to market. In the case of implantable sensors this is primarily because they struggle to maintain their function once implanted, due to the complex nature of the biological environment and its interaction with the sensor surface. Finally, many novel electroactive biomaterials have recently been developed which could be used to overcome the challenges associated with implantable bioelectronics.

1.6.2 Aims

Based on the rationale above 3 aims were established for this work.

1. Create an electroactive surface which is capable of detecting and monitoring the concentration of tricyclic antidepressants, based on their unique redox behaviour.
2. Develop a blend of conductive, biocompatible and biodegradable polymer which could be used to create a biodegradable electroactive surface.

3. Using knowledge from aims 1 and 2 construct a platform which uses an electroactive and biodegradable surface to detect TCA in a biologically relevant solution.

The following thesis describes the work which was carried out in an attempt to achieve these aims.

2 Methods

2.1 Fundamental Electrochemistry

Electrochemistry lies at the overlap between physics and chemistry; it studies the relationship between the movement of electrons and subsequent chemical changes. The simplest reaction within electrochemistry is the reversible movement of electrons between a chemical species and an electrode surface:

$$O\ (aq) + \ n^{e-}\ (s) \rightleftharpoons \ \ R^{n-}(aq)$$

Equation 1

in which *O* and *R* represent an oxidised and reduced redox couple in aqueous media (*aq*), respectively. This type of redox reaction is driven by the supply, or removal, of a number of electrons (n^{e-}) through an electrode surface (*s*). This movement of electrons is the foundation of electrochemistry, however, to understand electrochemical reactions in greater detail it is necessary to look at not only the movement of individual electrons but how that movement changes the surrounding environment. Based on that the following discussion will highlight the key components of the electrode solution interface as well as the transport and kinetic mechanisms which occur in an electrochemical cell. This will be followed by a summary of the electrochemical techniques which have been used to gather the subsequent data presented in this thesis.

2.1.1 Understanding the electrode solution interface

An electrochemical cell consists of an electrolyte, a solution which is capable of transporting charge, and various electrodes. In a three electrode electrochemical cell these electrodes are: a working electrode (WE), where the redox reaction of interest occurs, a reference electrode (RE), which contains a known reaction in which the cell potential can be measured against, and a

counter electrode (CE) to complete the electrical circuit of the cell. Finally, there is usually an analyte of interest which will be the subject of the redox reaction (Figure 2-1)**Error! Reference source not found.**.

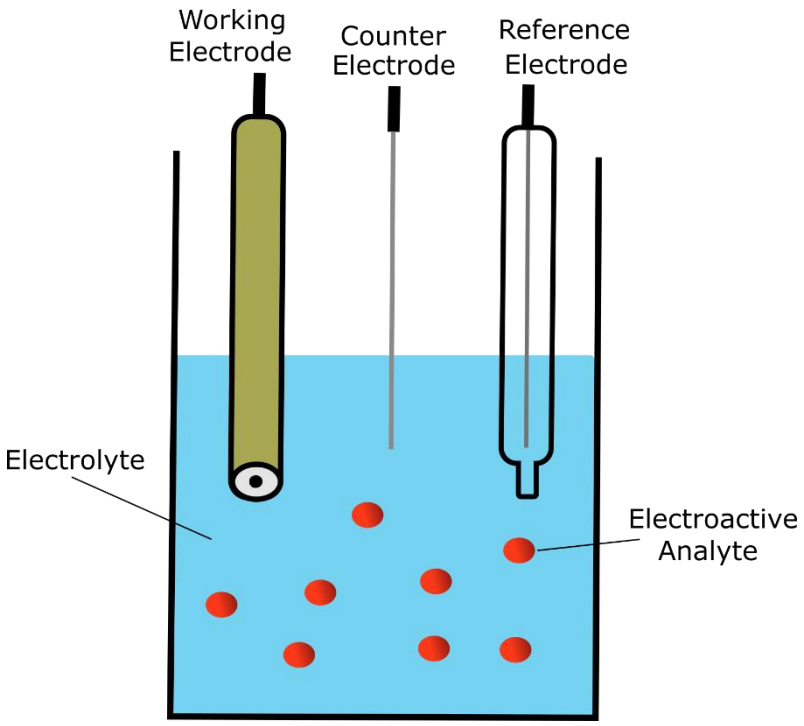

Figure 2-1- Schematic showing the key components used in an electrochemical cell using a three electrode setup.

All of the components used to create this electrochemical cell can be adjusted according to a desired need. For instance, any conductive material could be used as a WE; as long as it can act as either a source or sink for electrons to drive a redox reaction. Many WEs which are currently used are based on inert materials such as gold, platinum or carbon (e.g. glassy carbon). Similarly, due to its relatively inert nature the most common CE is platinum wire. RE are used to provide a stable, known and well-defined electrochemical potential; this potential will remain effectively constant allowing the potential at the working electrode to be measured. Previously, the most well-known RE was the standard hydrogen electrode (SHE), also referred to as the normal hydrogen electrode (NHE)[199]. This electrode is formed by passing hydrogen gas through an acidic solution in the presence of a platinum surface. An alternative to the SHE is the

saturated calomel electrode, which consists of mercury paste and liquid mercury saturated in potassium chloride solution. However, the SHE requires constant pressure, temperature and concentration, which can be difficult to maintain, likewise mercury is now considered a serious hazard, as such other RE have grown in popularity. In particular, the silver/silver chloride (Ag/AgCl) RE is commonly used.

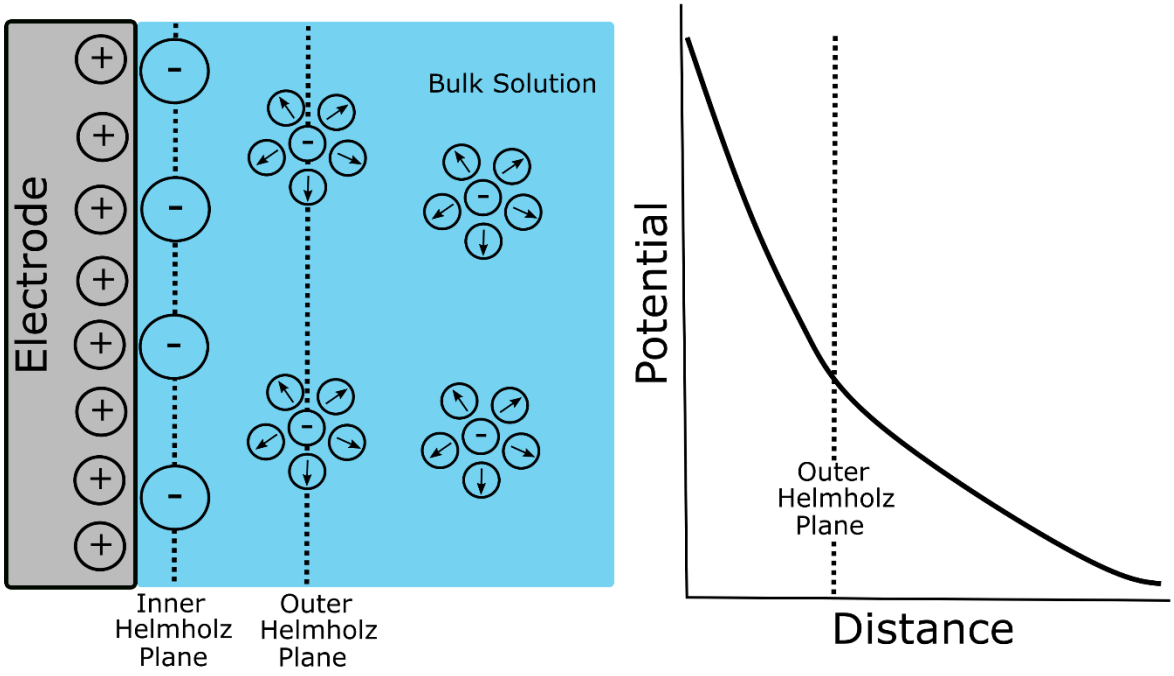

Figure 2-2 Schematic showing the structure of the electrical double layer and the location of Inner and Outer Helmholz planes, alongside the change in potential profile with increasing distance from electrode surface

In an electrochemical redox reaction electrons will only move when given sufficient energy to move between electronic bands. In an electrochemical cell the WE is used to provide that potential energy. When this occurs the movement of electrons causes a change in the immediately area surrounding the electrode surface. When the electrode surface is charged a heterogeneous system is set up within the vicinity of the electrode surface, this is known as the electrical double layer (Figure 2-2)[200]. If the electrode surface is positively charged it will attract negative ions present in the electrolyte solution, and vice versa. This is done to ensure the

interface remains neutral and results in the formation of several distinct layers. Firstly, there is the Inner Helmholz Plane (IHP) which is made of solvent molecules and ions which are adsorbed to the electrode surface. Following this there is the Outer Helmholz Plane (OHP) which consists of ions which are loosely attracted to the surface by coulombic force and are non-specifically adsorbed to the surface. Finally, beyond these planes, there is the diffuse layer, which contains molecules and ions which are diffusing towards the electrode surface, which then leads into the bulk solution.

The electrical double layer is often compared to a capacitor; the charged electrode and opposite charge in the IHP represent the two plates of the capacitor. This creates two potential-distance profiles; initially a linear increase in potential occurs up until the OHP is reached, at which point an exponential change in potential occurs within the diffuse layer. However, despite these profiles the overall charge present in the IHP, OHP and diffuse layers is always equal to that of the net charge at the electrode. The structure and size of these planes can impact the kinetic behaviour observed within an electrochemical cell; for instance a heavily charged particle will take longer to cross the helmholz planes resulting in slower electrode kinetics. Likewise, it is worth noting that the discussion above relates to the structure of electrical double layer at a standard flat electrode; the structure of this layer at porous film electrodes, such as those made using conductive polymers, will differ slightly. As opposed to a single double electrical layer, a multi-layered system exists, based on the Gouy-Chapman-Stem model (GCS), which involves a series of the double-layer capacitance made up of the Helmholtz capacitance, and the diffuse layer capacitance, this is called the Gouy-Chapman capacitance CG.

2.1.2 Mechanisms involved in simple electrode reactions

As shown the movement of molecules in an electrochemical cell is driven by the charge at an electrode surface. However, when examining chemical reactions at the electrode surface the

movement of molecules, charged or uncharged, is not always consistent and can occur through various modes of transport (Figure 2-3)[200]. Firstly, there can be standard diffusion, which involves spontaneous movement of molecules driven by a concentration gradient; whereby molecules move from areas of high to low concentration. Secondly, there is convection which involves transport caused by physical movement, usually driven by mechanical energy such as the flow or stirring of a solution. Finally, there is migration caused by the movement of charged particles due to electrostatic charges.

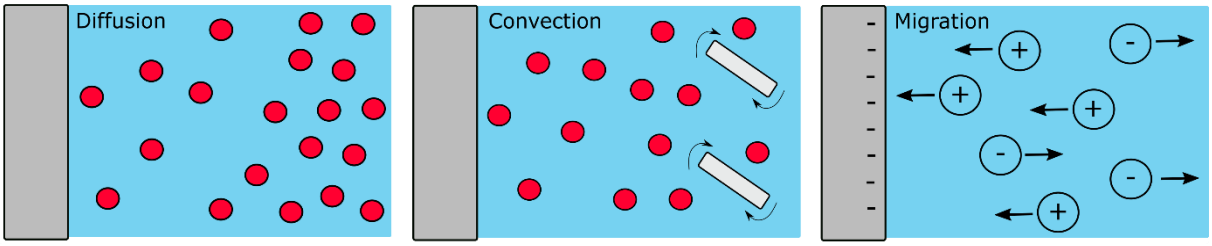

Figure 2-3 - Schematic showing three types of mass transport; diffusion, convection and migration.

The rate of mass transport is measured using flux (J), which is a mathematical method to describe the overall mass transport of a given number of molecules, in a unit area within a unit of time. In the case of diffusion the flux of molecules is described using Ficks two laws of diffusion, the first of which is:

$$J = D\,\frac{\delta C_O}{\delta x}$$

Equation 2

in which D and C_O are the diffusion coefficient and the concentration of molecules in the bulk, respectively, *x* represents position and δ is the depth of the diffusion layer in the system. In its simplest form this law states that when a system is diffusion controlled the flux of the molecules is proportional to the concentration gradient present in the system.

Fick's second law of diffusion describes how, under linear diffusion, flux is also time-dependent:

$$\frac{\delta C_O}{\delta t} = D\left(\frac{\delta^2 C_O}{\delta x^2}\right)$$

Equation 3

in which *t* represents time. This law describes how the change in rate of concentration influences the change in concentration gradient; specifically, it demonstrates that the rate of diffusion is proportional to the concentration gradient.

During an electrochemical reaction, at an electrode surface, the rate at which the reaction occurs is governed by the slowest process involved in the overall system. The simplest electrochemical reactions, or those which occur rapidly, will be limited by the mass transport of electroactive species to the surface of the electrode. In contrast, more complex reactions could include electrochemical or chemical steps, in which case the rate of reaction is limited by either transport or the rate of electron transfer, usually determined by the specific experimental conditions. Reactions controlled exclusively by the rate at which electroactive species are transported to the electrode surface are known as mass-transport-limited reactions. These types of reaction are also known as Nernstian reactions; they follow a thermodynamic relationship described by the Nernst-Planck equation:

$$J = -D\left[\nabla c + \frac{z\,F}{RT}c(\nabla \Phi)\right]$$

Equation 4

where *z* is the valence of ionic species, *F* is the faraday constant, *R* is the gas constant, *T* is the temperature and Φ is the electric potential. A system is described as Nernstian if it satisfies the Nernst equation. Likewise, a diffusion-controlled system will display several key characteristics. Specifically, the peak potential at which a reaction occurs will be independent of the rate at which the potential is scanned. Similarly, the scan rate and current peak intensity will be proportional to the square root of the scan rate[201]. The effect of scan rate on peak current, for simple reversible redox reactions, is governed by the Randles–Sevcik equation:

$$i_p = 0.04463nFAC\left(\frac{nFvD}{RT}\right)^{\frac{1}{2}}$$

Equation 5

where i_p is the maximum current, n is the number of electrons transferred in a redox event, A is the surface area of the electrode, F is the faraday constant, D is the diffusion coefficient, C is the concentration of analyte, v is scan rate, R is the gas constant and T is temperature.

2.2 Electroanalytical techniques

This thesis relies on electroanalytical techniques to characterise both redox active therapeutic compounds and electroactive materials. The following section provides an overview of the theory behind some of these electroanalytical techniques[202].

2.2.1 Cyclic voltammetry

Cyclic voltammetry (CV) is one of the most common electroanalytical techniques used to study electrochemical reactions. Its popularity is fuelled by its rapid ability to provide in-depth thermodynamic information about redox kinetics, electron transfer and surface processes. During CV a potential is applied (E) to a stationary working electrode (WE) while the response, a change in current (i) caused by the potential change, is measured. Over the course of a cycle the potential at the WE is taken from a starting potential up to a stop potential, this is called the forward scan, the potential is then scan back to the initial potential, called the reverse scan. The change in current throughout this cycle is displayed a voltammogram (Figure 2-4).

CV can be used to study any redox active compound, and the voltammogram that is produced will be unique to that compounds redox behaviour. A common probe used during electrochemical studies is the ferri/ferro cyanide redox couple $[Fe(CN)_6]^{3-/4-}$, an example of the voltammogram produced by this couple is presented in Figure 2-4 along with the concentration profiles of each couple. During a cycle the potential of the WE electrode is scanned from a

starting potential (point 1), where initial concentrations of each component are consistent. As the potential becomes increasingly positive oxidation of $[Fe(CN)_6]^{3-}$ begins to occur, producing an increase in the measured current as electrons move from the analyte to the electrode surface (point 2). Eventually the current at the electrode is limited by the delivery of additional reactant to the electrode surface, producing a peak current (point 3). At this point the product, in this case $[Fe(CN)_6]^{4-}$, increases in local concentration while reactant decreases at the electrode surface, while bulk concentration remains consistent. As the potential continues in the positive direction the rate of diffusion of reactant to the electrode surface begins to slow, causing a decrease in current (from point 3 - 4). This causes an increase in the size of the diffusion layer, further changing the concentration of reactant and analyte. When the switching potential is reached (point 4) the reverse scan is initiated. At the electrode surface, the $[Fe(CN)_6]^{4-}$ generated during the forward scan is now reduced back to $[Fe(CN)_6]^{3-}$ (points 5 - 6).

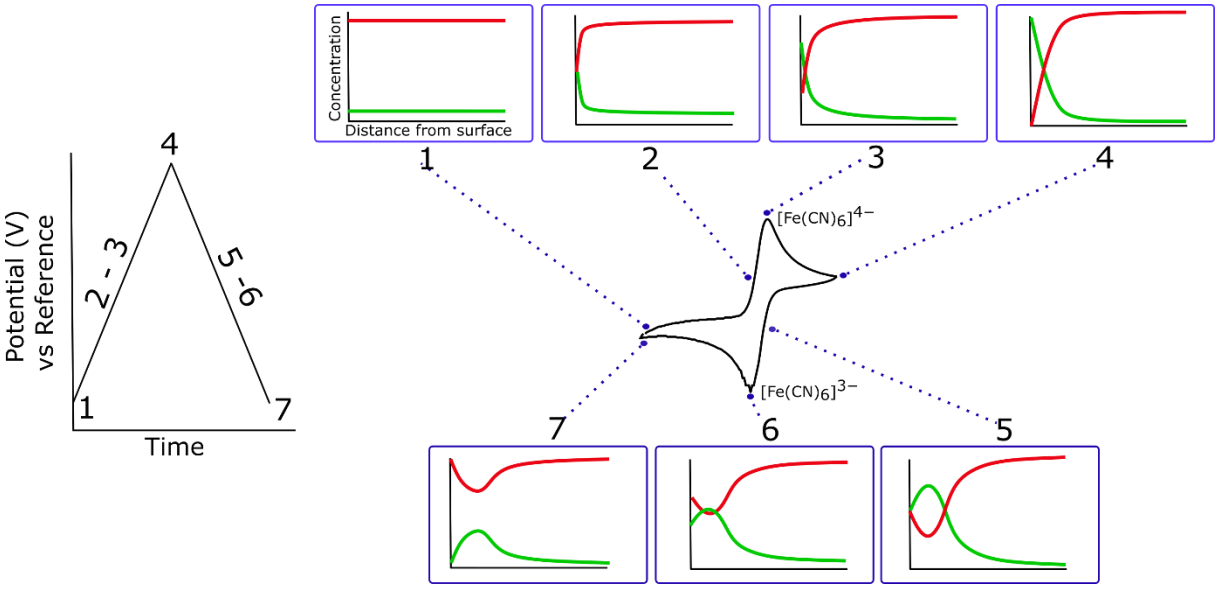

Figure 2-4 Schematic of the potential profile of cyclic voltammetry and the resulting change in current. Voltammogram is an example of the oxidation/reduction of $[Fe(CN)_6]^{3-/4-}$ alongside the change in concentration over the course of the cycle. Adapted from Elgrishi *et al*[201]

Voltammograms produced using CV technique can be used to generate diagnostic data for studying redox reaction mechanisms. In the case of a chemically and electrochemically

reversible reaction, an example of which was shown above, certain criteria have been established. An electrochemical reaction can be considered reversible if the heterogeneous rate constant (k_s), which takes into account the forward and reverse rate constants for the reaction, is > 0.020 cm/s[203]. For an electrochemically reversible reaction the difference between the oxidative and reductive peaks (peak separation) will be 57 mV. If the reaction is fully reversible and diffusion limited the ratio of the peak currents will also be equal to one and the peak current function, which is calculated by dividing the peak current by the square root of scan rate (v), will be independent of the rate at which the potential is scanned. These criteria, however, represent the ideal situation and not every reaction will be fully reversible and will not always adhered perfectly to these specifications.

It is also possible to study more complex reactions using a similar approach[204]. When discussing these types of reaction mechanisms, and the steps which are involved, the nomenclature E and C are used to describe either a redox or chemical step, respectively. Examples of more complex reactions include EC reactions; whereby once an electrochemical step has taken place a subsequent chemical reaction can occur:

$$O + n^{e-} \rightleftharpoons R$$

$$R \leftrightarrow X$$

Where X represents the product of a chemical step. Likewise, the reverse process can occur during which a chemical reaction must occur prior to an electrochemical step:

$$X \leftrightarrow O$$

$$O + n^{e-} \rightleftharpoons R$$

Furthermore, multi-step processes are common, such as the ECE mechanism, which involves multiple electron transfer events with a chemical reaction in-between:

$$O + n_1^{e-} \rightleftharpoons R$$

$$R \rightleftharpoons X$$

$$X + n_2^{e^-} \rightleftharpoons Y$$

The exact mechanism which occurs will depend on the analyte in question; the redox behaviour will be determined by that compounds unique chemical structure. Likewise, the kinetics of the reaction will be determined by the speed at which these steps can occur. All of these factors will have an impact on the shape and data produced by the voltammogram.

2.2.2 Square wave voltammetry

An additional voltammetric technique commonly used when carrying out electroanalytical studies is square wave voltammetry (SWV). During this technique rather than a potential cycle, as with CV, a square wave form is superimposed onto the potential (Figure 2-5)[205,206]. Furthermore, the resulting current is not just a raw value; the current is sampled at two times - once during the forward potential pulse and once on the reverse potential pulse. The net current is obtained by taking the difference between the forward and reverse currents generated during the pulse (Figure 2-5, inset). The potential pulse continues to increase linearly from a baseline to a final potential, sampling the current at specified intervals - determined by the forward and reverse pulses.

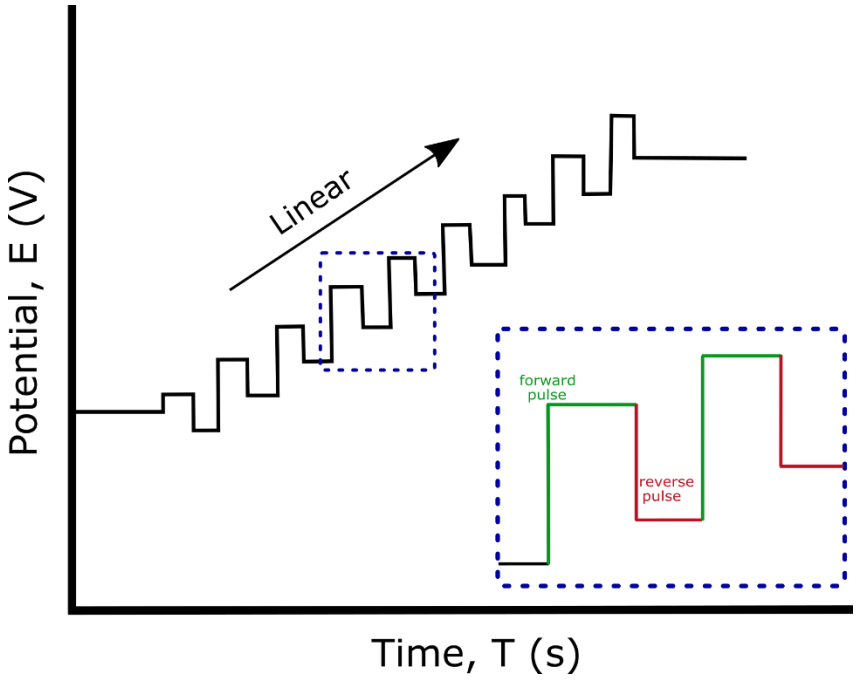

Figure 2-5 – Schematic outlining the wave form used during SWV sampling

SWV offers one significant advantage when compared to CV, the current sampling approach minimises the background signal which arises due to capacitive current, also known as non-faradaic current, at the electrode surface. While SWV can be an effective method to study reaction mechanisms the ability to limit the effects of non-faradaic current provides the increased sensitivity which is often needed when designing an electrochemical sensor. Based on this it has become a popular method when lower currents are being generated or when background signal is expected to be high.

2.3 Surface and materials analysis

2.3.1 Atomic Force and Scanning Microscopy

Scanning probe microscopy (SPM) is a group of techniques which generate high resolution surface imagery by scanning a probe over a surface and measuring the interaction between the probe and the surface. The types of data which can be produced vary depending on the specific type of method used. Of the different SPM techniques atomic force microscopy (AFM) receives

significant attention, especially given recent technical developments which have opened up new avenues of research.

During AFM a probe is scanned across the surface of interest. The probe consists of a sharp tip made from silicon or silicon nitride attached to a semi-flexible cantilever. The force sensitive cantilever is used to measure the interaction between the probe and the sample; as the tip is scanned the overlapping electron clouds of the tip and surface produce repulsive forces which fluctuate in accordance with the topography of the surface[207]. The movements of the tip across the surface are translated using a laser which is reflected onto the reverse side of the cantilever. The laser signal is then captured by a four diode photodecetor which converts the signal produced by the laser into a digital map of the topography of the sample.

AFM has become a popular technique for surface analysis due to the flexibility it offers. It can be operated in a range of modes, including contact and non-contact modes, as well as using either constant force or height, depending on both the type of sample and the type information that needs to be generated. Likewise, as the tip-surface interaction is dependent on force, rather than electrical interaction, it can be used to study both conductive and non-conductive samples. However, AFM is limited with regard to analysing the chemical makeup of a sample; force is independent of the chemical structure of the sample.

Different AFM modes are available; each offering advantages and disadvantages depending on both the type of surface and properties which are being investigated. Contact Mode relies on continuous contact between the probe and the surface as the probe raster scans the sample. In contrast, Dynamic Mode involves the oscillation of the cantilever at a high frequency. The probe tip is then held at a fixed distance from the surface; where attractive forces between the surface and tip can occur. Additional modes, subsets of both Contact and Dynamic, exist for studying specific properties of surfaces, this includes; conductive AFM, (C-AFM), piezoresponse Force Microscopy (PFM), Magnetic Force Microscopy (MFM).

Recent advances in AFM technology have led to new modes and improved capabilities. For instance, Peak Force Tapping mode, a relatively recent development by Bruker Ltd, can perform high resolution, non-destructive imaging of surfaces while simultaneously generating nano mechanical data[208,209]. In this mode, the probe and sample are brought together and pulled apart rapidly (tapped) so that the tip makes intermittent contact with the surface for a short period; this reduces the lateral forces exerted on both the tip and sample.

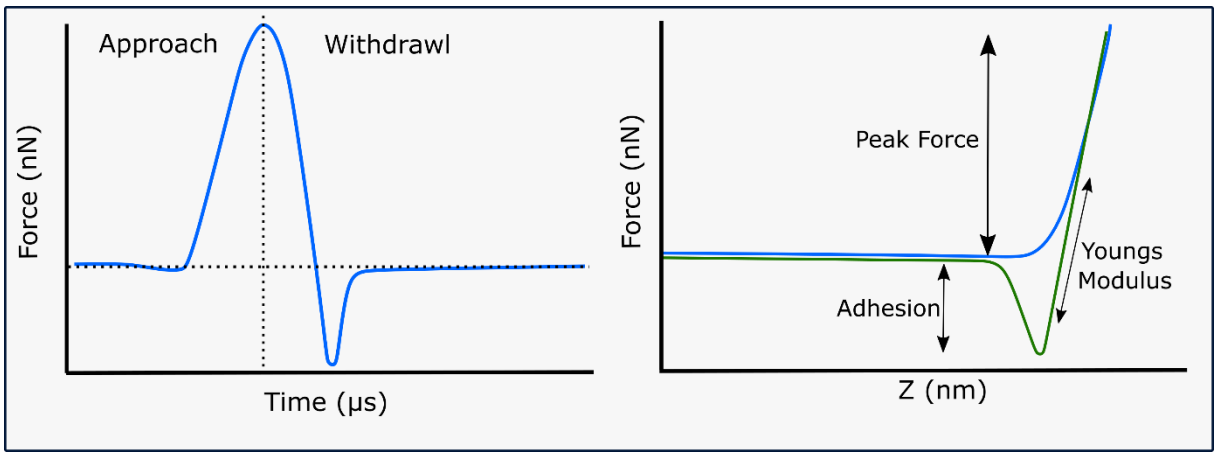

Figure 2-6 Schematic showing the curved produced as an AFM tip approaches a surface and the data which can be generated using Peak Force tapping mode.

During a tip cycle the maximum force (peak force) which is applied to the tip is measured and a force curve is generated every time the tip contacts the sample (**Error! Reference source not found.**). This force curve is then extracted and used to generate both peak force data alongside mechanical data, such as adhesion and Youngs Modulus. During Peak Force AFM as the tip approaches the surface attractive forces, such as van der Waals, pull the cantilever toward the surface, creating a slight dip in the force curve. Following this the attractive forces of the tip-surface interaction overcome the stiffness of the cantilever drawing the tip towards the surface. The tip then remains in contact/near-contact with the surface until a peak is reached. Then the probe begins to withdraw until the tip eventually detaches from the surface, known as the pull-off point.

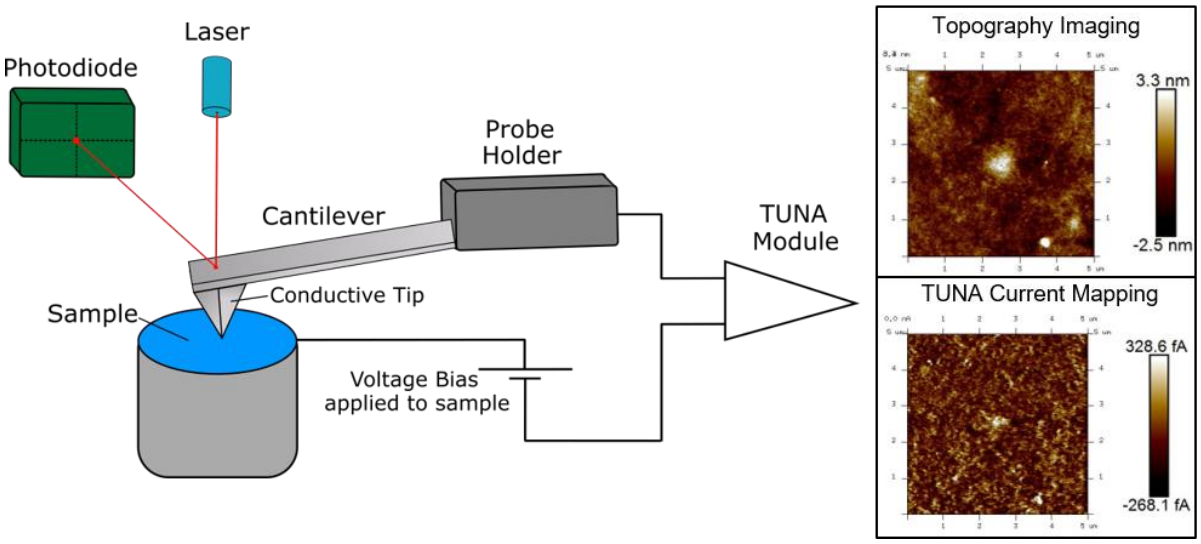

Figure 2-7 – A schematic outlining the key components involved in PF-TUNA AFM

Additional properties, alongside topographical and mechanical data, can be investigated using advanced AFM techniques. Of particular interest is electrical characterisation at both the micro and nano scale, which can be carried out using tunnelling AFM (TUNA AFM)[210]. During (Figure 2-7) TUNA AFM a conductive tip, such as platinum, is scanned across the surface

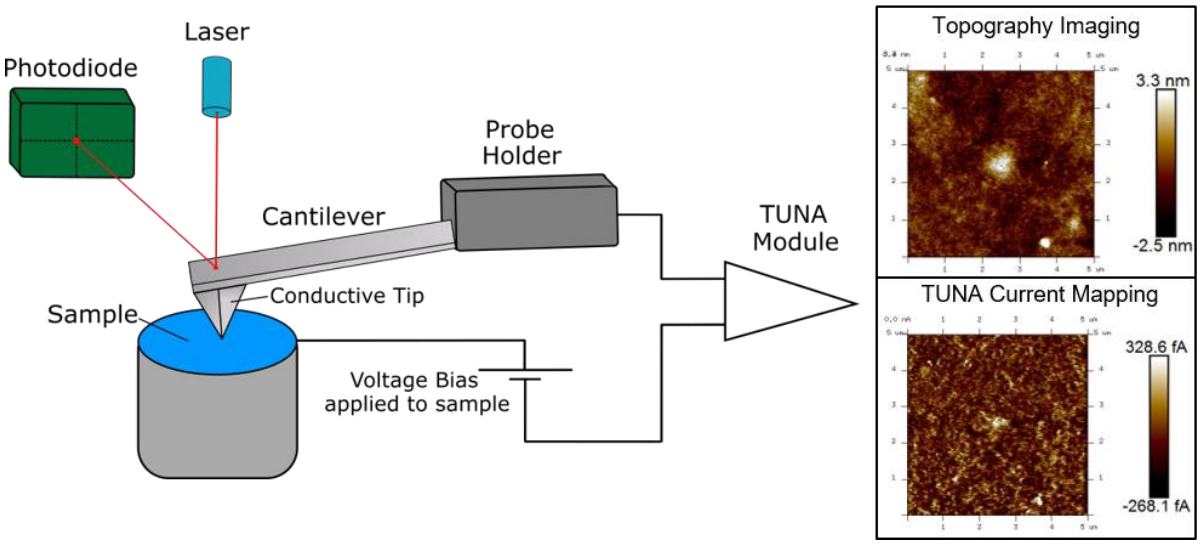

. The surface is connected to an external circuit, allowing a voltage bias to be applied. As the tip moves, and the circuit is complete through contact with the sample, a current map is produced alongside the topographic measurements. When combined with Peak Force Tapping

mode this method provides lower force control than previous methods, allowing it to maintain tip shape and sample integrity which leads to improved spatial resolution alongside the ability to characterise nano mechanical and nano electrical properties.

Despite the advantages Peak Force and TUNA AFM offer there has been limited literature which has applied this method to studying electroactive surfaces. Thus far work has focused on characterising electronic materials for engineering applications, providing high resolution studies of a variety of surfaces including vapour deposited diamond films and solar cells[211,212].

3 Electroanalytical Comparison of Tricyclic redox behaviour at an unmodified glassy carbon electrode

3.1 Introduction

Tricyclic compounds (Figure 3-1) have previously been used to treat clinical depression, earning them the name Tricyclic Antidepressants (TCA). More recently, members of the TCA family have been used as pain management therapeutics, in particular amitriptyline[213,214]. Now, due to their narrow therapeutic window and risk of cardiovascular side effects, TCA compounds are rarely considered a viable treatment for depressive illness; they have been supplanted by safer alternatives such as selective serotonin reuptake inhibitors (SSRIs)[215,216].

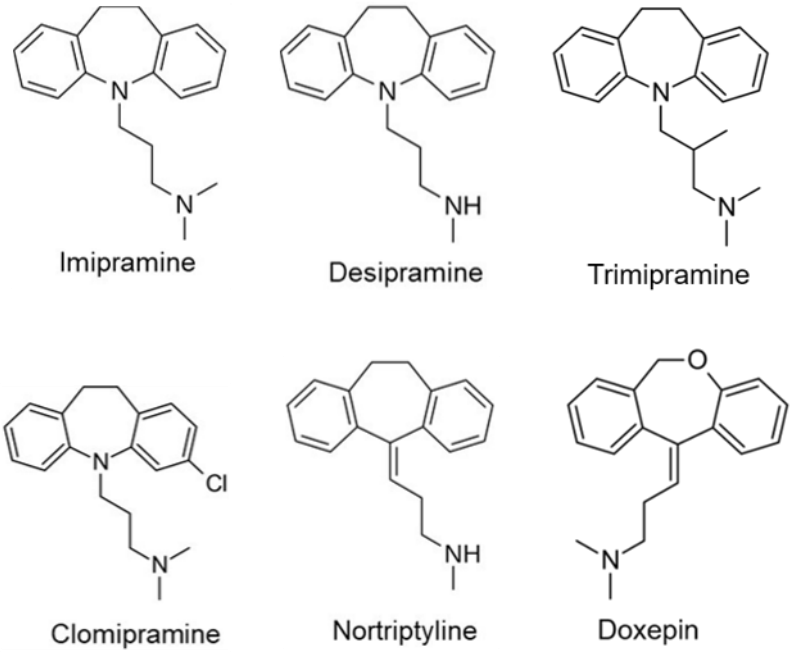

Figure 3-1 - Chemical structure of six tricyclic antidepressant compounds

To overcome the limitations associated with TCA usage attempts have been made to develop analytical techniques to detect the presence of TCA compounds in serum; therapeutic drug

monitoring would allow treatment to be tailored to an individual patient's pharmacokinetic profile, minimising the risk of overdose or adverse cardiovascular effects. This could re-establish TCA compounds as a potential treatment option[46,118]. Monitoring the active concentration of TCA in a patient's system would also provide pharmacokinetic data and physiological insight into how the body processes TCA, information which is currently limited[116].

Electroanalytical methods are popular in the design of therapeutic monitoring system since they can be performed rapidly, function in complex environments and are already used in commercial point of care sensors, such as glucose sensors. However, before an electroanalytical sensor can be developed it is necessary to have an in-depth understanding of the electrochemical behaviour of the target compound's redox behaviour.

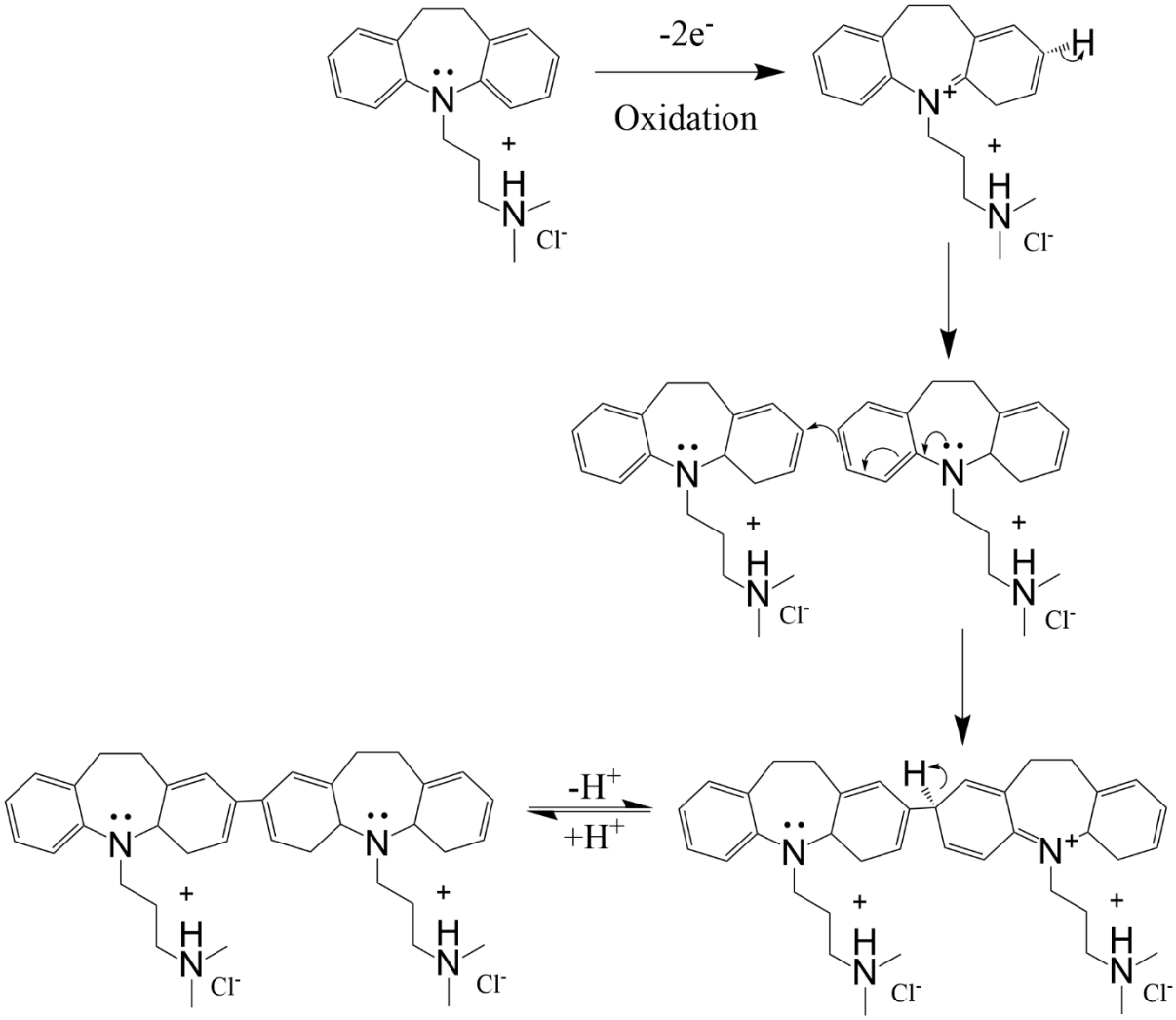

Figure 3-2 - Redox mechanism showing the oxidation of IMI, leading to formation of IMI dimer.

Previous work into the electrochemical behaviour of tricyclic compounds has focused on IMI as a model compounds, it is currently thought that the redox and transport mechanisms are characterised by chemical irreversibility and observed currents, at +0.878 V, are diffusion-limited[217]. Electroanalytical work has focused on the ability of modified electrode surfaces to sense these compounds rather than to investigate their redox behaviour. It is assumed that the redox reaction for IMI (

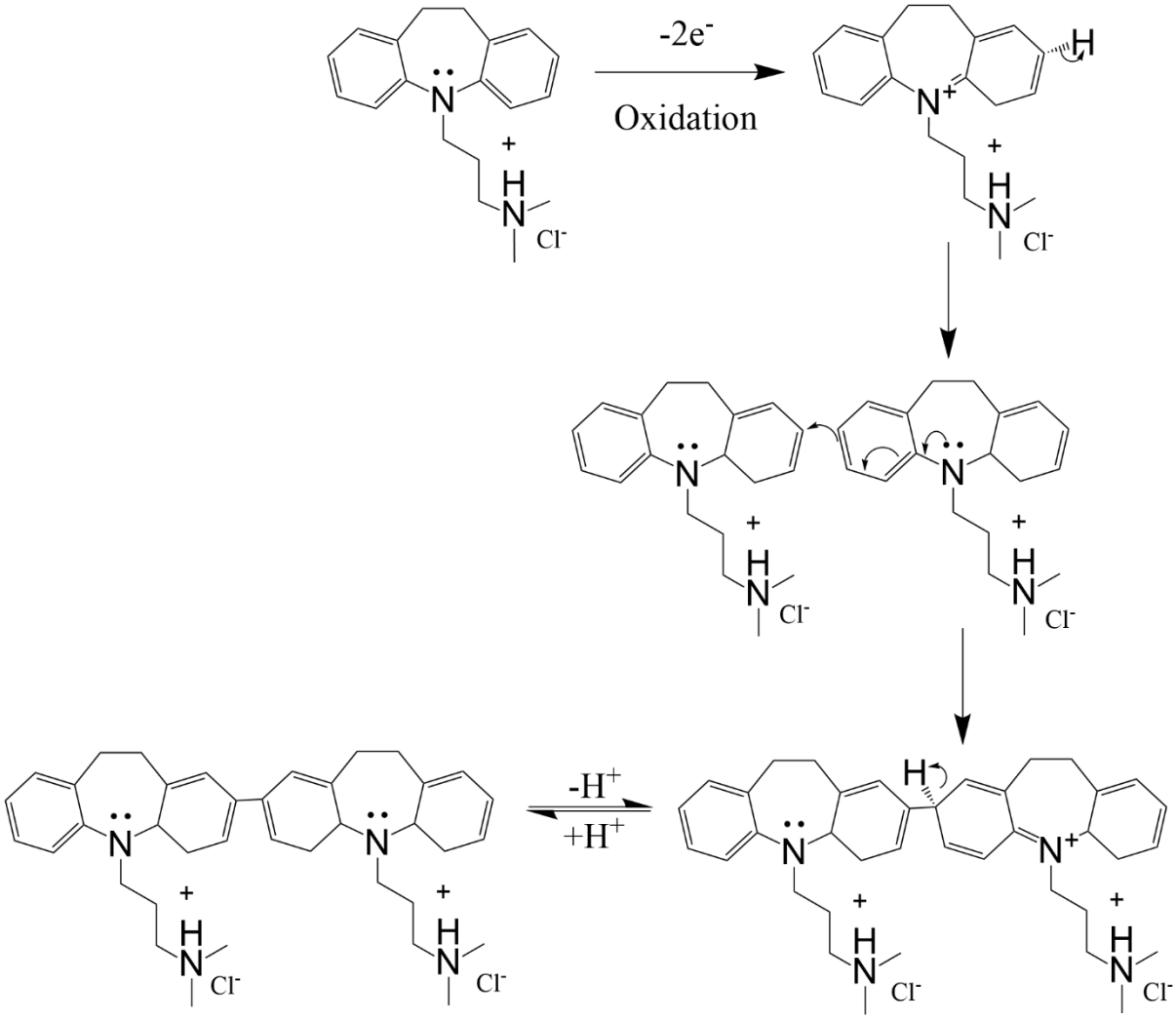

Figure 3-2) occurs in all tricyclic compounds, however limited work exists that directly compare a range of tricyclic redox behaviour[218]. However, given the structural differences between TCA compounds this count be an incorrect assumption. As shown in Figure 3-1 IMI consists of the core three rings with a central nitrogen, typical of TCAs, with a three carbon tail which possess a second nitrogen. DES and TRI are similar to IMI, however the second nitrogen of DES is joined to only one additional carbon, compared to IMIs two while TRI contains an additional carbon group part way down the three carbon tail. CLO consists of a similar structure to IMI, with the exception an additional Cl attached to the third tricyclic ring. Finally, NOR and DOX are similar in that the central rings of these structures do not contain nitrogen, instead DOX contains an additional oxygen atom.

The following work investigates the electrochemical behaviour of multiple TCAs at a simple unmodified electrode. In particular, we have performed an electroanalytical study and relied on the Nicholson-Shane diagnostic plots, which are commonly used for studying both electrode surfaces and chemical and biological analytes, to characterise and compare TCA redox mechanisms[202,219–221]. This work by *Nicholson and Shane* highlights the key types of reaction mechanisms that can be observed using cyclic voltammetry by measuring a combination of peak current, peak potential, scan rate and ratio of anodic and cathodic current.

This insight will provide further understanding of the electrochemical mechanisms involved in TCA redox behaviour, which may be useful in selecting suitable compounds to monitor when developing sensors.

3.2 Experimental

3.2.1 Materials and Equipment

Imipramine hydrochloride (IMI), clomipramine hydrochloride (CLO), desipramine hydrochloride (DES), nortriptyline (NOR), and doxepin (DOX) were all purchased from Sigma-Aldrich. Trimipramine maleate (TRI) was purchased from ApexBio. PBS tablets supplied by Sigma-Aldrich were used to obtain a 137 mM NaCl, 2.7 mM KCl and 10 mM phosphate buffer solution (PBS) (pH 7.4 at 25 °C). The glassy carbon electrode (1 mm diameter), Ag/AgCl reference electrodeand Pt wire electrode, were supplied by Biologic.

Voltammetric results were acquired using a Metrohm Autolab M204 potentiostat running Nova 2.1 software.

3.2.2 Cyclic Voltammetric analysis of tricyclic compounds

To perform cyclic voltammetry we used a three electrode system. This comprised of an unmodified glassy carbon working electrode (GCE), an Ag/AgCl reference electrode, and a Pt Wire counter electrode. 10 mL of PBS were placed in the electrochemical cell and cyclic

voltammetry was performed in the presence of the following tricyclic antidepressants (each of which had been dissolved in PBS); Imipramine hydrochloride, clomipramine hydrochloride, desipramine hydrochloride, nortriptyline, doxepin and trimipramine maleate. Prior to use, the GCE was polished with 0.05 µm polishing alumina on an alumina polishing pad. Samples were purged of oxygen prior to, and during, experimentation by gassing with nitrogen.

Cyclic voltammetry was performed on 10 mM solutions of either IMI, CLO, DES, NOR or DOX. Scans were performed at 100 mV/s with a starting potential of 0.5 V and a switching potential of 1.2 V, and an end potential of 0.5 V. Following this a scan rate study was performed with the scan rate being varied from 5 – 1000 mV/S (for a full list of scan rates see figure legend of Figure 3-4). This data was then used to generate Nicholson-Shane diagnostic plots, by plotting the values according to the literature[219].

Statistics

Numerical data are given as mean ± standard deviation (S.D) for all samples, where S.D is provided n = 3. Statistical analyses were performed using Graphpad PRISM Ver. 9.0. Statistical significance was assigned when $p < 0.05$.

3.3 Results and Discussion

3.3.1 Comparison of oxidative peaks across TCA compounds

Cyclic voltammetry was performed with solutions containing each individual TCA compound to determine the presence, or absence, of redox behaviour at a standard glassy carbon electrode (GCE)**Error! Reference source not found.**. Of the six TCA compounds tested, four showed an oxidative peak (O1) between +0.87 and +0.92 V (Figure 3-3), specific peak potential and peak current for each compound are listed in Table 3-1. The current generated during O1 is thought to correspond with the loss of electrons on the central nitrogen[217,222]. Our data suggests that the number of electrons involved, in this case, the lone pair of electrons on the central ring

nitrogen which is readily oxidised, was the same for all four compounds. This is in line with early work which studied TCA redox behaviour and found that for TCAs with similar structure the central nitrogen produces a single oxidation peak between +0.8 and +0.9V[218,223]. In contrast, the two compounds without central nitrogen in their structure, NOR and DOX, showed no discernible redox peak at similar potential.

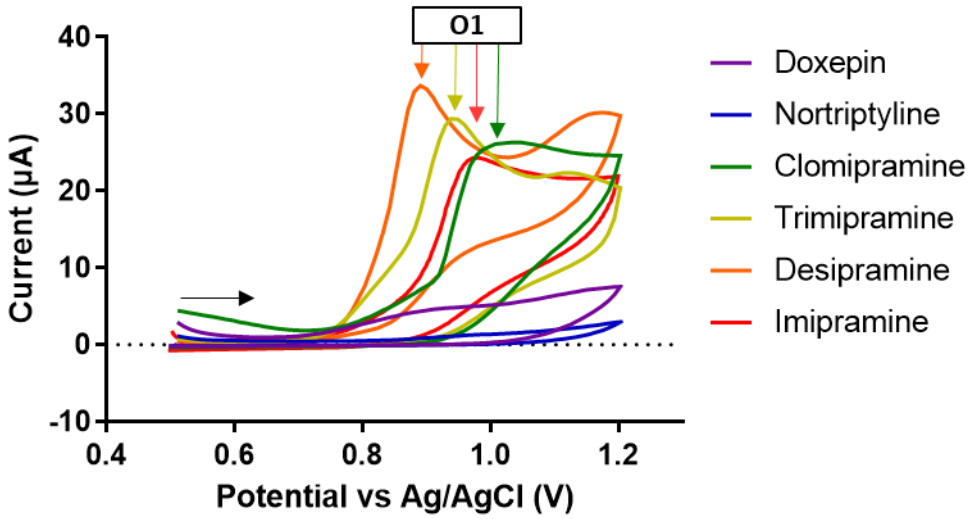

Figure 3-3- Typical CVs obtained from solutions containing one of the six different TCA compounds, each at 10 mM, carried out in 0.01 M PBS at 100 mV/s (Inset: 0.01 M PBS control, 100 mV/s).

Of the four compounds which showed similar oxidation current, DES and TRI displayed a less well-defined peak at approximately +1.1 V. We tentatively suggest this is due to the adsorption of the compound on the electrode surface, a hypothesis previously suggested by Oliveira et al when studying IMI at a boron-doped diamond electrode[224]. Interestingly, DOX, which showed no O1 peak, displayed two broad peaks, one in the region of O1 and another in the region of the adsorption peak. Little investigation has been carried out in TCA compounds that lack central nitrogen. Furthermore, pre-wave adsorption peaks can also be observed, in particular with TRI and CLO, indicating analyte adsorption at the electrode surfaces. This is the first report of this phenomenon (Figure 3-3).

Using a rearrange form of the Randles–Sevcik equation (Equation 5) it is possible to calculate diffusion coefficients, and compare them across the different members of the TCA family (Table 3-1). Previously, diffusion coefficients for members of the TCA family have not been calculated using this approach, as such there is no comparable data in the literature.

Analyte	O1 Peak Current (μA)	SD	O1 Peak Potential (E_{pa})(V)	SD	O1 Half-peak Potential ($E^{p/2}$)(V)	SD	Diffusion coefficient (D)
Imipramine	19.02	1.17	0.92	0.005	0.04	0.003	6.845×10^{-8}
Desipramine	26.3	0.55	0.89	0.011	0.04	0.005	1.3088×10^{-7}
Trimipramine	17.67	3.44	0.95	0.023	0.08	0.004	5.908×10^{-8}
Clomipramine	12.8	1.73	0.99	0.011	0.08	0.006	3.1×10^{-8}

Table 3-1- list of peak current, peak potential and half-peak potential for each TCA compound, measured directly from voltammograms and diffusion coefficients and number of electrons.

When comparing the O1 peak CLO appears to produce significantly broader peak than its TCA counterparts; indicating a slower electron transfer. Similarly, the peak potential for CLO is higher than that of the other compounds (Table 3-1) which suggests the Cl- has an electron withdrawing effect, increasing the energy needed to produce the TCA radical during oxidation. Thus far no literature has observed a difference between CLO and other members of the TCA family. These results suggest that there is a minor difference. As a means to compare redox potentials in irreversible systems the half-peak potential ($E_{p/2}$), of both CLO and TRI showed no difference (0.08 V SD+/- 0.006; P = 0.7), this highlights possible similarity between the redox behaviour of these TCA members. Specifically, we hypothesise that the electronegative effect of the Cl- ion, bonded to the third tricyclic ring, results in slower electron transfer kinetics. As chlorine is an electron withdrawing group it likely withdraws electrons from the tricyclic ring, decreasing the electron density and stabilising the tricyclic ring structure; making it harder to undergo the initial oxidation of the central nitrogen observed in other TCA. While this has yet to be observed in TCA, similar effects have been documented on any ring structure with Cl- ion present, including porphyrins and chlorinated benzene[225,226].

Overall, a comparison of the voltammograms of TCA compounds at a simple unmodified electrode provides an understanding of reaction mechanisms. These observations and understanding are essential for sensing.

3.3.2 Scan rate studies and mechanistic comparison

To investigate and compare the redox mechanism of TCA compounds a scan rate study was performed (Figure 3-4). Of the four compounds which generated O1 an increase in peak current with the square root of scan rate is observed in all cases (Figure 3-4 a – d), indicating the current associated with O1 is diffusion limited. In contrast, only imipramine produce a peak potential in the reverse (reductive) scan direction. However, this reductive peak was not observed in

between 5 mV/s to 100 mV/s, this is likely due to slow electron transfer at slower scan rates, supported by the fact that as scan rate increases the reductive peak increases with scan rate. This finding suggests that the rate of reduction is much slower than the rate of oxidation. The reduction of the analyte is so slow that this reaction can be considered an irreversible reaction.

Plots of the O1 peak current versus square root of scan rate are commonly used to determine the mechanisms involved in a redox reaction. A diffusion-limited system will display a peak current that is proportional to the square root of scan rate; this is described by the Randles-Sevcik equation (Equation 5). In comparison, when a linear trend is not observed the limiting factor is instead adsorption of the analyte to the electrode surface. In the case of IMI, DES, CLO and TRI, all display a linear trend as the scan rate increases; indicating a diffusion-limited reaction.

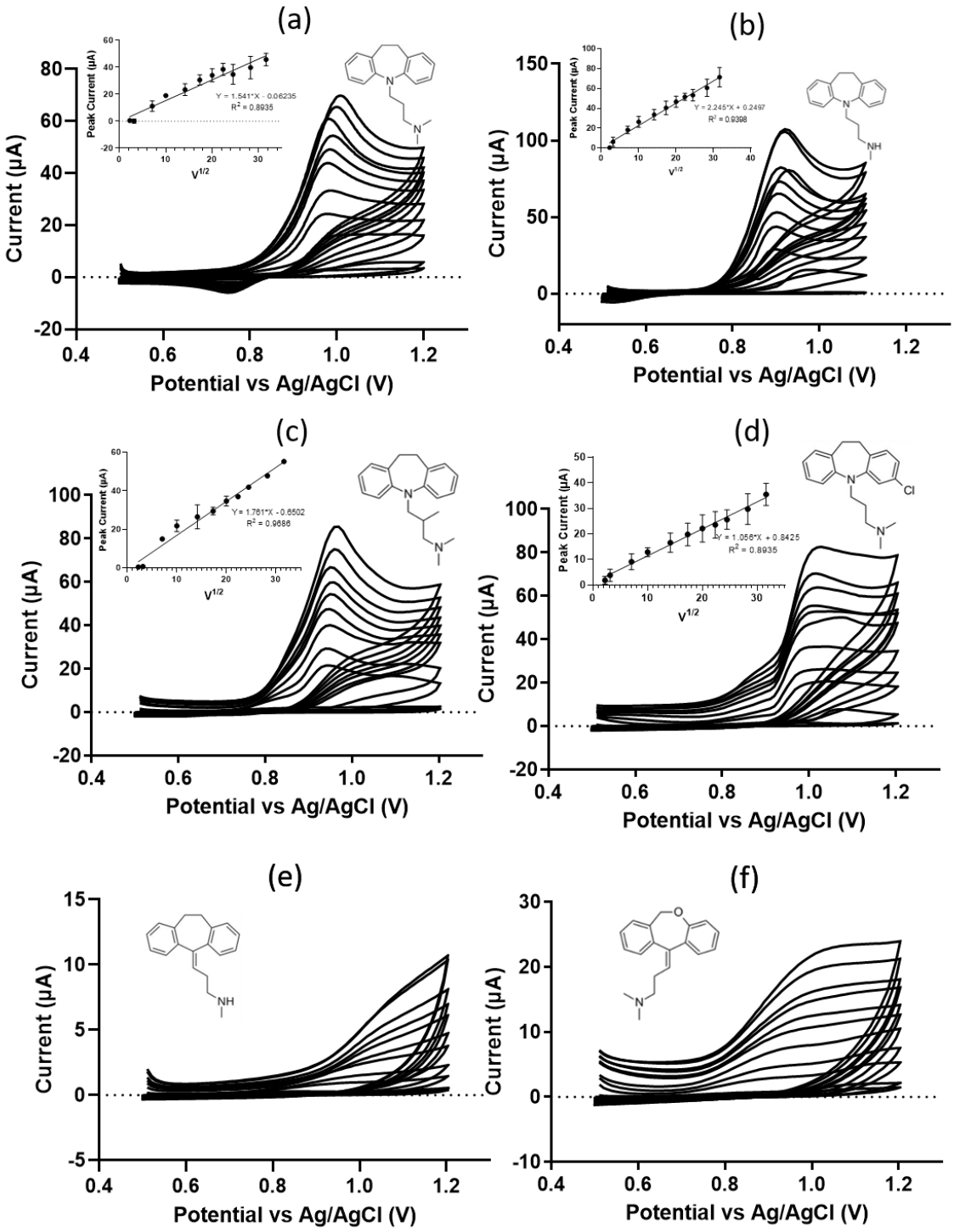

Figure 3-4 - CVs of 10 mM TCA compounds carried out at a range of scan rates (5, 50, 100, 200, 300, 400, 500, 800 and 1000 mV/s). (a) IMI (b) DES (c) TRI (d) CLO (e) NOR (f) DOX. Insets: (a – d) plot of peak oxidative current versus square root of scan rate ($V_{1/2}$)

As mentioned only IMI displayed a reductive current therefore a diagnostic plot of the peak anodic and cathodic peak ratio could only be plotted for this compound (Figure 3-5). The reductive peak has previously been attributed to the reduction of a dimer, which is formed when the radical produced during O1 reacts with additional IMI molecules. Given that the other TCA compounds display an O1 peak it would be expected that they would also form a dimer; the loss of electrons from the central nitrogen should trigger the formation of a radical in all four compounds. There are two possible explanations for this observation. Firstly, the other TCA compounds could not form a dimer following their oxidation. However, given the similarity in structure, this is unlikely. Therefore, it is more likely that as we used a plain unmodified GCE we were just not observing the reduction of the dimer. This indicates that the kinetics of this reaction is slower than IMI; slow electron transfer kinetics are favoured at fast potential scan rates[227]. This explains why the majority of the literature has focused on IMI as an ideal analyte. This difference in the rate of dimer formation has not been observed elsewhere; it has been assumed that the resulting radical reacted similarly across all TCA compounds with central nitrogen. The results presented here suggest that there is in fact variation between TCA compound dimer formation.

As IMI was the only compound that displayed oxidative and reductive peaks the ratio of anodic to cathodic peak current could only be plotted for this compound. As such this is the only compound for which this diagnostic plot can be used to determine the redox kinetics. Based on the Nicholson-Shane criteria as IMI displays linearity between both oxidation and reduction (both with R^2 >0.9) this suggests that the mechanism involved is either a chemical reaction preceding a reversible charge transfer or a charge transfer followed by an irreversible chemical reaction. Given that previous work has confirmed that dimer formation is irreversible these results confirm that the reaction mechanism entails a charge transfer followed by an irreversible chemical reaction.

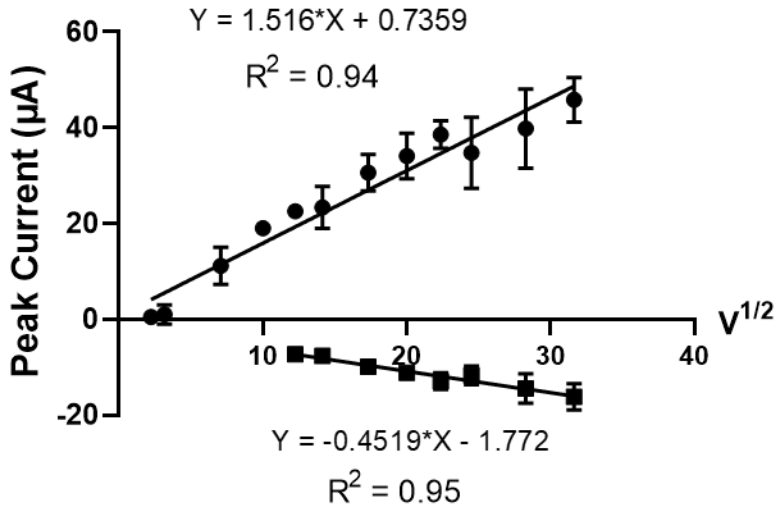

Figure 3-5 - Plot of peak anodic and cathodic current versus V1/2 for IMI.

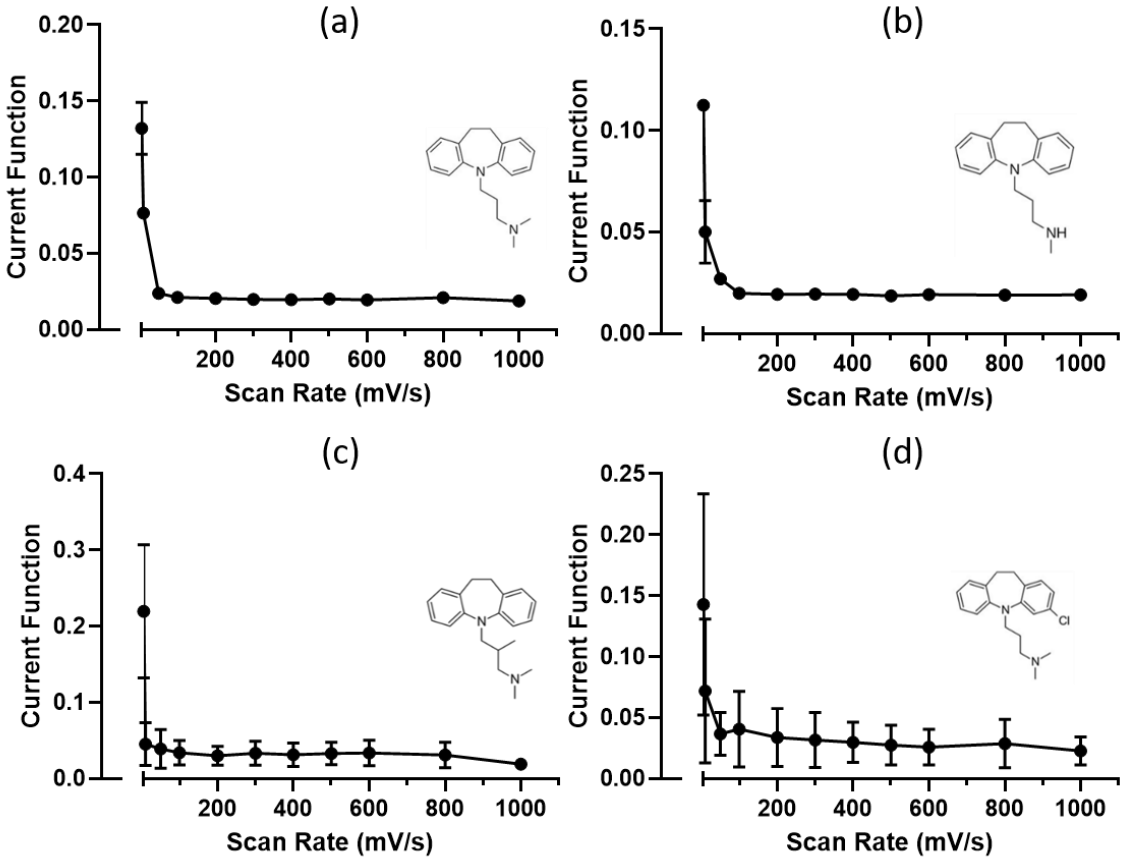

Figure 3-6-Plot of current function versus scan rate for (a) IMI (b) DES (c) TRI and (d) CLO.

To confirm the type of reaction mechanism involved in TCA redox current function plots were plotted (Figure 3-6). The current function is calculated from the Nicholson-Shain equation using values obtained from the CV scans and is a useful method to determine the electron transfer reactions involved in an unknown system.

For all TCA compounds which undergo oxidation, the current function plots display a general decrease in current function as scan rate increases. This indicates that the mechanism is one of the following: a charge transfer followed by an irreversible chemical reaction; a catalytic reaction with a reversible charge transfer or a catalytic reaction with an irreversible charge transfer[219]. It is possible to rule out both types of catalytic reactions; firstly earlier data indicates the reaction is irreversible. Likewise, any catalytic reaction would show a rapid, sharp increase in current in the voltammogram, as well as large differences in the magnitude of peak current between each scan rate as the concentration of the analyte, would increase throughout the reaction. Therefore, the current function plots confirm that all of the TCA compounds undergo an electron transfer followed by an irreversible chemical reaction. This supports our earlier hypothesis that due to structural similarity all of these compounds forms dimes; even if the dimer reduction cannot be detected at a simple electrode surface.

3.4 Conclusions

Electroanalytical studies are crucial for analytes of therapeutic interest; a detailed understanding of a target's redox behaviour is needed if a successful sensing platform is going to be designed. The TCA family of compounds has received interest previously, with a focus on the use of modified electrode surfaces. However, many of these studies have focused solely on sensing or have only compared two or three TCA compounds.

The work presented here focuses on comparing the redox behaviour of multiple TCA compounds at a simple unmodified electrode, to better understand the redox mechanisms

involved. Previous work has shown that redox of TCA involves the loss of 2 electrons at the central ring nitrogen in the formation of a radical and the loss of 2 protons during a dimerisation process. The work presented here confirms that this reaction was irreversible and diffusion-limited. However, we have also shown that within the TCA family of compounds there are variations that depend on TCA structure. Specifically, the most notable impact is the electron drawing effect of Cl- ion in CLO.

Understanding electrochemical behaviour in an ideal environment is useful; it provides insight that forms the foundation to develop new sensing platforms. This understanding will be important for future therapeutic sensing of TCA compounds.

4 Characterisation of PEDOT:PSS electrochemical surfaces using atomic force microscopy

4.1 Introduction

Progress in soft polymer electronics has opened up new avenues of research; from the development of low-cost solar cells, the functionalisation of nanomaterials for aerospace technology or the large scale production of consumer devices[228–234]. Conductive polymers (CPs) have laid the foundation for many of these developments, of particular interest has been those which can be used to design soft electronics; they are flexible, easy to manufacture and have a tuneable level of conductivity[232,235,236].

The ability to modify and tune CP properties, both physical and electronic, makes them an attractive material for novel engineering applications. CP properties can be altered according to the desired application; this can be done through the simple addition of compounds via direct blending or it can involve more complex procedures such as electrospinning or chemical conjugation[237–239]. For those interested in electronic engineering applications there is a focus on mechanical strength and recyclability, in contrast when developing a for biomedical application the focus can be biocompatibility and hydrophobicity[240,241].

One CP that has been of particular interest is the polymer mixture poly(3,4-ethylenedioxythiophene) polystyrene sulfonate (PEDOT:PSS)(Figure 4-1). PEDOT:PSS consists of PEDOT and PSS chains, with positive and negative charges, respectively. Due to the charges present the chains are loosely attached via columbic interaction. While PEDOT can be prepared by itself, using electrochemical or chemical oxidative polymerisation of the monomer ethylenedioxythiophene (EDOT), it is primarily used with the surfactant PSS. This

combination is used for two reasons, firstly PSS acts a counter for charge-balancing but it is also used to allow the dispersion of PEDOT in aqueous an aqueous environment, specifically PEDOT:PSS is only stable in water in the presence of excessive PSS.

Previous work has shown that PEDOT:PSS excels in both electronic engineering and biomedical applications; it has been used to produce high power thermoelectric films, flexible actuators, supercapacitors and power storage devices[242–244]. Likewise, PEDOT has been used to develop various wearable electronic devices, most recently this includes a supercapacitor for sweat based sensing, a 3D printed optical and electrical sensor, stretchable self-powered temperature sensors and a range of textile based sensing platforms[245–248]. For biological applications, PEDOT hydrogels have been developed for use in implantable bioelectronic devices, alongside other PEDOT based bio-scaffolds which can interact with and influence various tissue and cell types[249–252].

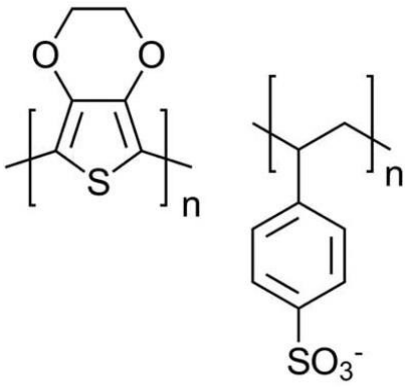

Figure 4-1- Chemical structure of PEDOT:PSS

When studying CP surfaces there are two main goals. Firstly, to better understand the fundamental processes that occur at CP surfaces and secondly to use this understanding to improve the design of novel electronic devices. Various surface analytical techniques can be used when investigating CP properties and attempting to achieve these goals. One technique is atomic force microscopy which uses the deflection of a probe scanned across a surface to generate topographic information about the sample[253,254]. For additional background on AFM I

refer the reader to section 2.3.1 which specifically discusses atomic force and scanning microscopy.

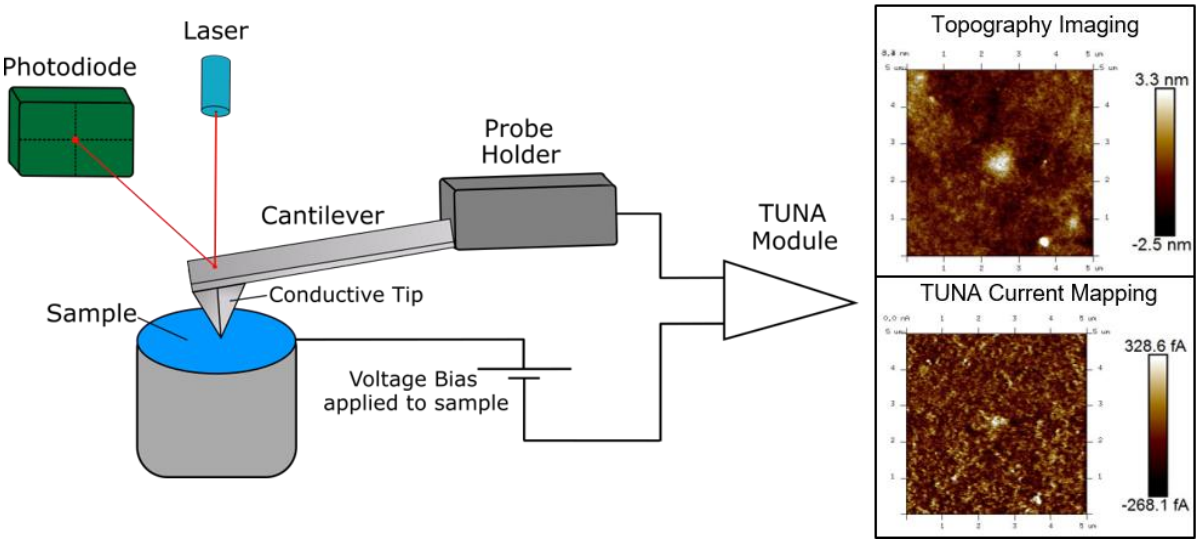

Figure 4-2- Schematic of Peak Force TUNA tip and probe and electrical circuit and examples of topographic and electrical data produced.

Developments in AFM technology have made it possible to gather information beyond topographical measurements; now a combination of electrical, nanomechanical and electrochemical data can be obtained. Recent advances which can collect this wealth of data include Peak force tapping (PF) mode and Tunnelling AFM (PF-TUNA AFM). Peak Force tapping relies on a probe that periodically taps a sample surface and measures atomic force interaction at a pN-level based on cantilever deflection; providing both mechanical and topographical measurements. In contrast, TUNA AFM provides high-resolution current mapping by measuring the current passing through regions of a sample when a current bias is applied to the sample (Figure 4-2). Together these methods allow unparalleled investigation into a materials electrical, mechanical and topographic properties, thus far however the use of PF-TUNA has been limited and it has yet to be widely applied to the study of conductive polymer films.

Previous force microscopy work has studied conductive polymer films and characterised their nanoscale topography and electrical properties, however this work has often been carried out

using conductive AFM (C-AFM) which can produce inaccurate current mapping due to tip degradation or a narrow current dynamic range; which limits the scope of the current map[255]. Likewise, C-AFM can suffer capacitive background current which will produce inaccuracy during current measurements[256]. PF-TUNA is able to overcome these limitations; tapping mode prevents tip damage and reduces build-up of capacitive current, while the wide current range used during TUNA, from -10 V to + 10 V, provides a wide dynamic range.

Understanding how topographical morphology influences the electrical behaviour of CPs can provide insight which can lead to the more effective design of CP based devices. For instance, it has been suggested that there is a close relationship between the morphology and electrical conductivity of PEDOT:PSS; due to the structural network responsible for the conductivity of PEDOT:PSS[257,258]. This has been supported by evidence which links the morphology of PEDOT to the resulting optical and electronic properties[259,260]. This evidence suggests that if a device is going to be designed using PEDOT:PSS understanding about film morphology and conductivity will be crucial; it will inform the design and optimisation of more effective devices.

In this work, we use PF-TUNA AFM to study a blend of PEDOT:PSS and PVA and investigate how changes in a PEDOT:PSS formulation impact the electrical behaviour of a polymer film. We provide evidence that PF-TUNA is an ideal method for simultaneously characterising multiple properties of CP films. We then use this method to investigate the impact electronic and cross-linking additives have on the properties of thick PEDOT:PSS films.

4.2 Experimental

4.2.1 Materials and equipment

Poly(3,4-ethylene dioxythiophene):polystyrene sulfonate (PEDOT:PSS) (1.3 % wt) dispersion, Dimethyl sulfoxide (DMSO) and (3-Glycidyloxypropyl)trimethoxysilane (GOPS) were

supplied by Sigma Aldrich. Ethylene glycol (EG) and Polyvinyl Alcohol (PVA), 88% hydrolysed with an average molecular weight of 88,000 – 120,000, were both supplied by Acros Organics. Divnyl Sulfone was provided by Merck. Glass slides for sample preparation were ground glass microscope slides (1.0 - 1.2 mm) supplied by Fisher Scientific. Silver conductive ink was obtained from Alfa Aesar.

Atomic Force Microscopy (AFM) was conducted using a Bruker Dimension Icon with a Peak Force TUNA application module attached. Spark 150 AFM platinum-coated probes (spring constant: 18 N/m, resonant frequency: 150 kHz) were supplied by NuNano (Bristol, UK).

4.2.2 Fabrication of PEDOT:PSS:PVA surfaces

To produce electroactive surfaces PEDOT:PSS dispersion was mixed directly with PVA stock solution. A 10% w/v solution of PVA stock was produced by dissolving PVA in milli-q water, then after stirring for 24 hours at room temperature the PVA stock solution was left to sit for a further 24 hours to remove any bubbles from the solution.

The PVA solution was then used to produce a range of PEDOT:PSS:PVA blends by mixing PEDOT:PSS dispersion with PVA at a range of concentrations, from 10 % PEDOT up to 90 %, increasing with 10 % intervals. The solution was left to mix for 60 minutes at room temperature, to ensure the PEDOT:PSS and PVA mixed.

Once thoroughly mixed 100 µL of the solution was pipetted onto microscope slides, which were then placed in a vacuum desiccator and dried for 24 hours under vacuum at room temperature. Samples were then visually inspected to determine macro imperfections (e.g. bubbles or cracking) which could interfere with AFM imaging. If no imperfections were present samples were then imaged.

To fabricate additive modified electroactive surfaces, PEDOT:PSS dispersion was mixed with components that are commonly used to alter either the electrical or physical properties of

PEDOT:PSS surfaces. The following additives were added at 2 %; DMSO, EG DVS and GOPS. As above, the additives were mixed for 60 minutes at room temperature, then pipetted onto slides and dried under vacuum desiccation for 24 hours.

4.2.3 Peak Force TUNA characterisation of PEDOT:PSS:PVA blends and additive-enhanced surfaces

To characterise the electrical behaviour of PEDOT:PSS films the samples must be connected to the AFM stage, this was achieved using conductive silver ink. A brush was to used apply silver ink to the edge of the dried PEDOT:PSS samples then dried for 20 minutes in an oven at 40ºC. This ink provide a connection between the sample and the underside of the microscope slide, which then provides electrical connection to the stage so that a bias can be applied during imaging.

To ensure that samples could be accurately compared all Peak Force TUNA measurements were acquired under the same conditions, using the following settings:

Scan size	5 µm
Scan rate	0.496 Hz
Peak Force Amplitude	220 nm
DC sample bias	10 V

Following image capture images were processed using Nanoscope software (V1.9). Images were flattened and plane fit. The same software was also used to acquire roughness (R_q), Peak force and TUNA current values. Graphpad was used to perform all data analysis, including one-way ANOVA to determine statistical significant, set at $P = 0.05$, and calculate standard error of the mean (SEM).

4.3 Results and discussion

4.3.1 Investigating the relationship between topography and electrical behaviour of blended PEDOT:PSS:PVA films

The topography, Peak Force and tunnelling current (TUNA) maps of pure PVA and PEDOT:PSS films are shown in . PVA films appear uniformly flat with few distinguishing features, and a mean R_q value of 0.87 nm. In contrast, PEDOT:PSS films are heterogeneous with a high number of aggregates causing a rough surface, with an R_q value of 14.93 nm – a value significantly different from PVA (P = 0.0135). There was no uniformity across PEDOT:PSS films and the aggregates appear to occur at random, this is likely responsible for the increased variability in the R_q value of PEDOT compared to PVA. This matches early results investigating PEDOT:PSS which show that PEDOT films consist of large grains dispersed throughout a semi-smooth matrix[261].

Previous force microscopy work studying PEDOT:PSS has found that pristine PEDOT films possess roughness values between 1 – 1.5 nm[259,260]. This value, lower than that presented here, could be due to two factors; firstly the area which was studied here was greater than previous measurements which makes it difficult to compare roughness values. Secondly, differences in production method of the PEDOT films could be contributing; previous evidence suggests that the method by which a polymer film is produced has a significant impact on the films mechanical and topographic properties[262]. Despite different methods of production the topographic structure of PEDOT:PSS appears, visually, to agree with the work mentioned above; suggesting that thin films of PEDOT:PSS consistently display granular aggregates.

Low levels of TUNA current were observed on the PVA samples, which was expected due to the absence of π electrons that are typically required for conductive polymers[263]. In comparison PEDOT:PSS films display a greater level of TUNA current compared to the PVA only; 6.02 pA versus 0.22 pA, respectively. Previous C-AFM results have shown that pure PEDOT films

display conductivity within the pico and nano amp range[259,264]. The average level of conductivity measured here is similar to previous work, however once again there are differences in the size of the area which has been studied; previous work has measured 1 μm^2 compared to the 5 μm^2 which was measured during this work[264]. This suggests that while the average current level of unmodified PEDOT films may vary, the films do display a high level of conductivity regardless of varying levels of aggregation.

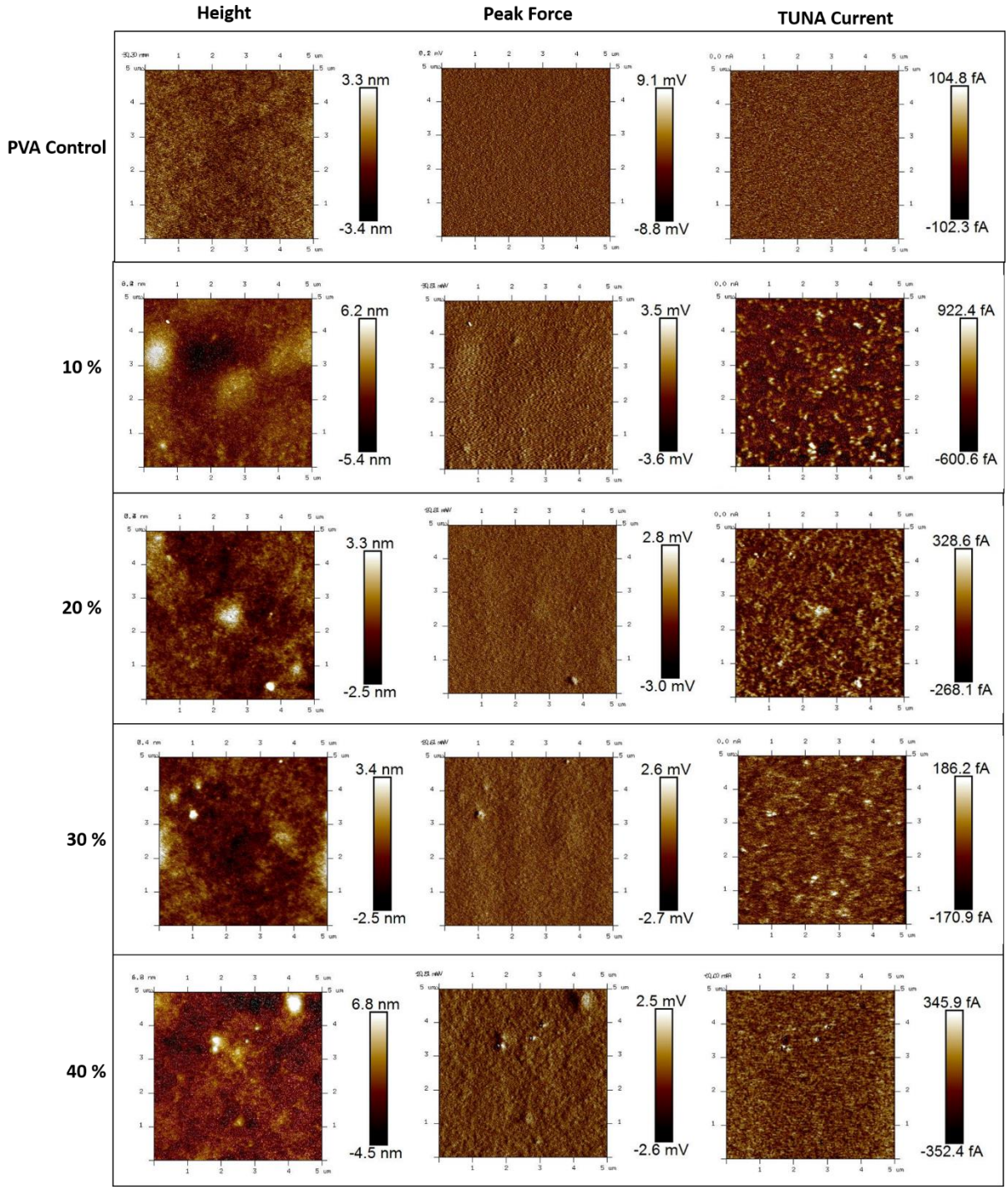

Figure 4-3- Representative images of PEDOT:PSS:PVA films, with increasing concentration of PEDOT from 10% - 90%, including pure PVA and PEDOT:PSS films. Images include height, peak force and TUNA current data.

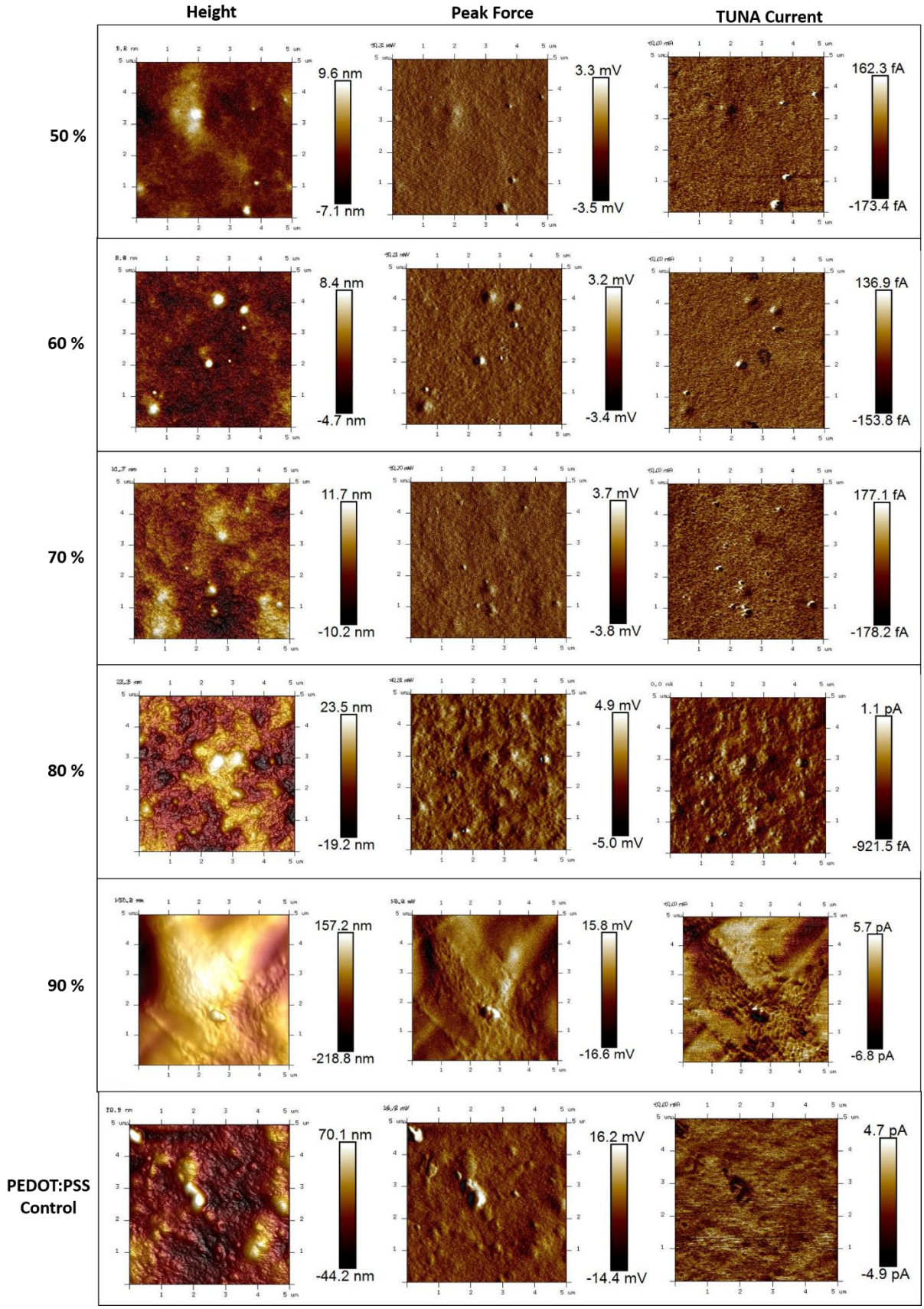

Figure 4-3 (Cont.)

Figure 4-3**Error! Reference source not found.** shows a representative image from each blend of PEDOT:PSS:PVA, from 10% up to 90%. As can be seen in both height and adhesion (Peak Force) images, increasing the concentration of PEDOT in the blend did not appear to cause an increase in the number of aggregates or alter the roughness of the sample until a concentration above 80% was reached. However, by counting the number of aggregates greater than 0.5 μm^2 it is possible to observe an increase in aggregate number from 60% PEDOT up to 80%; beyond that it is difficult to count the number of aggregates because the ability to resolve individual aggregates is lost in the overall morphology of the film (Figure 4-4).

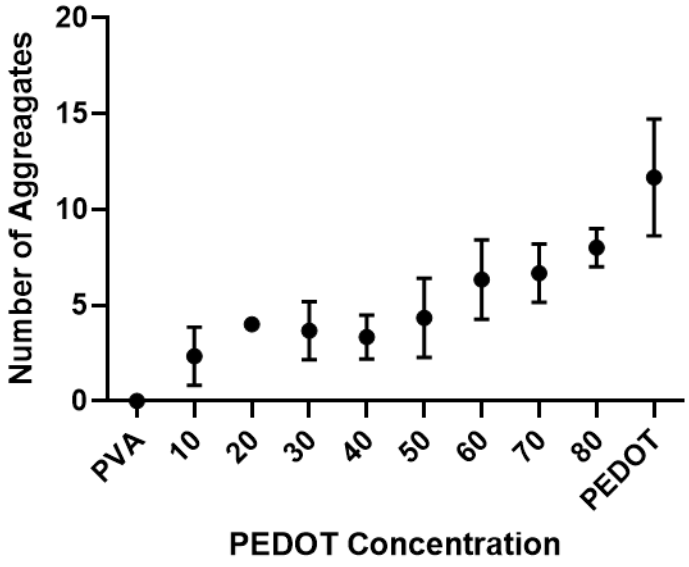

Figure 4-4 – A comparison of the number of aggregates above 0.5 μm^2 observed on PEDOT films with increasing concentration of PEDOT

As shown in Figure 4-5**Error! Reference source not found.** (a) the mean roughness (R_q) for PEDOT is statistically greater than all blends below 70% (P = 0.048), at which point the 80% blend was not significantly different (P = 0.074). However, at 90% PEDOT the roughness increased to a point that was significantly greater than all blends as well as PEDOT only (P = 0.0019). A similar trend can be seen in the topography and peak force images; the 90% blend

appears to have larger aggregates and a more rough appearance (Figure 4-3**Error! Reference source not found.**).

Extensive work has been carried out developing and characterising the electrical, mechanical and thermal properties of both pure and modified PEDOT films[265–267]. However, there has been few publications characterising blends of PEDOT:PSS with PVA, in particular none have carried out investigation of the nanoscale electrical properties of PEDOT:PSS:PVA films. Research has instead focused on studying the microscopic structure, tensile strength and chemical properties of PEDOT:PSS:PVA surfaces[261,262,268,269]. Previous evidence indicates that a range of factors can impact the electrical behaviour of the final film. For instance, it has been shown that the surface morphology of PEDOT has a significant impact on the subsequent electrical and optical properties[259,270]. Likewise, it has been observed that the method of production used to produce a PEDOT film can influence a combination of morphology and electrical behaviour[264,271,272]. Many of the production methods used to produce PEDOT films, in particular PEDOT:PSS:PVA blends, are more complex than those presented here. These include electrospinning for the production of blended nanofibers, spin-coating followed by high-temperature drying or the addition of chemical additives[273–275]. Previous work which does use production methods similar to the one presented here, a simple drying procedure, do not investigate the relationship between PEDOT and PVA, and focus on the impact of conductivity enhancers such as carbon nanotubes or instead look at the mechanical properties of the films[276,277]. This makes it challenging to compare the roughness and surface characterisation in previous literature to the results presented here. The closest comparison is work that blended PEDOT:PSS with PVA for the development of flexible optoelectronic materials, which found that a film containing 40% w/v of PEDOT possess a roughness of 110 ± 80 nm, greater than any of the values found here[278]. This variation could be due to difference in scale; the area measured here was 5 μm compared to the millimetre size measurements taken previously. At

the micro-scale these films could appear less rough compared to the millimetre scale; variation over a larger area could be responsible for an increase in roughness. It is also possible that the production method that we used impacted the roughness of these films; during the production of our films samples were placed under vacuum desiccation. This would remove excess air trapped in the PEDOT:PSS:PVA structure, due to the porous nature of PEDOT, causing the film to adhere more firmly to the underlying substrate, resulting in a less rough surface.

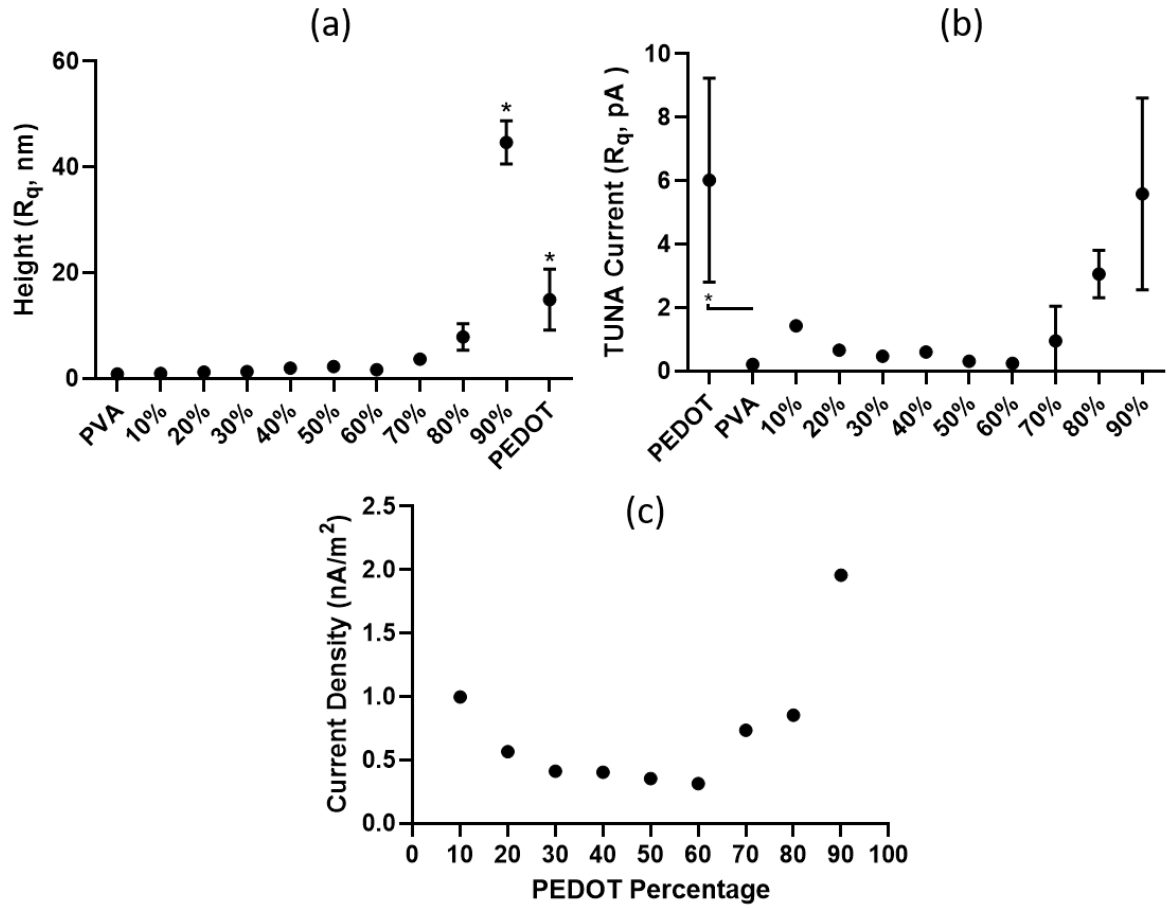

Figure 4-5-analysis of PEDOT:PSS:PVA blended films. (a) mean Rq values of height (b) mean R_q values of TUNA current and (c) plot of current density against increasing concentration of PEDOT (SEM, n = 3), * indicates significant difference ($P \leq 0.05$).

As the concentration of PEDOT increased in the blended films it was expected that the conductivity of the polymer blend would also increase. A similar trend was predicted with roughness; it is already known that PEDOT forms aggregates and therefore it would be likely

that an increase in the number of PEDOT aggregates would also cause an increase in film roughness[279,280]. The average current for both PEDOT control and polymer blends above 70% displayed a high level of variability, in some cases, this variability was 3 pA (±SEM). This variability is likely the cause for the lack of statistical significance between the PEDOT only film and other blends. A similar phenomenon was observed by *Kemerink et al* when studying PEDOT:PSS films using spectroscopic techniques[281]. They observed that PEDOT films displayed a high level of three-dimensional inhomogeneity, which produced nanoscale variations in the local conductivity, similar to those seen here. *Kemerink et al* attributed this variation to the presence of a top layer that contains a higher level of PSS, resulting in decreased conductivity, compared to the lower layers which contain more PEDOT and therefore have greater conductivity. In a similar way, the samples produced here may contain a top layer of PSS, caused by separation of PSS from the PEDOT:PSS:PVA blend. The varying thickness of this top layer then provides greater or lesser access to the PEDOT rich area beneath, depending on the thickness of that layer; which in turn causes variation in the conductivity of the film.

To further investigate the relationship between topography and surface area, a plot of current density (Current/surface area) was produced (Figure 4-5**Error! Reference source not found.**, c). At higher concentrations, 70% and above, current density increased with increasing concentration of PEDOT, however, there is no linearity, and the relationship appears U-shaped. This lack of linearity suggests that any increase in electrical conductivity is due to increased PEDOT concentration, and the PEDOTs increased ability to carry charge, as opposed to an increase in surface area.

4.3.2 Determining the properties of pure PEDOT films modified with electrical and physical additives using TUNA-AFM

PEDOT films are often modified to improve their electrical, chemical or physical properties, this can include chemical conjugation, post-production vapour deposition, or doping via simple blending methods[282–284]. Previous work has already shown that the electrical conductivity of PEDOT:PSS devices can be improved through the addition of solvents such as ethylene glycol (EG) and dimethyl sulfoxide (DMSO)[285–287]. Likewise, it has been shown that the conductivity and physical properties of PEDOT films can be tailored with the addition of cross-linking compounds, including (3-glycidyloxypropyl)trimethoxysilane (GOPS) and divinylsulfone (DVS)[288,289]. Work regarding the modification of PEDOT:PSS films has focused on determining how modification, with the above mentioned compounds, impacts the function of larger scale device such as PEDOT solar cells, transistors or textiles[285,286,290,291]. In contrast, we sought to investigate the effect these additives had on PEDOT:PSS films at the micro and nano scale; in particular we wanted to determine how addition of electrical and physical compounds altered the roughness and electrical current. Figure 4-6**Error! Reference source not found.** shows the impact EG, DMSO, DVS and GOPS had on PEDOT film topography and electrical properties.

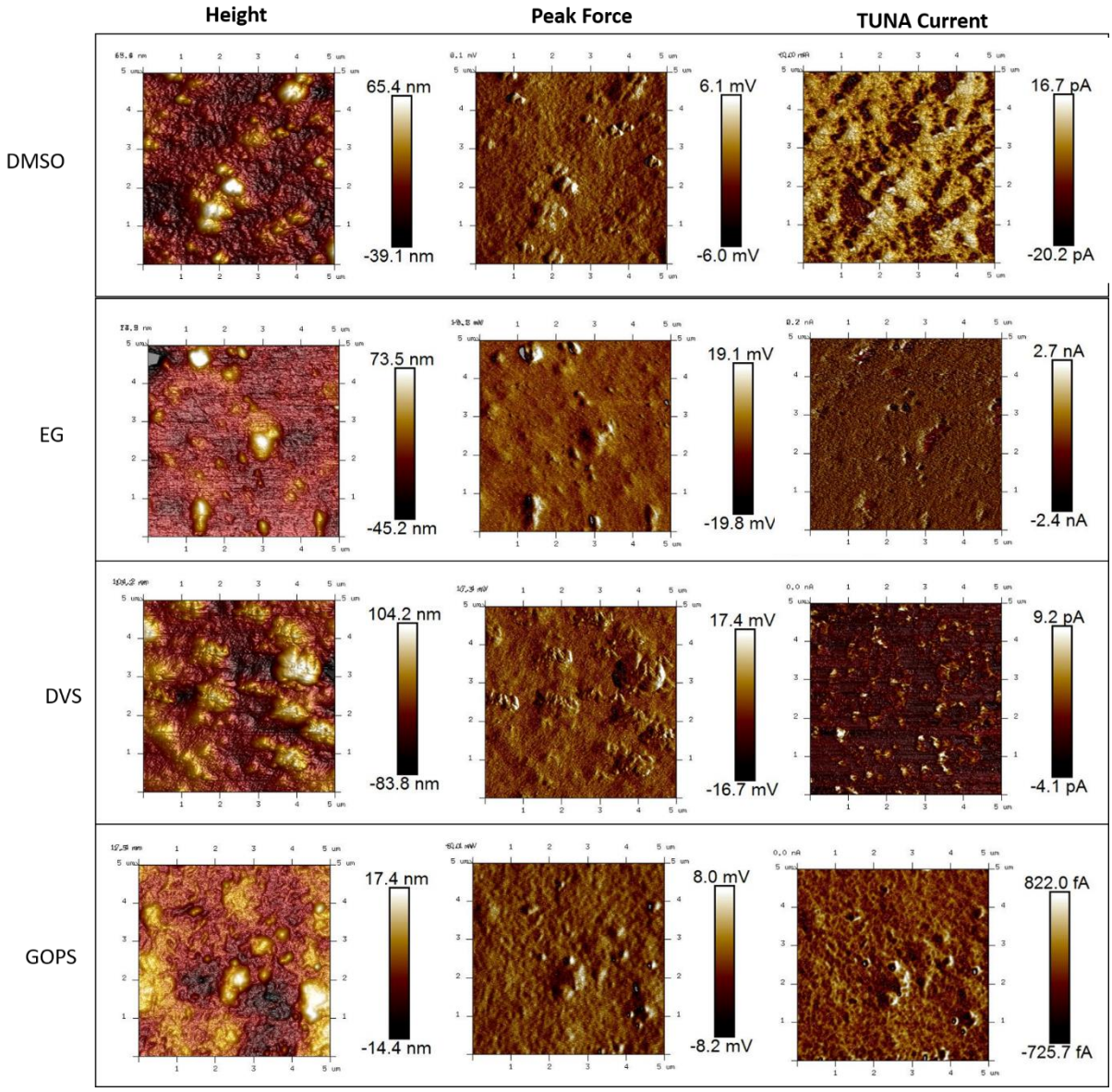

Figure 4-6 - Representative images of PEDOT:PSS films doped with DMSO, EG DVS and GOPS all at 2% w/v. Images include height, peak force and TUNA current data.

Topography and Peak force images reveal that all four samples, irrespective of the presence of additive, displayed PEDOT aggregation. However, R_q values indicated that the addition of EG significantly increased roughness compared to all other additives, from 14.93 nm in PEDOT only films to 42.1 nm in EG blended films ($P = 0.014$) (**Error! Reference source not found.**, a). This matches previous AFM studies of PEDOT:PSS films which contained EG, which

observed increased roughness and increased PEDOT aggregation[242,292]. *Yan and Okuzaki* proposed that the addition of EG causes an increase in the aggregation of primary particles, which, if accurate, could be occurring here and be responsible for the increased surface roughness[293].

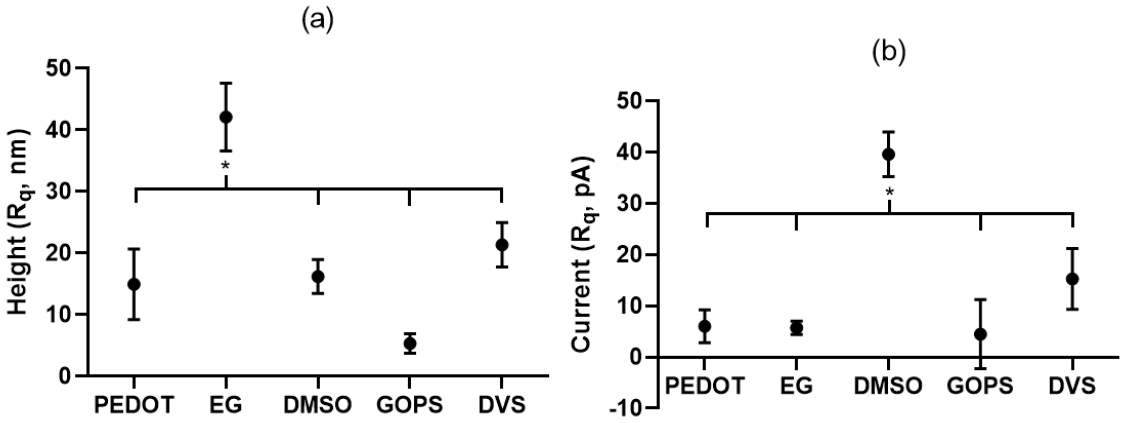

Figure 4-7 - analysis of PEDOT:PSS films with the addition of either electrical (DMSO and EG) or physical (GOPS and DVS) additives. (a) mean R_q values of height (b) mean Rq values of TUNA current (SEM, n = 3).

In contrast, films containing GOPS displayed decreased variability and lower roughness compared to all other samples, however this difference was not significant. This is similar to previous studies of GOPS supplemented films which, over an area of 1 × 1 μm^2 found a decrease in roughness, from 2.1 nm in PEDOT down to 0.83 nm in GOPS containing films, a value lower than the mean roughness presented here[289]. In contrast, the addition of DVS created a slight increase in roughness, which is unexpected as both DVS and GOPS are cross-linking agents and it might be expected they would have a similar effect on film roughness. Currently there is no literature which uses AFM to compare the impact of cross-linking compounds on the structure of PEDOT films. We hypothesise that the mechanisms involved are different depending on the cross-linker being used (Figure 4-8). The silane present in GOPS allows the film to adhere more firmly to the underlying glass substrate, reducing the height of the PEDOT aggregates and causing a reduction in roughness compared to PEDOT only films. A similar

phenomenon has been observed in polymer films on indium tin oxide (ITO) and polymer composites deposited on glass substrates[294,295]. In contrast to GOPS, DVS cross-linking is based on the reaction of vinyl groups with nucleophiles such as the hydroxyl groups in PEDOT:PSS[291]. This suggests that DVS cross-linking does not impact the adhesion of the film to the substrate and instead increases cross-linking within the film but has little impact on the formation of aggregates and therefore does not cause the decrease in roughness observed in PEDOT GOPS films; and in fact causes a slight, if none significant, increase in roughness.

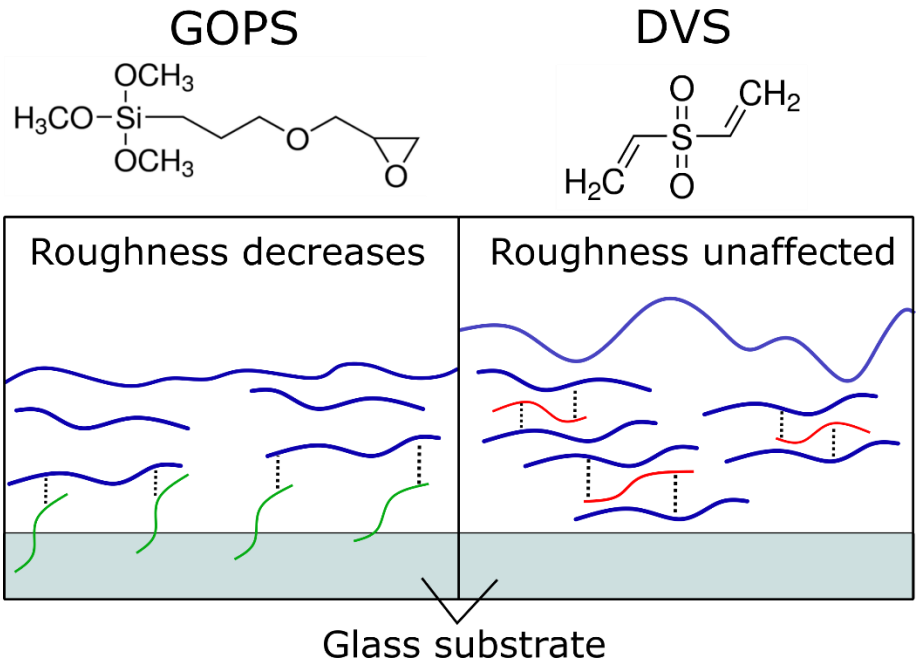

Figure 4-8 - Schematic demonstrating the impact GOPS (left) and DVS (right) have on PEDOT film roughness

TUNA current mapping revealed that the only films which displayed significantly increased current were those treated with DMSO (P = 0.028) (Figure 4-7**Error! Reference source not found.**, b). It was expected that both EG and DMSO would cause an increase in conductivity; both compounds are used as secondary dopants to enhance the electrical properties of PEDOT[260,296–298]. While DMSO was responsible for a significant increase in TUNA current,

EG did not cause any noticeable change in current. Previous investigation into the mechanism behind PEDOT secondary doping using these additives has yet to define a single mechanism. However, in the case of DMSO evidence suggests that DMSO dissolves PSS altering the ratio of PEDOT to PSS, causing an increase in conductivity[299,300]. Furthermore, it has also been suggested that secondary dopants, such as DMSO, cause phase separation between PEDOT and PSS which can also increase conductivity[301]. Currently, no conclusive mechanism has been proposed for the mechanism by which EG alters PEDOT conductivity or morphology. Some evidence suggests that changes in conductivity are due to an increase in the number of polarons in EG treated PEDOT films[302]. It is also possible that EG causes an indirect increase in surface area, by increasing roughness, which then leads to the increased conductivity observed in EG treated film. For instance during a force microscopy study by Yan and Okuzaki results suggested that addition of EG to PEDOT:PSS thin films removes excess PSS causing an aggregation of PEDOT which then form conductive grains causing an increase in both surface roughness and increase in conductivity[293]. This is reinforced by analysis of the crystal structure of PEDOT:PSS films; solvents such as EG can increase the number of PEDOT grains causing measurable changes in film morphology[303,304]. It has also been suggested that, as with DMSO, addition of EG causes phase segregation leading to increased conductivity[301,305]. Based on the results shown here we suggest that a combination of mechanisms could be involved. EG could be causing phase segregation, resulting in the formation of more PEDOT aggregates, causing the observed increase in film roughness, but due to the relatively small area measured here (5 μm^2) the change in roughness did not result in an increase in current as observed by others, who have measured changes at the macro scale.

As with EG, neither GOPS nor DVS caused a significant change in current; previous evidence indicates that GOPS can cause a decrease in conductivity while DVS can cause an increase[288,297]. However, GOPS has primarily been used in PEDOT films to alter physical rather

than electrical properties, while DVS has rarely been used and therefore it was unclear how significant an impact it would have on PEDOT films. The results shown here indicate that at the micrometere scale neither have a significant impact on the films electrical properties (Figure 4-7).**Error! Reference source not found.**

4.4 Conclusions

In this study, we have presented the use of Peak Force TUNA AFM for the characterisation of PEDOT:PSS films. By blending PEDOT:PSS and PVA, we were able to study the relationship between surface topography and electrical behaviour, and determine the impact PEDOT concentration had on this behaviour. We also investigated the impact commonly used additives had on PEDOT films. In particular, we used current mapping to characterise the impact electrical additives, DMSO and EG, had on PEDOT films – with DMSO doped films displaying a significant increase in electrical conductivity. Likewise, we found that the additives GOPS and DVS, chemical cross-linkers used in the production of PEDOT devices, had no significant impact on electrical and topographic properties.

Together these studies demonstrate that PF TUNA is an ideal method for simultaneously characterising multiple properties of CP films. This type of insight will be essential given the growing interest in PEDOT:PSS as both an engineering and bioelectronic material. In the context of this thesis it this knowledge can inform which additives to use when PEDOT:PSS to design an electroactive surface as part of a biosensor.

5 Development of PEDOT:PSS loaded biodegradable scaffolds for electroanalytical drug detection

5.1 Introduction

The success of early implantable bioelectronic devices, which aimed to interface electronic components with biological systems for therapeutic benefit, were restricted by the materials available at the time. For instance, the first widely available cardiac pacemakers were made from stainless steel wires surrounded by Teflon or polyethylene[127]. Likewise, early cochlear implants were manufactured using platinum-iridium wires coated in silicone[306]. While early bioelectronics devices were effective, and still represent the foundation of commercial bioelectronic technology, advanced materials have opened avenues for the development of the novel bioelectronic devices. A commercially successful example is the leadless micro pacemaker produced by Medtronic that relies on nickel titanium alloy (Nitinol) and displays improved biocompatibility; they decrease the risks that are associated with previous cardiac pacing systems[307–309]. Likewise, the company Advanced Bionics have used gold wires reinforced with high-density polymer fibres to produce flexible Cochlear implants[310,311]. Two key areas of focus for the design of bioelectronic implants have been the enhancement of biocompatibility and tuneable biodegradability. Biocompatibility has broadly been defined as "the ability of a material to perform with an appropriate host response in a specific application"[312]. In a commercial or clinical setting this definition involves meeting regulatory standards and determining the biological response to the material, this includes, but is not limited to, an assessment of cytotoxicity, irritation, and immune response[313,314].

In an attempt to improve the biocompatibility of bioelectronic devices, materials have been developed with physical properties that more closely match target tissues. For instance, where semiconductors, such as silicon, are relatively rigid and have a high Young's Modulus (~100GPa), advanced materials such as conductive polymers and hydrogels have a significantly lower Modulus (~1GPa), are more flexible and more closely resemble biological tissue [163,315]. It is also possible to optimise the porosity, stiffness and chemical properties of bioelectronic materials to maximise the interaction between device and biological environments[316–318]. Improving the continuity between device and target tissue reduces the likelihood of problems associated with device implantation; the more closely a device resembles biological tissue the less likely it is to trigger an immune response which cam severely limit the functionality of an implanted device[314].

The conductive polymer poly(3,4-ethylenedioxythiophene) polystyrene sulfonate (PEDOT:PSS) is already a popular choice for the design of bioelectronic devices. Most recently this includes highly conductive hydrogels, soft microelectrodes for neural interfacing and flexible wearable electrodes for physiological monitoring[249,319,320]. This interest has led to a growing body of data concerning the biocompatibility of PEDOT. Evidence indicates that PEDOT is cytocompatible, triggers a minimal immune response and has no significant impact on cell growth when interacting with a range of tissue and cell types[321–325]. In contrast, there remains limited data about the biological breakdown and elimination of PEDOT materials. PEDOT is not inherently degradable; it does not biodegrade at a molecular level. As such there exists limited work exploring the biodegradability of PEDOT and instead previous work has focused on developing PEDOT structures and devices which can be made biodegradable through blending with other polymers or additives, such as modified nanotubes and silk composites[321,326]. In place of studying the biodegradation of PEDOT work has also focused on *in vitro* characterisation, short term implantation, or long-term stability, and therefore there is

a lack of long-term biodegradability data[327–329]. Another reason for the lack of data concerning PEDOT breakdown is the instability of pure PEDOT films; when dried PEDOT films are exposed to an aqueous environment the film has no structural integrity and falls apart. This means that a pure PEDOT film could not be used as an implant; it would be too unstable. As such there is a need to increase the stability of PEDOT, using additives as mentioned above, or by housing the PEDOT in a more stable structure. One possibility is to create a biodegradable scaffold that would contain the PEDOT, preventing its immediate dissolution when in contact with an aqueous environment, which could then degrade either when the PEDOT became too unstable or the implant was no longer needed.

the majority of recent work studying biodegradable implantable materials has focused on controlling the release of therapeutic compounds, examples include biodegradable nanocarriers loaded with anticancer agents, scaffolds which can deliver cellular regenerative compounds and resorbable gels for sustained protein delivery[330–332]. Alongside controlled release of therapeutic compounds the design of biodegradable electronic devices is of growing interest. In certain clinical situations a bioelectronic implant may only be needed in the short term, this can include the temporary monitoring of physiological parameters following injury, such as brain trauma or musculoskeletal injury, or the acute modulation of biological signalling[333–337]. In these cases, invasive surgery to implant and then remove a device after a short period increases the risk of complications. By comparison, a device that can be implanted and completely degrades when no longer required reduces the risks associated with the surgical removal of a device.

While new materials expand the opportunities for designing an implantable device one challenge will always remain: fouling of the surface following implantation. This is a particularly important challenge for implantable sensors; fouling can severely impact the accuracy and function of the sensor. Fouling can be reduced through the design of porous structures to filter out contaminants, such as ion selective-membranes and nanoporous thin

films[338,339]. Chemical approaches can also be taken which rely on the use of surface chemistry to produce antifouling properties, this includes the use of zwitterionic surfaces and the addition of polyethylene glycol (PEG), both of which can help a device resist protein fouling[340–342]. Likewise, work is being carried out to produce novel screening methods to identify biomaterials that can resist sources of fouling or interference, such as biofilms[343,344].

Development of biodegradable materials offers another possible solution to the fouling problem; as the materials degrade they can replenish a surface reducing interference due to biological fouling. One commercial family of biodegradable polymers are RESOMER®, produced by Evonik Operations GmbH. Thus far these materials have been used for the controlled release of therapeutic compounds, such as the use of microspheres and nanoparticles loaded with antiviral and anticancer agents[345,346]. There have been limited examples of implantable devices developed using RESOMER®, the only examples are limited to a prosthetic blood vessel and 3D printed filaments designed to cultivate stem cells[347,348].

Previous work has attempted to develop biodegradable conductive devices, with a focus on tissue engineering applications. This work involved modifying biodegradable scaffolds with conductive components, such as carbon nanotubes or conductive polymers[349–351]. Thus far there has been no attempt to combine RESOMER® with conductive polymers, despite the promising biocompatibility and degradability properties of RESOMER®.

One possible reason for this is the inability to easily combine RESOMER® with conductive polymers. For instance, PEDOT:PSS can be purchased in aqueous solution, however when directly mixed with Resomer the aqueous solution causes RESOMER® to form an immiscible mixture consisting of RESOMER® and liquid PEDOT:PSS. As such if the biodegradable RESOMER® is going to be combined with PEDOT:PSS an alternative strategy is required.

Based on this we aimed to use a RESOMER® polymer to produce a biodegradable scaffold that could house a PEDOT:PSS; creating a long-term biodegradable bioelectronic platform. In this work, we demonstrate the fabrication and electrochemical characterisation of these scaffolds. We then go on to demonstrate that they can be used to detect the redox behaviour of the TCA compound imipramine, which was previously discussed in chapter 3.

5.2 Experimental

5.2.1 Materials and equipment

RESOMER® polymer LR708 (Poly(L-lactide-co-D,L-lactide) was provided by Evonik Operations GmbH. Poly(3,4-ethylenedioxythiophene) polystyrene sulfonate (PEDOT:PSS) was supplied by Sigma Aldrich. Divnyl Sulfone was supplied by Merck. Ethylene glycol was supplied by Acros Organics. Two part epoxy resin was obtained from Gorilla Glue.

Scaffolds were designed using BioCad software and printed using a RegenHu 3D Discovery Extrusion Printer. All consumables for the printing, including 3 cc syringes and 27 gauge needles, were obtained from Adhesive Dispensing Ltd.

All electrochemical measurements were obtained using a Metrohm Autolab M204 potentiostat running Nova 2.1 software. A three-electrode setup was used, using scaffolds as a working electrode, a platinum wire counter electrode and an Ag/AgCl reference electrode, stored in 3 M KCl.

5.2.2 3D Printing of RESOMER® Scaffolds

To print scaffolds, RESOMER® was dissolved in analytical grade dichloromethane (DCM). Initially, various percentage w/v concentrations were used, from 10 – 40% (see Table 5-1), to determine an optimal concentration. When dissolving RESOMER® in DCM to create "RESOMER® ink" RESOMER® was left to dissolve in DCM at room temperature for 24 hours.

Following dissolution, RESOMER® ink was loaded into a 3 cc syringe with a 27 gauge needle attached. This was then attached to the 3D extrusion printer.

To identify ideal printing parameters a range of RESOMER® concentrations, printing speeds, printing pressure and layer height were tested, all of the parameters tested are listed in Table 5-1. Initially, RESOMER® scaffolds were printed on aluminium foil, however, once suitable parameters had been identified the substrate was changed to glass microscope slides.

Once scaffolds were printed they were left to dry in front of a fan spinning at 1100 rpm, to maintain the temperature at 19ºC. Following drying, scaffolds were inspected for any macro-scale errors which would limit their ability to function.

5.2.3 Fabricating PEDOT:PSS loaded RESOMER® Scaffolds

Once RESOMER® scaffolds were dried the edge of a pipette tip was used to apply epoxy to the edge of the scaffold, where the scaffold met the glass slide. This was done to secure the scaffolds to the slide and prevent electrolyte dislodging the scaffold during electrochemical analysis. The epoxy resin was left to dry for 24 hours.

The RESOMER® scaffolds were then loaded with a mix of PEDOT:PSS and physical and electrical additives. This formulation consisted of PEDOT:PSS (1.3% aqueous solution), ethylene glycol, divinyl sulfone and polyethylene glycol diglycidyl ether (PEGDE) at 10, 5 and 3 % v/v, respectively. This formulation was stirred at room temperature for 1 hour, after which approximately 2 µL was added to each well of the RESOMER® scaffold. The loaded scaffolds were then placed in an oven at 45ºC for 20 minutes to dry the PEDOT formulation. Once loaded with PEDOT formulation and dry scaffolds were stored at room temperature and characterised within 48 hours of production.

5.2.4 Voltammetric analysis using RESOMER®:PEDOT Scaffolds

PEDOT loaded scaffolds were initially characterised using cyclic voltammetry. A glass cutter was used to trim the microscope slide, with the RESOMER® scaffold attached, so that it could be placed in a multi-well plate.

The RESOMER® scaffold was attached to a potentiostat using a platinum (Pt) wire inserted into the central well of the scaffolds. A three-electrode setup was then used to perform cyclic voltammetry using a Pt counter electrode and Ag/AgCl counter electrode. Approximately 3 mL of 0.01 M phosphate buffer saline (PBS) was added to each well; just enough to create contact between the outer surface of the scaffold and the other electrodes.

Scan rate studies were performed in both 0.01 M PBS and 10 mM of the FIC/FOC redox couple. The scan rates used were: 50, 100, 200, 300, 400, 500, 800, 1000, 2000, 3000, 4000 and 5000 mV/s. Stability studies were carried out by performing 100 sequential scans at 1 V/s in both PBS and 10 mM FIC/FOC.

Finally, square wave voltammetry was used to determine how effective PEDOT loaded RESOMER® scaffolds were at detecting a TCA. Square wave voltammetry was carried out, from -0.4 to +0.9 V, in the presence of an increasing concentration of the tricyclic antidepressant Imipramine (IMI).

5.3 Results and discussion

5.3.1 Optimisation of 3D extrusion printed RESOMER® scaffolds

3D extrusion printing is a well-established method for the printing of polymers, it is easily optimised and can rapidly print specific structures, making it an ideal approach for creating RESOMER® scaffolds. Previous methods used to create biodegradable conductive polymer scaffolds are more technically demanding and can involve multiple processing steps, such as freezing or the addition of complex molecules[352,353]. In contrast, we sought to develop a process

which was less technically demanding and more rapid than previous methods, hence the use of 3D extrusion printing.

Two scaffolds were designed, A (a square grid, 15 mm × 15mm) and B (a rectangular grid, 14 mm × 6 mm). Initially scaffold design A was used to determine three key factors:

1) If it would be possible to print RESOMER® ink
2) Which parameters impacted scaffold printability
3) Once printed if PEDOT:PSS could easily be loaded into the scaffolds wells

In contrast, scaffold design B was an attempt to reduce the size of the scaffold to examine the resolution that could be achieved when using extrusion printing to print RESOMER® and determine if a smaller scaffold could be generated which could be manually loaded with PEDOT:PSS.

Table 5-1 lists the parameters which were varied when printing scaffold design A while Figure 5-1 provides visual examples of a failed or successful scaffolds, alongside the parameters used during printing and an explanation for the printing error.

		Variable Printing Parameters		
		Ink concentration (% w/v)	**Print speed (mm/s)**	**Pressure (MPa)**
		40	5 - 8	0.4 – 0.6
		30	5 - 8	0.4 – 0.6
		20	5 - 8	0.4 – 0.6
		18	2 – 8	0.3 – 0.5
		15	2 - 8	0.3 – 0.5
Final Print Settings	**Design A**	**18**	**5**	**0.35 – 0.4**
	Design B	**18**	**3.6**	**2.5 – 3**

Table 5-1- a list of the parameters which were tested when optimising printing of RESOMER® scaffolds

The parameters which were adjusted during printed included: concentration, print speed, layer height and pressure. The first parameter tested was ink concentration (RESOMER®: DCM % w/v). Initially, 40, 30 and 20% were tested, however, due to extremely high viscosity a high pressure was needed to allow the nozzle to extrude the ink onto the substrate. If the pressure was lower than 0.6 MPa the ink would not extrude from the printing nozzle, in contrast when the pressure was at 0.6 MPa the nozzle extruded an excess of ink (Figure 5-1, images a and b). A lower ink concentration was tested to determine if a lower pressure could be used to overcome this problem. At 15% the RESOMER® ink was less viscous and a lower pressure, down to 0.3 MPa, could be used during printing. However, at 15% the viscosity was too low, once again causing an excess of the solution to be extruded during printing (Figure 5-1, image c).

Concentrations between 15 – 20% were then tested and the ink and the most viable viscosity was 18%; it produced ink that could be printed at a pressure between 0.2 – 0.6 MPa and did not result in excess ink extrusion. Based on this 18% RESOMER® ink was used for all subsequent printing.

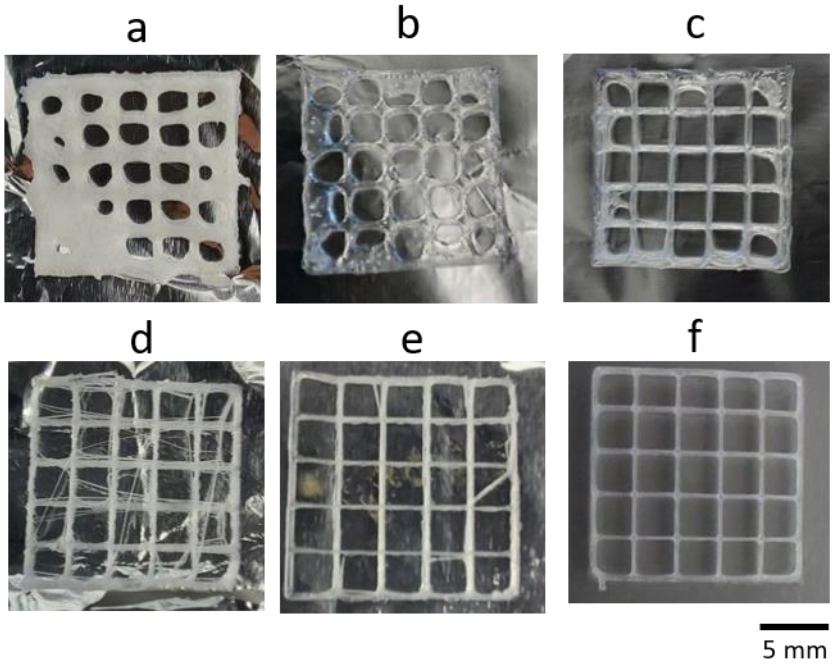

Scaffold image	Parameters	Error
a	Ink Concentration: 30% Print Speed: 6 mm/s Pressure: 0.6 MPa	High viscosity required high pressure to extrude, leading to excess ink extrusion
b	Ink Concentration: 20% Print Speed: 6 mm/s Pressure: 0.6 MPa	As above
c	Ink Concentration: 15% Print Speed: 6 mm/s Pressure: 0.3 MPa	Lower viscosity allows for lower pressure, but also leads to excess extrusion
d	Ink Concentration: 18% Print Speed: 3 mm/s Pressure: 0.3 MPa	Lower printing speed leads to drying errors
e	Ink Concentration: 18% Print Speed: 4 mm/s Pressure: 0.3 MPa	As above
f	Ink Concentration: 18% Print Speed: 5 mm/s Pressure: 0.4 MPa	None

Figure 5-1- a list of the parameters tested during printing of 15 X 15 mm scaffolds (Design A), with images demonstrating the type of error and an explanation for the source of the error. Scale bars represent 5 mm.

Once a suitable ink viscosity was identified we attempted to optimise the remaining printing parameters. The printing speed was reduced from 6 to 3mm/s, however, this resulted in drying

errors (Figure 5-1image d). This likely occurred as the slower printing speed gave the filaments increased time to dry but as the filaments dried they began to constrict. As the filaments dried we observed that these constrictions caused them to interfere with the printer nozzle, entangling with the subsequent layer. To counteract this error we increased the print speed to 4 mm/s, this reduced the number of errors; however, some errors still occurred (image e). Finally, we increased the print speed further to 5 mm/s and increased the pressure to 0.4 MPa; the increased speed reduced the volume of ink extruded. With these parameters (image f) we were able to produce viable 15 × 15 mm RESOMER® scaffolds.

The 15 × 15 mm scaffolds were proof of concept that the RESOMER® LR708 could be printed into a scaffold structure. The dimensions of this scaffold are similar to those of existing bioelectronic implants; such as cardiac pacemakers which are comparable to the size of a matchbox and in some cases are be larger than the scaffold developed here[354]. However, we decided to create design B, which is a 14 × 6 mm rectangle, to reduce the overall size of the scaffold. This was done to produce scaffolds which more closely resemble miniaturised bioelectronic implants which are currently in development[355,356]. Likewise, while there is no legally defined limit to the size of an implantable device any design should minimise the damage caused by implantation. Reducing the size of an implant is one way to achieve this goal; a smaller implant will create less scar tissue when implanted and be less likely to trigger an immune response which could negatively affect the function of the device[357]. We therefore undertook a process of designing and optimising the smaller scaffold, design B (Figure 5-2). While design B is smaller it is worth noting that the size of the scaffold was also limited by the resolution of the printer and if further miniaturisation was required it would involve using a printing methods with greater resolution.

Initially, the same parameters used for the larger scaffold were used, however, this resulted in failed scaffolds (Figure 5-2, image a). This likely occurred due to the difference in scaffold

design. This design was smaller than the previous scaffold design, therefore the RESOMER® ink had less time to dry as each subsequent layer was added. As each new layer was added residual unevaporated solvent remained trapped in that layer preventing it from fully drying. This resulted in a lack of structural integrity, eventually causing the layers to merge together and the scaffold to collapse.

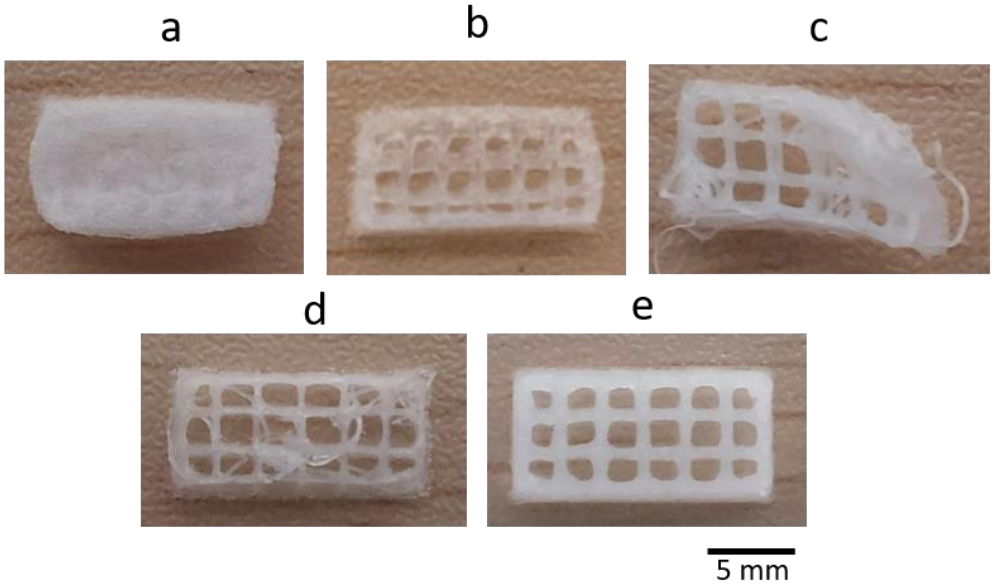

Scaffold image	Parameters	Error
a	Ink Concentration: 18% Print Speed: 5 mm/s Pressure: 0.4 MPa	Smaller scaffold design caused build of ink
b	Ink Concentration: 18% Print Speed: 4 mm/s Pressure: 0.3 MPa	Excess ink extruded
c	Ink Concentration: 18% Print Speed: 3 mm/s Pressure: 0.2 MPa	Rapid drying caused scaffold contraction
d	Ink Concentration: 18% Print Speed: 4 mm/s Pressure: 0.2 MPa	As above
e	Ink Concentration: 18% Print Speed: 3.6 mm/s Pressure: 0.25 MPa	None

Figure 5-2 - a list of the parameters tested during printing of 14 × 6 mm scaffolds (Design B), with images demonstrating the type of error and an explanation for the source of the error. Scale bars represent 5 mm.

To prevent the RESOMER® scaffolds collapsing during printing each layer needs to dry sufficiently. This could be achieved by either adding a drying step between each layer or adjusting the printing parameters. We chose not to add a drying step because if each layer were to dry too much then the layer height could shrink. This would mean that as each subsequent layer was printed and allowed to dry inaccuracies and errors could develop due to variation in layer height, instead we chose to adjust the printing parameters. Specifically we decreased both pressure and print speed; which would in turn decrease the volume of ink and increase the drying time between each layer without adding a full drying step. While this improved the resolution there was an excess of ink being extruded (image b). To account for this we further decreased the pressure from 0.3 MPa to 0.2 MPa to reduce the amount of ink that was being extruded and decreased the pressure to account for the slower print speed. This caused a decrease in the thickness of the filament decreased, suggesting a decrease in the volume of ink being extruded (image c). As with the larger scaffolds, this resulted in faster drying and caused the filaments to contact; causing the scaffold to shrink and deform. Based on this we increased the print speed to prevent the scaffold from drying too rapidly. While this did improve the outcome by reducing the shrinkage, some errors still occurred (image d). Finally, a print speed between 3 and 4 mm/s and a pressure between 0.2 and 0.3 MPa was selected and identified as the optimal value for these parameters (image e).

5.3.2 Loading of PEDOT:PSS and voltammetric characterisation

Once the RESOMER® scaffolds could be consistently printed we could then attempt to load them with a conductive polymer formulation. PEDOT:PSS was chosen because it can be processed into a structure based on the desired application, from 3D printed textiles to polymer films for biological and engineering applications[358–361]. Likewise, as shown in chapter 4 the electrical and physical properties of commercially available PEDOT:PSS can easily be

modified through the addition of additive agents. We chose to include ethylene glycol, which improves the conductivity of PEDOT, divinyl sulfone, which stabilises PEDOT films and acts as a secondary dopant, and finally poly(ethylene glycol)diglycidyl ether (PEGDE), which improves the water stability of PEDOT:PSS surfaces[302,322,362].

PEDOT:PSS Additive Formulation (% v/v)	
Ethylene glycol	10%
Divinyl sulfone	5%
Polyethylene glycol diglycidyl ether	3%

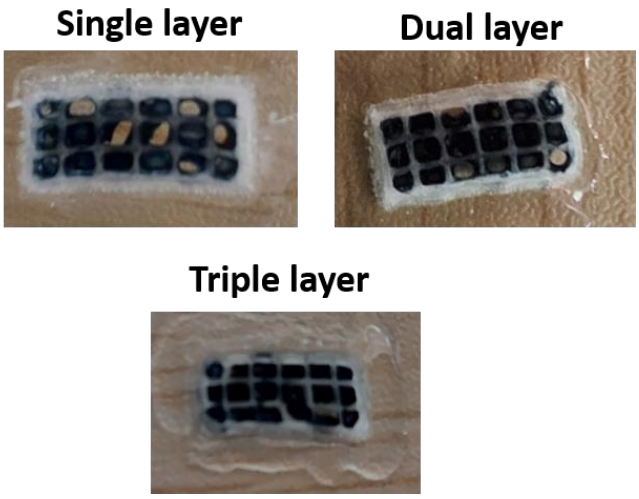

Figure 5-3 - a list of the additives used to create the PEDOT:PSS loading formulation and example images of single, dual and triple loaded scaffolds.

The formulation, the specific composition of which is shown in Figure 5-3, was loaded into each well of the RESOMER® scaffold. When this solution was dried the PEDOT inside each scaffold well formed a thin layer. However, during the drying process, the PEDOT did not dry evenly; in some cases it adhered to the side of the well, creating an uneven layer. Based on this we added a second layer to each well and allowed it to dry. While this reduced the number of wells that lacked a complete PEDOT layer some wells still had only thin layers of PEDOT. Finally, we added a third layer to each well and this proved to fill each well with enough PEDOT to create a continuous layer within each well of the scaffold.

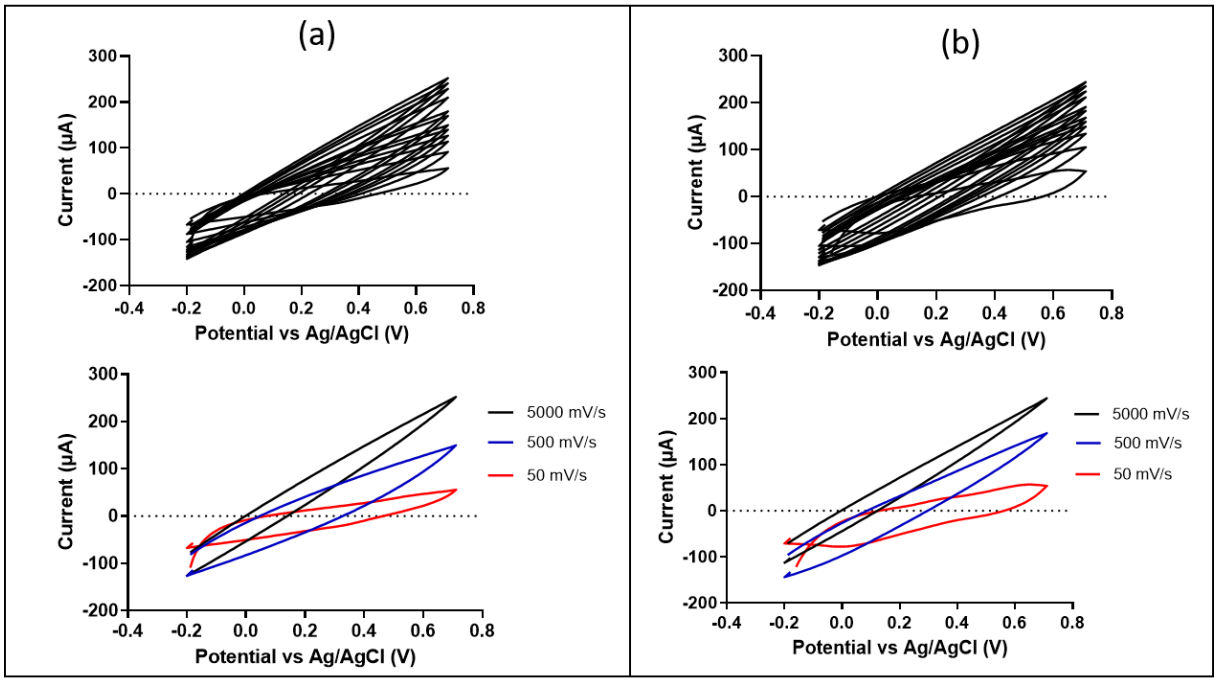

Figure 5-4 - Scan rate studies performed in either (a) 0.01 M PBS alone or (b) in the presence of 10 mM of the FIC/FOC redox couple. The upper voltammogram show overlays of all scans while the lower highlight only 50. 500 and 5000 mV/s scans. Scans were performed

Following the loading of the RESOMER® scaffolds with the PEDOT:PSS formulation we used cyclic voltammetry to characterise the electrochemical activity of the scaffolds. This was carried out using the redox couple ferri/ferro cyanide (FIC/FOC). Initially, scan rate studies were performed in both PBS alone and PBS containing FIC/FOC (Figure 5-4). In both cases, a single scaffold was tested and the scan rate increased. For both PBS and FIC/FOC the initial scan showed primarily capacitive behaviour; while possible peaks are visible at the lower scan rates they are not clearly discernible due to the capacitance. As the scan rate was increased the behaviour of the scaffold became more resistive and at the highest scan rate (5000 mV/s) no peaks are visible. Previous work has noted that PEDOT:PSS can undergo over-oxidisation resulting in inactivation[363]. However, over-oxidation is thought to occur at potentials above +1.4 V, and given the potential during these experiments did not exceed +0.8 V this suggests over oxidation is unlikely. One possible explanation has been proposed recently by *Markoulidis et al* when studying pseudocapacitance using a lithium-ion electrolyte and electrode containing

PEDOT:PSS[364]. At higher scan rates there is less time for redox processes to occur at the PEDOT:PSS surface; redox processes will occur more slowly than capacitive processes. As such any redox processes either do not occur or are obscured by the strong capacitive behaviour of PEDOT:PSS. This hypothesis would explain the lack of peaks at higher scan rates.

To investigate the stability of the scaffolds we performed 100 sequential scans, once again in PBS alone and in the presence of FIC/FOC. As shown in Figure 5-5 a scaffold produced using exactly the same process (a technical replicate) could produce three different types of behaviour when loaded. In some cases (Figure 5-5, a) the scaffolds displayed strong capacitive behaviour in PBS but they were able to detect the redox of the FIC/FOC couple. This produced a peak typical of the FIC/FOC redox couple, with oxidation occurring at ~0.4 V and reduction at ~0.1V. Over the course of 100 scans the peak current did not vary, increasing from 45.8 mV in scan 1 to 46.7 mV in scan 100, and from -39.0 to -36.3 mV for oxidation and reduction, respectively (Figure 5-5, a - inset). Peak-to-peak separation (ΔE_p) for this reaction was found to be 332 mV at all scans. This is greater than the typical ΔE_p for FIC/FOC, which in an ideal situation would be 59 mV, in order to satisfy the Nernst-Planck equation (Equation 4). This indicates the PEDOT:PSS surface was not acting as an ideal electrode; interfering with the redox kinetics which occurred at the surface. It is possible that a combination of solution resistance and ohmic drop are response for this large ΔE_p[201]. This is likely caused by the porous nature of PEDOT:PSS; the electrolyte absorbed into the surface would cause a significant increase in solution resistance. To confirm this hypothesis further work examining the porous structure of the PEDOT:PSS surface is required.

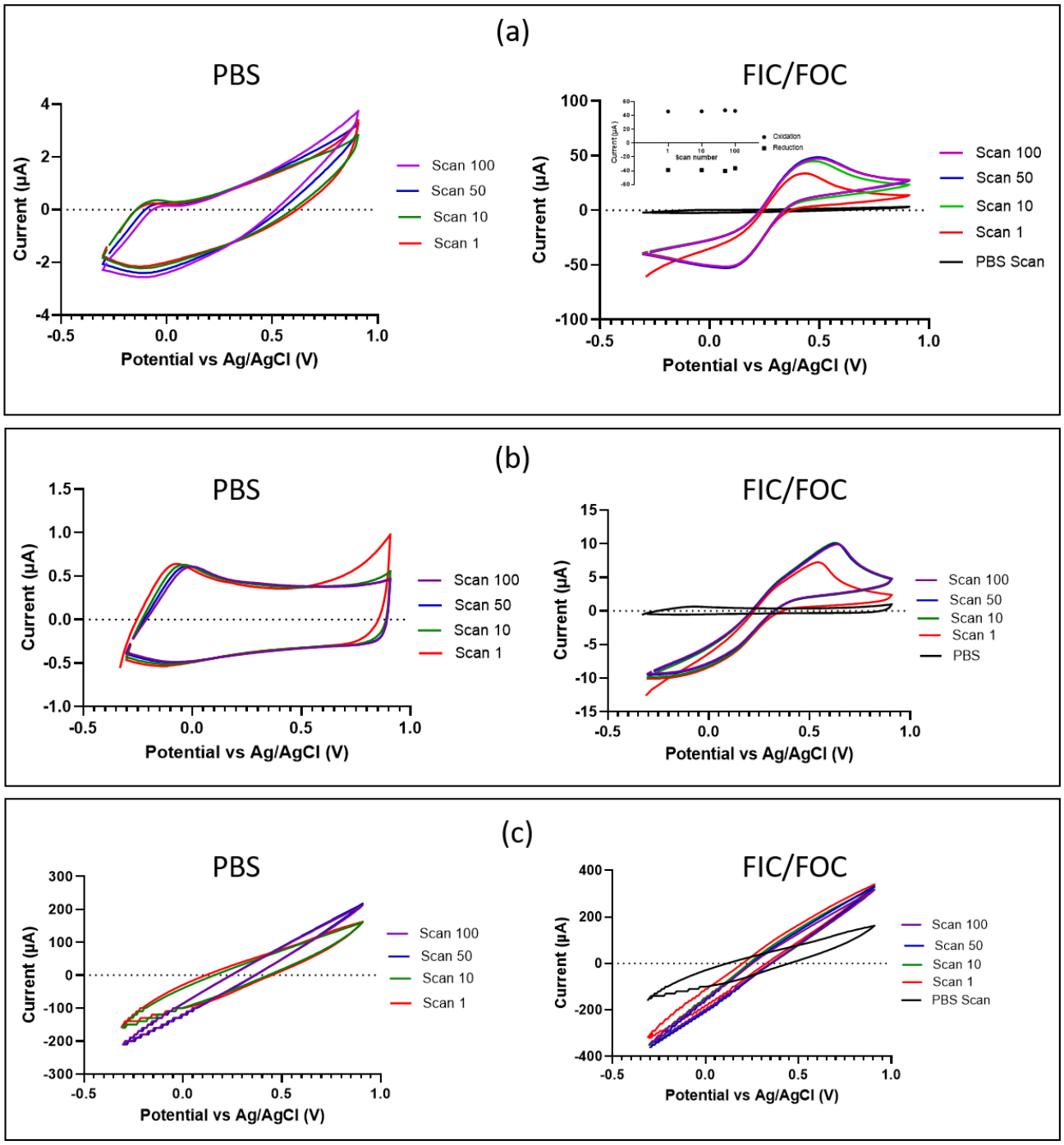

Figure 5-5 - Voltammograms of 100 repeated cycles, each panel (a-c) represents a single PEDOT:RESOMER® scaffold which had been pritned and loaded with the same PEDOT formulation and was tested first in 0.01 m PBS (upper) and then 10 mM FIC/FOC redox couple (lower).

The second type of behaviour exhibited by the RESOMER®:PEDOT scaffolds can be seen in Figure 5-5, b. In this case the redox which could be detected was predominantly oxidative; the

reduction peak was less well defined. In this case the peak was produced at 0.61 V, with a peak current of 8.9 mV. These values differ from the previous scaffold; indicating a change in surface behaviour. The source of this variation is unknown, however it could relate to the crude production method used to load the scaffolds. Variation in the amount of PEDOT:PSS formulation between each sample would change the surface area, thus changing the amount of current that could be detected.

Finally, the third type of behaviour which was observed was strongly resistive and was similar to that from scan rate studies (Figure 5-5, c). There are two possible sources for this behaviour; either the PEDOT:PSS loading formulation or the RESOMER® scaffold. It is possible that during the printing and subsequent drying of the RESOMER® scaffolds the pores, which allow the electrolyte to make contact with the internal PEDOT surface, are prone to variation. It is known that the degradation of RESOMER® involves the diffusion of aqueous solution into pores on the polymer surface[365]. However, beyond that there is limited published work studying the surface properties and structure of the RESOMER® family of polymers. As such additional characterisation techniques, such as scanning electron microscopy, would need to be performed to understand the level of porosity and variation present at the RESOMER® surface. Variation in the pore structure, between RESOMER® samples, could lead to varying amounts of electrolyte, and thus analyte, gaining access to the PEDOT electroactive surface.

In contrast to RESOMER® the behaviour of PEDOT in aqueous environments is well studied and it has previously been noted that PEDOT undergoes swelling when in contact with any liquid[366]. It has been suggested that as PEDOT swells there is an increase in the electrical resistance[367]. Based on this, we hypothesis that the three different behaviours relate to the volume of electrolyte gaining access through the RESOMER® structure. In situation C there is an excess of electrolyte causing swelling of the PEDOT resulting in resistive behaviour. While in situations A and B there is less electrolyte in contact with PEDOT. Likewise, the variation

between A and B can be explained by swelling of PEDOT; in situation B there is still an excess of electrolyte and due to the low reduction potential used oxygen in the excess electrolyte is being reduced and interfering with the reduction of the analyte. In contrast, in situation A sufficient electrolyte is gaining access but not so much as to cause interference of oxygen or swelling of the PEDOT.

The results presented here have focused on the initial optimisation of PEDOT:PSS loaded RESOMER® scaffolds. The primary goal was to determine if the 3D printed scaffolds could be loaded with a PEDOT:PSS formulation, and what characteristics those loaded scaffolds displayed.

The formulation presented in this section acted as an initial proof-of-concept and was therefore used as the basis for the work which follows, However, additional work is needed to determine the effect the PEDOT loading formulation has on the types of behaviour discussed above. This is particularly relevant considering the results shown in the chapter 4 of this thesis; as shown different additives can have varying effects on the electrical behaviour of PEDOT.

5.3.3 Application of PEDOT:RESOMER® scaffolds for sensing therapeutic compounds

Despite variability during the production of the PEDOT:RESOMER® scaffolds they did display an ability to detect redox behaviour. Therefore, we tested their ability to detect a therapeutically relevant analyte, specifically, a member of the tricyclic antidepressant (TCA) compounds which were characterised in chapter 3. TCAs are rarely prescribed due to their narrow therapeutic window and high risk of overdose and would benefit from a therapeutic monitoring device. Currently, monitoring TCA concentration, to reduce the risk of side effects and tailor treatment to individuals, requires labour intensive and expensive equipment such as high-pressure liquid chromatography. An implantable sensor that could rapidly monitor TCA concentration would

be of clinical significance, as such we choose to use one of the TCA compounds, Imipramine (IMI) to determine if the scaffolds could detect a clinically relevant therapeutic target.

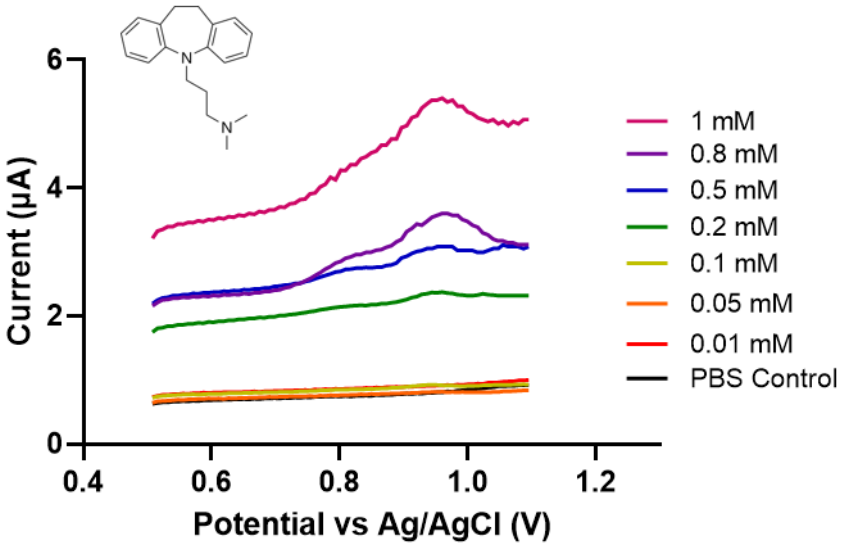

Figure 5-6 - square wave voltammetry of increasing concentration of IMI carried out in 0.01 M PBS.

Using the PEDOT:RESOMER® scaffolds we performed square wave voltammetry on increasing concentration of IMI in PBS. Previous literature, in combination with results presented early, confirm that TCA compounds which possess a central nitrogen in their chemical structure under oxidation. As shown in Figure 5-6 above 0.1 mM the PEDOT:RESOMER® scaffolds can detect an oxidative signal, with a peak at +0.94 V. This matches previous work developing electrochemical sensors for TCA which show an oxidative peak for IMI at a similar position[224]. As with the previous characterisation of the scaffolds, each scaffolds showed a high level of variability when attempting to detect TCA compounds. In particular, the batch-to-batch variability was such that insufficient replicates were carried out to perform further analysis. From a batch of 4 scaffolds only a single one could be used to generate the data seen in Figure 5-6; indicating a high level of variability, a 25% success rate when n = 4. This suggests that significant optimisation of either the RESOMER® scaffold or the PEDOT:PSS loading formulation is needed. Despite the level of variability peaks are

observable when IMI is at 0.2 mM and above. This suggests that given further develop this platform could perform as a TCA sensor; the therapeutic concentration of TCA compounds in the bloodstream is between 0.5-1.25 mM, which is clearly within the capability of this scaffold. Previous methods for detection of tricyclic compounds have been able to achieve nano and pico molar resolution, greater than the limits presented here[368,369]. However, these methods rely on complex analytical approaches such as chromatography and mass spectrometry; methods which are costly and time consuming. More recent electrochemical methods have been used to achieve detection of 1 – 50 µM[370]. This work used a telluride-graphite nanofiber electrode to detect IMI in both blood and urine with a greater range and sensitivity than the work presented here. This highlights the need for further optimisation of the platform which we have attempted to develop.

5.4 Conclusion

Additive manufacturing techniques have opened new possibilities for the production of medical devices. Here we have demonstrated an ability to use 3D extrusion printing to print a biodegradable scaffold using the commercially available RESOMER® (LR708). Furthermore, we have shown that, via loading with a PEDOT:PSS formulation, we can create an electroactive scaffold that can detect both ideal analytes and therapeutically relevant compounds. This latter conclusion however comes with the caveat that the production method gives rise to a high level of variability; only 1 in every 3 scaffolds can reliably detect redox behaviour. This variability is likely caused by variation in pore size on the outer scaffold; which allows varying amounts of electrolyte into the inner regions of the scaffold, resulting in variation in the electrical behaviour of the PEDOT. Further optimisation of the printing process and additional characterisation to confirm the source of the variability is required. Likewise, we have not confirmed the degradation of the scaffolds, either unloaded or loaded with PEDOT:PSS. While previous work using RESOMER® polymer demonstrates the degradation for drug delivery

applications there is no work exploring the impact 3D printing has on the degradation profile of the scaffolds[371]. This is an avenue that would need to be explored prior to any further development of the scaffolds presented here.

Overall, this demonstrates that it is possible to create biodegradable scaffolds which house electroactive polymers, thereby creating a biodegradable sensing platform. If successfully developed this platform could be used to create a biodegradable electroactive device that would allow for the *in vivo* measurement of therapeutic compounds, one that once no longer needed could biodegrade.

6 Conclusions and Future Work

6.1 Conclusions

The aim of this work was to develop an electrochemical sensor for the *in vivo* monitoring of tricyclic antidepressants. The work presented here has shown the progress made towards this aim.

Firstly, an electroanalytical study was performed to better understand the redox behaviour of TCA compounds. Cyclic voltammetry was used to study six TCA compounds and their redox behaviour was compared to identify any similarities or differences. The redox behaviour for almost all of the compounds was similar to previous literature, with some minor exceptions - in particular clomipramine. Based on scan rate studies an alternate redox mechanism was proposed for this compound. The work presented in chapter 3 confirms that any electrochemical sensor which relies on detecting the oxidation of TCA compounds could theoretically detect any TCA compound which possess a central nitrogen; oxidation of this atom generates a redox signal. This work also confirmed that the potential window needed to detect these compounds lies between +0.8 to +0.9 V. This chapter provided fundamental insight into the redox mechanism of TCA and laid the foundation for the design on an electroanalytical sensor for TCA compounds.

Next, the conductive polymer PEDOT:PSS was chosen to develop an electroactive sensing surface. PEDOT:PSS was chosen was chosen because it is commercially available, it has been used in previous sensing devices and it is easily processed and modified. A blend of PEDOT:PSS and PVA was used to create polymer films which were characterised using Peak Force Tunnelling AFM; a relatively recent advance in AFM technology which can simultaneously gather nano topographic, mechanical and electrical data. This method was used to characterise PEDOT:PSS films supplemented with various additives to modify both the

physical and electrical properties of PEDOT:PSS films. This reinforced previous work into the effect additives have on the electrical and physical properties of PEDOT surfaces; understanding can inform the design of a PEDOT based sensor.

Finally, 3D extrusion printing was used to generate scaffolds using the biodegradable polymer RESOMER®. Following optimisation of printing parameters scaffolds were loaded with a PEDOT:PSS formulation, based on a combination of previous work into PEDOT:PSS and the results presented in chapter 4, and the resulting conductive scaffolds were characterised using cyclic voltammetry. This work revealed a high level of variability in scaffold manufacturing; the scaffolds displayed various types electrical behaviour. One possible explanation for this variability is microscopy variations in the pore size of the scaffolds. Depending on the pore size varying amounts of electrolyte will gain entry into the scaffold, causing PEDOT:PSS to swell which can in turn increase the electrical resistance of PEDOT. Despite the observed variation it was still possible to use the PEDOT:PSS loaded scaffolds to detect redox events. The RESOMER® scaffolds were used to detect the oxidation of the TCA imipramine; square wave voltammetry was able to detect a range of concentrations in PBS. While the concentrations which were detected were within a clinically relevant range the success of that detection was influenced by variations in the scaffolds design.

The work presented here lays the foundation for the development of a novel therapeutic monitoring device. Therapeutic monitoring is a key element in personalised medicine; it can provide crucial insight which informs clinical decision making. Previously therapeutic monitoring relied on lab based techniques to perform analysis of therapeutic target compounds however, there is growing investment in point-of-care technologies for therapeutic monitoring; with a focus on simple, rapid and reliable devices. Likewise, while the field of implantable sensing stands to make a significant impact in personalised medicine it must tackle the challenge all implantable devices must face - the body’s natural response to a foreign object.

The work presented here attempted to address this challenge by designing an implantable electroanalytical sensor which could degrade, providing a means to minimise foreign body response, thus removing the need to explant a device once it is no longer required.

6.2 Future work

While the work presented here provides new insight, as well as progress towards the development of a novel sensing technology, some areas remain unexplored. The following is an attempt to highlight these areas, and describe how best to investigate any areas of future interest.

6.2.1 TCA Redox Behaviour

The results presented here provide insight into the mechanisms involved in TCA redox behaviour. To complete the design and development of an effective TCA sensor, and provide additional fundamental electrochemical understanding, further into the redox mechanism of TCA compounds is needed. Firstly, the electrochemical characterisation presented here should be repeated in a more relevant electrolyte; PBS is a simple solution with very few components that could interfere with the detection of TCA compounds. If an effective sensor is going to be designed it would be useful to determine which components that are present in a complex biological solution could reduce the accuracy of an electrochemical sensor. Any biological electroactive species, such as ascorbic acid, uric acid, or other therapeutic compound, could negatively impact a sensors ability to detect TCA redox. Based on this, the work carried out here should be repeated in a complex biological solution, such as simulated body fluid that has been supplemented with possible interfering species or, ideally, using real patient samples. This information is crucial when designing any electrochemical sensor; it may be necessary to enhance the sensor surface to maximise an analytes signal or reduce background signal.

Secondly, more detailed electrochemical studies would provide deeper understanding of TCA redox behaviour; in particular it would be useful to have additional data about the mechanism involved in dimer formation and the differences between TCA compounds. Previous work has shown that once a TCA dimer is formed it can undergo reversible protonation. Likewise it has been suggested that protons could influence the redox behaviour of TCA compounds prior to dimer formation. In lower pH solutions the presence of increased H+ ions could change the behaviour of both IMI and other TCA compounds, potentially making it easier to detect dimer formation. To determine the impact pH has on TCA redox behaviour more scan rate studies and multi-scan comparisons should be carried out in solutions of various pH. As highlighted the presence of Cl- on the tricyclic ring results in different kinetics for CLO, therefore it would also be useful to determine if varying pH influences this reaction; it could reveal more insight into this mechanism.

Finally, further electrochemical studies of TCA compounds could be carried out using the novel sensing platform developed in subsequent chapters. The electrode used in chapter 3 to study TCA redox was an unmodified glassy carbon electrode. While this electrode provides a good enough surface to carry out electroanalytical studies a modified surface, such as the PEDOT surface developed in later chapters, could provide additional, and more relevant, insight into electron transfer kinetics. As such the RESOMER®:PEDOT scaffold developed in later work could be used not only as a sensor but as an analytical device for studying redox behaviour. The increased surface area provided by the porous nature of PEDOT could improve the signal produced by TCA oxidation and the dimer reduction, thereby making it possible to study these redox events in more detail.

6.2.2 Characterisation of polymer blends using PF-TUNA AFM

The work presented in chapter 4 demonstrates the capability of PF-TUNA AFM as a method for characterising polymer blends and studying the impact additives have on polymer film behaviour. However, significantly more work could be carried out to provide fundamental understanding of the properties of conductive polymer films and study their surface behaviour to support the development of novel bioelectronic devices**.**

Firstly, the approach shown here could be used to characterise additional polymer blends; to develop a greater understanding of how PEDOT:PSS blends with other polymers. As discussed PEDOT has already been blended with PVA to create various types of films for bioelectronic purposes. However, it has also been combined with other polymers and more advanced materials for a range of purposes. This includes electrodes made from PEDOT which have been chemically modified with ethylene glycol, blended with polyurethane, or mixed with acrylic acid[275,372,373]. In all of these cases, the materials could be studied using AFM-TUNA to provide insight into how PEDOT interacts with other polymers and additives.

Additional work could also focus on how other advanced materials impact the PEDOT:PSS:PVA blend; for instance carbon nanotubes (CNTs). CNTs have already been mixed with PEDOT for a range of applications; with a focus on the development of neural electrodes for tissue engineering applications and the sensing and recording of neural electrical signals[374–376]. However, there has been limited investigation of the surface topography and nanoscale electrical behaviour of these materials. As PF-TUNA can provide nanoscale resolution it could be used to determine how CNTs interact with PEDOT and the impact they have on PEDOT films; to provide insight for the development and design of novel surfaces.

While the PF-TUNA data presented here provides an initial characterisation of the PEDOT:PSS:PVA electrode surfaces, if this material were to be used for sensing applications additional electrochemical characterisation is needed at both the macro and nano scale. At the

nanoscale this could be achieve by additional probe microscopy techniques, in particular scanning electrochemical microscopy (SECM). SECM uses a scanning probe to measure the local electrochemical activity of a surface[377]. When in close proximity to a surface an electrical signal is measured by the probe as it interacts with a redox mediator that is present in the solution surrounding the probe and surface. The signal that is produced is affected by the probes proximity to the surface and the surfaces conductivity. By measuring the resulting signal SECM can produce a map of electrochemical activity and topography. Previously, SECM relied on ultramicroelectrodes which were between 5 - 25 μm; this made it difficult to achieve sub-micrometre resolution. However, recent advances in SECM have coupled the technique with AFM and reduced the size of the probe to the nanoscale; improving the resolution of both topography and electrochemical measurements to the nanoscale[378].

Alongside the PF-TUNA results presented here SECM could be used to provide an understanding of the electrochemical activity of the PEDOT:PSS:PVA films. Understanding the electrochemical properties of the PEDOT:PS:PVA blend at the nanoscale would provide fundamental understanding about the redox events that occur at the PEDOT:PSS:PVA surface. This understanding is important because it is necessary to determine if the PEDOT surfaces act as either macro, micro or nano electrodes. This is because macro and micro electrodes have predictable characteristics and the movement of electroactive species to the surface will occur under either planar or radial diffusion[379]. However, at nanoelectrodes diffusion can be a mix of the two; therefore SECM could provide insight into how diffusion at a PEDOT surface occurs. Furthermore, SECM can provide additional insight into how polymer blending and the presence of additives impacts the films redox activity. All of this information is important because PEDOT:PSS is becoming a common choice for the design of bioelectronic materials. Likewise, nanoscale devices are also a popular choice for bioelectronic devices due to the advantages they offer in biocompatibility. As such understanding how PEDOT:PSS, polymer blends of PEDOT

and PEDOT additives behave at the nanoscale could be crucial to designing more effective bioelectronic devices.

Further work is also needed to characterise the PEDOT:PSS:PVA electrodes at the macroscale. This would involve a combination of electrochemical impedance spectroscopy (EIS) and voltammetric methods. EIS involves applying an alternating current potential to an electrochemical cell and then measuring the resulting current[202,380]. This technique would allow the design of equivalent circuits and provide information on the surface phenomenon taking place at the PEDOT:PSS:PVA surface. Comparing these properties across different samples would provide insight into which blends and which additives have the greatest impact on the conductive properties of PEDTO:PSS:PVA films. Likewise, cyclic voltammetry could be used to determine if the PEDOT:PSS films have any inherent redox properties and determine how effective they would be at detecting the redox behaviour of other analytes. Previous work has shown that PEDOT can suffer from over-oxidation which causes degradation of the polymer[363]. However, some evidence indicates that over oxidised PEDOT films actual show an improved capacity for ion sensing[381]. Based on this, it would be useful to determine if PEDOT:PSS:PVA films behave in a similar way; whether they show a change in electroactivty following overoxidation.

A combination of macro, micro and nano scale analysis would provide a detailed understanding of the electrical properties of PEDOT:PSS:PVA blends and the impact of additives, this knowledge would then inform the design of PEDOT electrodes which could be optimised for sensing.

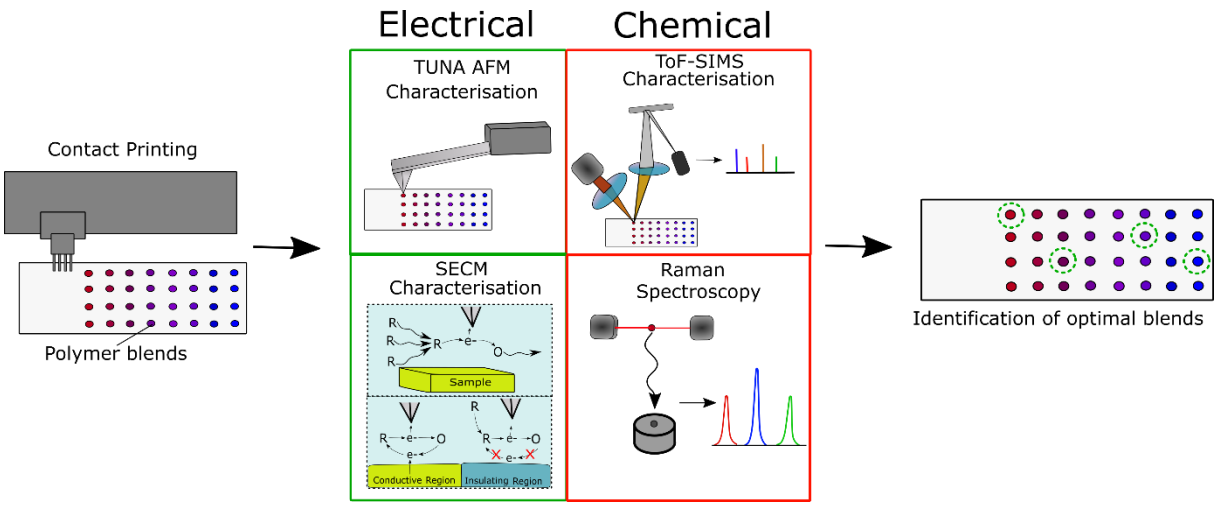

Figure 6-1 schematic outlining an optimised workflow for the electrical and chemical characterisation of PEDOT blends to identify target formulations

Finally, a more methodical and high-throughput approach could be used to characterise the PEDOT:PSS:PVA blend and additive modified films. One of the most significant drawbacks to the characterisation of the PEDOT:PSS:PVA films presented here was the time taken to produce samples; each film took 24 hours to produce. While multiple films were produced simultaneously, an alternative approach would speed up the process. This would allow more samples to be analysed, producing a greater volume of data about the properties of the PEDOT films. One solution would be the use of micro-manufacturing to produce a high number of micro films in rapid succession. This could be achieved using solid pin contact printing, which relies on pins to pick up several µL of pre-mixed polymer solution which is then depositing onto a substrate[382,383]. A contact printer can produce a micro-array of several hundred samples, significantly increasing the number of polymer blends which can be produced. In the work shown here increments of 10% PEDOT were used for the PEDOT:PSS:PVA blend. Likewise, only one concentration of additive was assessed, which was based on values presented in other literature. To improve these results a microarray printer could be used to produce samples with a greater number of variables; such as increasing PEDOT by 1% or including a range of additive

concentrations. Micro-array printing would enhance the production of samples, taking it from small scale production to high-throughput.

A similar method could be used for the analysis of samples (Figure 6-1). Once a micro-array has been produced each polymer sample could be analysed in rapid succession using various methods. Firstly, electrical characterisation could be performed using a combination of PF-TUNA and SECM. This would provide a detailed map of both topography and electrical current and assess the ability of each sample to initiate or sense redox activity. The polymer micro-array could then be chemically characterised. This would involve the use of Time-of-Flight Secondary Ion Mass spectrometry, which uses a primary ion beam to produce secondary ions which are measured using mass spectrometery. This would produce a chemical map which, in the case of polymer blends, would show how the polymers are distributed throughout the film. This approach has already been used for the high-throughput assessment of ink-jet printed acrylate monomers, therefore it could be used to assess the structure of PEDOT:PSS:PVA films[384]. Similarly, a secondary chemical mapping technique could be used, such as Raman spectroscopy or X-ray photoelectron spectroscopy, to generate additional chemical data from the polymer micro array.

Using a high-throughput approach would provide a means to assess an array of PEDOT samples and provide a wealth of knowledge including chemical mapping, electrical data and nanoscale redox characterisation. This approach could identify which samples on the PEDOT array possess the properties most suited for a desired application. In particular, understanding surface chemistry is crucial when designing a possible bioelectronic implant; it determines how the device will interact with biological tissue. Likewise, having a detailed understanding of electrical behaviour, at the micro and nanoscale, will inform the design of the surface; the surface may need to be modified to improve signal-to-noise or to target a specific analyte of interest.

This high-throughput approach has already been demonstrated, however much of this work has focused on the interaction between a biomaterial and small populations of cells[385,386]. In contrast, the approach suggested here would assess PEDOT blends and additives which are mostly likely to be effective as a bioelectronic material. If this approach were successful it could be adapted to assess other bioelectronic materials, which could provide insight to improve the design of numerous bioelectronic devices.

6.2.3 Development of RESOMER®:PEDOT Scaffolds

The work presented here highlights the design and initial optimisation of a PEDOT:RESOMER® scaffold for therapeutic sensing. While this acts as a proof-of-concept for a novel sensing platform further work is needed to validate and build on these results.

The PEDOT formulation, used to load the RESOMER® scaffolds, must be optimised to ensure the electroactive surface can specifically detect the target analyte, in this case TCA. As outlined above, this could be achieved using a high-throughput screening approach. Printing a range of PEDOT samples, containing various PEDOT additives, and analysing the electrical and chemical activity of dried micro-dots of PEDOT would provide insight into how additives impact surface behaviour. This insight could be fed forward to design a formulation with optimal properties. This would include high conductivity, a large surface area and the ability to detect redox events; these are essential properties for a device which is going to act as an electrochemical sensor. Based on this approach, one or more lead blends could be identified which are most likely to be effective as a loading compound in the RESOMER® scaffolds. Once a suitable loading formulation has been developed additional electrical characterisation would need to be performed; beyond the voltammetry which was presented in this work electrochemical impedance spectroscopy (EIS) could provide further insight into to the electrical behaviour of the scaffolds.

Next, the RESOMER® scaffolds themselves would need to be characterised. This would include additional surface characterisation, such as scanning electron microscopy (SEM) to study the surface structure of the RESOMER® scaffolds. This work would be used to investigate the source of the variation which was observed in the current scaffold design. SEM could be used to determine the size of the pores present on the outer scaffold, and how pore size varies between samples. This could then inform the design of more reliable scaffolds.

The scaffolds should also be chemically characterised, with a focus on the chemical composition of the dried scaffolds. While RESOMER® should be the primary component, the ink used to print the scaffolds contains dichloromethane (DCM), which is a volatile organic compound. Before the scaffolds could be developed further it would be necessary to determine that, during the drying process, the majority of DCM evaporates. This could be confirmed via ToF-SIMS; scaffolds could be analysed to determine if DCM is present once they have been dried, and at what concentration. RESOMER® is designed to degrade when implanted therefore if any DCM were present, as the scaffold degrades it would be released into the surrounding environment, which would pose a significant risk.

The aim of this work was to develop a device which could be implanted and measure TCA concentration *in vivo*. To achieve this aim we would need to understand how a loaded PEDOT:RESOMER® scaffold would behave in a biological environment, and if it could maintain its function over an extended period of time. Previous work using the biodegradable RESOMER® polymer has focused on drug delivery applications. This includes the development of nanoparticles for the delivery of anti-cancer agents, such as Sorafenib and Doxorubicin, and the use of polymeric microspheres for delivery of antivirals[345,346,387]. While RESOMER® has also been used in the development of degradable implants these examples are more limited; such as the design of bone matrix coatings for the release of a model protein and the development of a polyester prosthetic blood vessel with a RESOMER® coating[347,388]. While

this previous work has studied the degradation of RESOMER® there is no data concerning the degradation of 3D printed RESOMER® scaffolds. This is an area that would need to be explored, with a focus on the degradation rate of the scaffolds, their mechanical strength following contact with biological solution and how scaffold degradation impacts their ability to store the PEDOT loading formulation. Furthermore, different variations of RESOMER® are available; each made using different co-polymers and polymer ratios. This can be used to control the degradation time of the polymer; of those which are commercially available the time scale varies from 4 weeks to 3 years[389]. It would be useful to assess if these different RESOMER® polymers are as printable as the one presented here. This is especially important when considering the final application of the scaffolds; it may be necessary to tailor the degradation time to a desired application.

Additional characterisation of the PEDOT loaded scaffolds would also confirm that they are able to maintain their function in a complex biological environment. While the work here has shown that the scaffolds can detect the oxidation of the IMI, this was carried out in ideal conditions using a simply electrolyte (PBS). To further demonstrate proof-of-concept this would need to be repeated for multiple TCA compounds, in a more complex environment. Initially, this would include detection of TCA in simulated body fluids in the presence of possible interfering compounds. Following this, if the scaffolds were unable to detect TCA oxidation, either the loading formulation would need to be adjusted, to maximise signal, or an additional targeting component would need to be added. In the latter case, one possible solution would be the use of molecularly imprinted polymer (MIP), which would selectively bind TCA compounds, increasing the signal detected by the scaffolds. The use of MIP for detection of TCA has recently been achieved using thin films, therefore this option could be incorporated into the RESOMER® scaffold[390].

Once the scaffolds can reliably detect TCA in complex biological fluid, either simulated or using real patient samples, we would then need to determine how the loaded scaffolds interact with biological tissue. The interaction between RESOMER® polymers and cells has been well documented. Work which has examined the interaction between various RESOMER® types and stem cells has shown positive cytocompatibility, support of cell adhesion and proliferation and the inhibition of apoptosis[391,392]. This suggests that RESOMER® would have a positive interaction with biological tissue when implanted, however until more *in vivo* data has been generated this can only be hypothesised.

Additional data would need to be collected regarding the degradation and biological interaction of the PEDOT loading formulation. PEDOT is currently a popular bioelectronic material because of the data available concerning its biocompatibility. This includes the interaction of PEDOT both *in vitro* and *in vivo*[324,327,374]. Based on current literature PEDOT appears to be biocompatible, and will likely have little direct impact when used within an implant, such as the scaffolds presented here. However, currently there is limited data available regarding the degradation of PEDOT; there is no commercially available PEDOT implant. This is primarily because of difficulty with the approval of PEDOT. PEDOT cannot be approved as an individual polymer; a product containing PEDOT must be assessed based on its method of manufacture, the presence of additives or any chemical modifications which have taken place[393]. As such there is no data about how a PEDOT implant actually functions, if, or how, it degrades and whether it is excreted from the body. These are questions which would need to be answered before an implant containing PEDOT could be developed.

In the long term it would also be necessary to plan how this RESOMER®:PEDOT scaffold would function, if it were to become an implantable device. The biggest challenges with an implantable electronic device are keeping the device powered and ensuring it can communicate

with external components. In the case of this implant, one solution would be the use of an external device placed in near-contact with the implant. A similar approach has recently been used by the Freestyle Libre glucose sensing system. This sensor relies on an external applicator to pierce the outer layer of dermis, allowing the sensor to gain *in vivo* access and perform analysis and data collection[394]. This system could be adapted to suit the RESOMER®:PEDOT scaffold; a micro needle could be used to provide the electrical stimulation needed to generate a redox signal at the PEDOT surface.

The final limitation to the proposed sensor is how to transmit the signal from the surface of the electrode, when *in vivo*, to an external source for data analysis. Firstly, near-field communication could be used to both supply power to the device and receive the resulting signal. NFC is already an established technology which relies on the inductive coupling between two antennas. NFC technology is already being explored as a means to power *in vivo* electronics, as well as a communication tool for medical implants[395,396]. This technology could be implanted as part of the scaffold; the scaffold design could be altered to include a wireless coupling electrode. This approach would allow an electrical current to be generated at the surface of the electrode, which would then trigger the redox of TCA compounds present near the electrode, this data would then be transmitted back via the NFC system. This system would provide a novel method for the wireless detection of therapeutic compounds.

Overall, a number of avenues remain unexplored in regard to the development of the PEDOT:RESOMER® scaffolds presented here. However, the understanding of TCA electrochemical behaviour, analysis of the electrical properties PEDOT surfaces and the design and development of a biodegradable scaffold are the first steps in developing an *in vivo* TCA sensor. Further development of this work would push forward the field of bioelectronics by

opening new avenues of research, contribute to diagnostic technology and improve patient care. The work presented here lays the foundation for these developments.

7 References

1. Centers for Disease Control and Prevention (CDC. Ten great public health achievements--United States, 1900-1999. *MMWR. Morbidity and mortality weekly report* **48**, 241–243 (1999).
2. Lee, R. *The Eureka! Moment: 100 Key Scientific Discoveries of the 20th Century*. (Taylor & Francis, 2016).
3. Ventola, C. L. Progress in Nanomedicine: Approved and Investigational Nanodrugs. *P T* **42**, 742–755 (2017).
4. Dzobo, K. *et al.* Advances in Regenerative Medicine and Tissue Engineering: Innovation and Transformation of Medicine. *Stem Cells International* **2018**, 2495848 (2018).
5. Nair, A. B. & Jacob, S. A simple practice guide for dose conversion between animals and human. *J Basic Clin Pharm* **7**, 27–31 (2016).
6. GlaxoSmithKline plc. GSK 2019 Annual Report. *2019*.
7. Pasipanodya, J. G., Srivastava, S. & Gumbo, T. Meta-analysis of clinical studies supports the pharmacokinetic variability hypothesis for acquired drug resistance and failure of antituberculosis therapy. *Clinical Infectious Diseases* **55**, 169–177 (2012).
8. Fabbiani, M. *et al.* Pharmacokinetic variability of antiretroviral drugs and correlation with virological outcome: 2 years of experience in routine clinical practice. *Journal of antimicrobial chemotherapy* **64**, 109–117 (2009).
9. Rang, H. P. & Dale, M. M. *Rang and Dale's pharmacology*. (Elsevier Brasil, 2007).

10. Gedawy, A., Martinez, J., Al-Salami, H. & Dass, C. R. Oral insulin delivery: existing barriers and current counter-strategies. *Journal of pharmacy and pharmacology* **70**, 197–213 (2018).

11. M Ramesan, R. & P Sharma, C. Recent advances in the oral delivery of insulin. *Recent Patents on Drug Delivery & Formulation* **8**, 155–159 (2014).

12. Anderson, G. D. Gender differences in pharmacological response. *International review of neurobiology* **83**, 1–10 (2008).

13. Sarfati, D., Koczwara, B. & Jackson, C. The impact of comorbidity on cancer and its treatment. *CA: a cancer journal for clinicians* **66**, 337–350 (2016).

14. Pan, S., Zhu, L., Chen, M., Xia, P. & Zhou, Q. Weight-based dosing in medication use: what should we know? *Patient preference and adherence* **10**, 549 (2016).

15. Soldin, O. P. & Mattison, D. R. Sex differences in pharmacokinetics and pharmacodynamics. *Clinical pharmacokinetics* **48**, 143–157 (2009).

16. Shi, S. & Klotz, U. Age-related changes in pharmacokinetics. *Current drug metabolism* **12**, 601–610 (2011).

17. De Baerdemaeker, L. E., Mortier, E. P. & Struys, M. M. Pharmacokinetics in obese patients. *Continuing Education in Anaesthesia, Critical Care & Pain* **4**, 152–155 (2004).

18. Katzung, B. G., Masters, S. B. & Trevor, A. J. Basic & clinical pharmacology. (2004).

19. Hamberg, A. *et al.* A PK–PD model for predicting the impact of age, CYP2C9, and VKORC1 genotype on individualization of warfarin therapy. *Clinical Pharmacology & Therapeutics* **81**, 529–538 (2007).

20. Backman, J. T., Filppula, A. M., Niemi, M. & Neuvonen, P. J. Role of cytochrome P450 2C8 in drug metabolism and interactions. *Pharmacological reviews* **68**, 168–241 (2016).

21. Aschenbrenner, D. S. FDA's 2019 Annual Report Highlights New Drugs and New Uses. *AJN The American Journal of Nursing* **120**, 23 (2020).

22. Brittain, H. K., Scott, R. & Thomas, E. The rise of the genome and personalised medicine. *Clinical Medicine* **17**, 545 (2017).

23. Wilsdon, T., Barron, A., Edwards, G. & Lawlor, R. The benefits of personalised medicine to patients, society and healthcare systems. *Charles River Assoc* **2018**, 1–72 (2018).

24. Pauker, S. G. & Kassirer, J. P. Decision analysis. *New England Journal of Medicine* **316**, 250–258 (1987).

25. England, N. Creating a genomic medicine service to lay the foundation to deliver personalised interventions and treatments. 2017. (2017).

26. All of Us Research Program Investigators. The "All of Us" research program. *New England Journal of Medicine* **381**, 668–676 (2019).

27. Dean, L. Dabrafenib therapy and BRAF and G6PD genotype. *Medical Genetics Summaries [Internet]* (2017).

28. Endo-Tsukude, C. *et al.* Population pharmacokinetics and adverse events of erlotinib in Japanese patients with non-small-cell lung cancer: impact of genetic polymorphisms in metabolizing enzymes and transporters. *Biological and Pharmaceutical Bulletin* **41**, 47–56 (2018).

29. Nagel, B., Dellweg, H. & Gierasch, L. Glossary for chemists of terms used in biotechnology (IUPAC Recommendations 1992). *Pure and Applied Chemistry* **64**, 143–168 (1992).

30. Thévenot, D. R., Toth, K., Durst, R. A. & Wilson, G. S. Electrochemical biosensors: recommended definitions and classification1International Union of Pure and Applied Chemistry: Physical Chemistry Division, Commission I.7 (Biophysical Chemistry); Analytical Chemistry Division, Commission V.5 (Electroanalytical Chemistry).1. *Biosensors and Bioelectronics* **16**, 121–131 (2001).

31. Clark JR, L. C., Wolf, R., Granger, D. & Taylor, Z. Continuous recording of blood oxygen tensions by polarography. *Journal of applied physiology* **6**, 189–193 (1953).

32. Bhalla, N., Jolly, P., Formisano, N. & Estrela, P. Introduction to biosensors. *Essays Biochem* **60**, 1–8 (2016).

33. Healy, D. A., Hayes, C. J., Leonard, P., McKenna, L. & O'Kennedy, R. Biosensor developments: application to prostate-specific antigen detection. *TRENDS in Biotechnology* **25**, 125–131 (2007).

34. Saylan, Y., Erdem, Ö., Ünal, S. & Denizli, A. An alternative medical diagnosis method: biosensors for virus detection. *Biosensors* **9**, 65 (2019).

35. Meneghello, A., Tartaggia, S., Alvau, M. D., Polo, F. & Toffoli, G. Biosensing technologies for therapeutic drug monitoring. *Current medicinal chemistry* **25**, 4354–4377 (2018).

36. Justino, C. I., Duarte, A. C. & Rocha-Santos, T. A. Recent progress in biosensors for environmental monitoring: a review. *Sensors* **17**, 2918 (2017).

37. Clark, L. C. & Lyons, C. Electrode systems for continuous monitoring in cardiovascular surgery. *Ann. N. Y. Acad. Sci.* **102**, 29–45 (1962).

38. Weibel, M. K. & Bright, H. J. The glucose oxidase mechanism: interpretation of the pH dependence. *Journal of Biological Chemistry* **246**, 2734–2744 (1971).

39. Newman, J. D. & Turner, A. P. Home blood glucose biosensors: a commercial perspective. *Biosensors and bioelectronics* **20**, 2435–2453 (2005).

40. Rajendran, R. & Rayman, G. Point-of-Care Blood Glucose Testing for Diabetes Care in Hospitalized Patients: An Evidence-Based Review. *J Diabetes Sci Technol* **8**, 1081–1090 (2014).

41. Hiom, S. C. Diagnosing cancer earlier: reviewing the evidence for improving cancer survival. *British Journal of Cancer* **112**, S1–S5 (2015).

42. Vincent, J.-L. The clinical challenge of sepsis identification and monitoring. *PLoS medicine* **13**, e1002022 (2016).

43. Blix, H. S., Viktil, K. K., Moger, T. A. & Reikvam, A. Drugs with narrow therapeutic index as indicators in the risk management of hospitalised patients. *Pharmacy practice* **8**, 50 (2010).

44. Goodman, L. S. *Goodman and Gilman's the pharmacological basis of therapeutics*. vol. 1549 (McGraw-Hill New York, 1996).

45. Roberts, J. A., Norris, R., Paterson, D. L. & Martin, J. H. Therapeutic drug monitoring of antimicrobials. *British journal of clinical pharmacology* **73**, 27–36 (2012).

46. Kang, J.-S. & Lee, M.-H. Overview of Therapeutic Drug Monitoring. *The Korean Journal of Internal Medicine* **24**, 1–10 (2009).

47. Niemz, A., Ferguson, T. M. & Boyle, D. S. Point-of-care nucleic acid testing for infectious diseases. *Trends in biotechnology* **29**, 240–250 (2011).

48. Clerc, O. & Greub, G. Routine use of point-of-care tests: usefulness and application in clinical microbiology. *Clinical microbiology and infection* **16**, 1054–1061 (2010).

49. Saha, K., Agasti, S. S., Kim, C., Li, X. & Rotello, V. M. Gold nanoparticles in chemical and biological sensing. *Chemical reviews* **112**, 2739–2779 (2012).

50. Li, Y., Schluesener, H. J. & Xu, S. Gold nanoparticle-based biosensors. *Gold Bulletin* **43**, 29–41 (2010).

51. Ma, F., Li, C. & Zhang, C. Development of quantum dot-based biosensors: principles and applications. *Journal of Materials Chemistry B* **6**, 6173–6190 (2018).

52. Lin, Y.-Y. *et al.* A nanoparticle label/immunochromatographic electrochemical biosensor for rapid and sensitive detection of prostate-specific antigen. *Biosensors and Bioelectronics* **23**, 1659–1665 (2008).

53. Singh, R. D. *et al.* Quantum dot based nano-biosensors for detection of circulating cell free miRNAs in lung carcinogenesis: from biology to clinical translation. *Frontiers in genetics* **9**, 616 (2018).

54. Tîlmaciu, C.-M. & Morris, M. C. Carbon nanotube biosensors. *Frontiers in Chemistry* **3**, 59 (2015).

55. Choi, Y. *et al.* Dissecting single-molecule signal transduction in carbon nanotube circuits with protein engineering. *Nano letters* **13**, 625–631 (2013).

56. Schroeder, V., Savagatrup, S., He, M., Lin, S. & Swager, T. M. Carbon nanotube chemical sensors. *Chemical reviews* **119**, 599–663 (2018).

57. Snow, E., Perkins, F., Houser, E., Badescu, S. & Reinecke, T. Chemical detection with a single-walled carbon nanotube capacitor. *Science* **307**, 1942–1945 (2005).

58. Sarkar, T., Srinives, S., Rodriquez, A. & Mulchandani, A. Single-walled Carbon Nanotube-Calixarene Based Chemiresistor for Volatile Organic Compounds. *Electroanalysis* **30**, 2077–2084 (2018).

59. Murugathas, T. *et al.* Biosensing with insect odorant receptor nanodiscs and carbon nanotube field-effect transistors. *ACS applied materials & interfaces* **11**, 9530–9538 (2019).

60. Zhang, J. *et al.* A rapid, direct, quantitative, and label-free detector of cardiac biomarker troponin T using near-infrared fluorescent single-walled carbon nanotube sensors. *Advanced healthcare materials* **3**, 412–423 (2014).

61. Arkan, E., Saber, R., Karimi, Z. & Shamsipur, M. A novel antibody–antigen based impedimetric immunosensor for low level detection of HER2 in serum samples of breast cancer patients via modification of a gold nanoparticles decorated multiwall carbon nanotube-ionic liquid electrode. *Analytica chimica acta* **874**, 66–74 (2015).

62. Izadi, Z., Sheikh-Zeinoddin, M., Ensafi, A. A. & Soleimanian-Zad, S. Fabrication of an electrochemical DNA-based biosensor for Bacillus cereus detection in milk and infant formula. *Biosensors and Bioelectronics* **80**, 582–589 (2016).

63. Nantaphol, S., Chailapakul, O. & Siangproh, W. A novel paper-based device coupled with a silver nanoparticle-modified boron-doped diamond electrode for cholesterol detection. *Analytica chimica acta* **891**, 136–143 (2015).

64. Wang, Y. & Alocilja, E. C. Gold nanoparticle-labeled biosensor for rapid and sensitive detection of bacterial pathogens. *Journal of biological engineering* **9**, 1–7 (2015).

65. Ng, B. Y. *et al.* Rapid, single-cell electrochemical detection of Mycobacterium tuberculosis using colloidal gold nanoparticles. *Analytical chemistry* **87**, 10613–10618 (2015).

66. Wang, Y. *et al.* Loop-mediated isothermal amplification label-based gold nanoparticles lateral flow biosensor for detection of Enterococcus faecalis and Staphylococcus aureus. *Frontiers in microbiology* **8**, 192 (2017).

67. Gong, Y. *et al.* A portable and universal upconversion nanoparticle-based lateral flow assay platform for point-of-care testing. *Talanta* **201**, 126–133 (2019).

68. Bandodkar, A. J. *et al.* Tattoo-based noninvasive glucose monitoring: a proof-of-concept study. *Analytical chemistry* **87**, 394–398 (2015).

69. Kong, D. *et al.* Protein–inorganic hybrid nanoflower-rooted agarose hydrogel platform for point-of-care detection of acetylcholine. *ACS applied materials & interfaces* **11**, 11857–11864 (2019).

70. Jiang, C., Li, Y., Wang, H., Chen, D. & Wen, Y. A portable visual capillary sensor based on functional DNA crosslinked hydrogel for point-of-care detection of lead ion. *Sensors and Actuators B: Chemical* **307**, 127625 (2020).

71. Liu, S., Su, W., Li, Y., Zhang, L. & Ding, X. Manufacturing of an electrochemical biosensing platform based on hybrid DNA hydrogel: Taking lung cancer-specific miR-21 as an example. *Biosensors and Bioelectronics* **103**, 1–5 (2018).

72. Soler, M. *et al.* Multiplexed nanoplasmonic biosensor for one-step simultaneous detection of Chlamydia trachomatis and Neisseria gonorrhoeae in urine. *Biosensors and Bioelectronics* **94**, 560–567 (2017).

73. Li, Z. *et al.* Pen-on-paper strategy for point-of-care testing: Rapid prototyping of fully written microfluidic biosensor. *Biosensors and Bioelectronics* **98**, 478–485 (2017).

74. Lakey, A. *et al.* Impedimetric array in polymer microfluidic cartridge for low cost point-of-care diagnostics. *Biosensors and Bioelectronics* **129**, 147–154 (2019).

75. Mandal, N. *et al.* PSA detection using label free graphene FET with coplanar electrodes based microfluidic point of care diagnostic device. *Talanta* **222**, 121581 (2021).

76. Takemura, K. *et al.* Versatility of a localized surface plasmon resonance-based gold nanoparticle-alloyed quantum dot nanobiosensor for immunofluorescence detection of viruses. *Biosensors and Bioelectronics* **89**, 998–1005 (2017).

77. Wang, C. *et al.* Magnetic quantum dot based lateral flow assay biosensor for multiplex and sensitive detection of protein toxins in food samples. *Biosensors and Bioelectronics* **146**, 111754 (2019).

78. Wadhwa, S., John, A. T., Nagabooshanam, S., Mathur, A. & Narang, J. Graphene quantum dot-gold hybrid nanoparticles integrated aptasensor for ultra-sensitive detection of vitamin D3 towards point-of-care application. *Applied Surface Science* **521**, 146427 (2020).

79. Rong, Z. *et al.* Dual-color magnetic-quantum dot nanobeads as versatile fluorescent probes in test strip for simultaneous point-of-care detection of free and complexed prostate-specific antigen. *Biosensors and Bioelectronics* **145**, 111719 (2019).

80. Ziegler, A., Koch, A., Krockenberger, K. & Großhennig, A. Personalized medicine using DNA biomarkers: a review. *Human genetics* **131**, 1627–1638 (2012).

81. Siwy, J., Mischak, H. & Zürbig, P. Proteomics and personalized medicine: a focus on kidney disease. *Expert review of proteomics* **16**, 773–782 (2019).

82. Emamzadeh, F. N. & Surguchov, A. Parkinson's disease: biomarkers, treatment, and risk factors. *Frontiers in neuroscience* **12**, 612 (2018).

83. Ensom, M. H., Davis, G. A., Cropp, C. D. & Ensom, R. J. Clinical pharmacokinetics in the 21st century. *Clinical pharmacokinetics* **34**, 265–279 (1998).

84. Gross, A. S. Best practice in therapeutic drug monitoring. *British journal of clinical pharmacology* **46**, 95–99 (1998).

85. Ates, H. C. *et al.* On-site therapeutic drug monitoring. *Trends in Biotechnology* (2020).

86. Buclin, T. *et al.* The steps to therapeutic drug monitoring: A structured approach illustrated with imatinib. *Frontiers in pharmacology* **11**, 177 (2020).

87. Taylor, I. W. & Tattersall, M. H. Methotrexate cytotoxicity in cultured human leukemic cells studied by flow cytometry. *Cancer Research* **41**, 1549–1558 (1981).

88. Paci, A. *et al.* Review of therapeutic drug monitoring of anticancer drugs part 1–cytotoxics. *European journal of cancer* **50**, 2010–2019 (2014).

89. Parachalil, D. R. *et al.* Raman spectroscopy as a potential tool for label free therapeutic drug monitoring in human serum: the case of busulfan and methotrexate. *Analyst* **144**, 5207–5214 (2019).

90. Zhao, S. S. *et al.* Miniature multi-channel SPR instrument for methotrexate monitoring in clinical samples. *Biosensors and Bioelectronics* **64**, 664–670 (2015).

91. Yockell-Lelièvre, H., Bukar, N., Toulouse, J., Pelletier, J. & Masson, J.-F. Naked-eye nanobiosensor for therapeutic drug monitoring of methotrexate. *Analyst* **141**, 697–703 (2016).

92. Breda, M. & Barattè, S. A review of analytical methods for the determination of 5-fluorouracil in biological matrices. *Analytical and bioanalytical chemistry* **397**, 1191–1201 (2010).

93. Baj-Rossi, C., Micheli, G. D. & Carrara, S. Electrochemical detection of anti-breast-cancer agents in human serum by cytochrome P450-coated carbon nanotubes. *Sensors* **12**, 6520–6537 (2012).

94. Alvau, M. D. *et al.* Enzyme-based electrochemical biosensor for therapeutic drug monitoring of anticancer drug irinotecan. *Analytical chemistry* **90**, 6012–6019 (2018).

95. Aslam, B. *et al.* Antibiotic resistance: a rundown of a global crisis. *Infection and drug resistance* **11**, 1645 (2018).

96. Bruch, R. *et al.* Clinical on-site monitoring of ß-lactam antibiotics for a personalized antibiotherapy. *Scientific reports* **7**, 1–10 (2017).

97. Kling, A. *et al.* Multianalyte antibiotic detection on an electrochemical microfluidic platform. *Analytical chemistry* **88**, 10036–10043 (2016).

98. Zhu, Y. *et al.* Simple, rapid and sensitive detection of antibiotics based on the side-by-side assembly of gold nanorod probes. *Biosensors and Bioelectronics* **26**, 4387–4392 (2011).

99. Ranamukhaarachchi, S. A. *et al.* Integrated hollow microneedle-optofluidic biosensor for therapeutic drug monitoring in sub-nanoliter volumes. *Scientific reports* **6**, 1–10 (2016).

100. Rawson, T. M. *et al.* Microneedle biosensors for real-time, minimally invasive drug monitoring of phenoxymethylpenicillin: a first-in-human evaluation in healthy volunteers. *The Lancet Digital Health* **1**, e335–e343 (2019).

101. Patsalos, P. N., Spencer, E. P. & Berry, D. J. Therapeutic drug monitoring of antiepileptic drugs in epilepsy: a 2018 update. *Therapeutic drug monitoring* **40**, 526–548 (2018).

102. van Dijkman, S. C., Wicha, S. G., Danhof, M. & Della Pasqua, O. E. Individualized dosing algorithms and therapeutic monitoring for antiepileptic drugs. *Clinical Pharmacology & Therapeutics* **103**, 663–673 (2018).

103. Patel, M. X. *et al.* Plasma olanzapine in relation to prescribed dose and other factors: data from a therapeutic drug monitoring service, 1999-2009. *Journal of clinical psychopharmacology* **31**, 411–417 (2011).

104. Mitchell, P. B. Therapeutic drug monitoring of antidepressant and antipsychotic drugs. in *Handbook of Analytical Separations* vol. 7 257–275 (Elsevier, 2020).

105. Astles, J. R. & Miller, W. G. Measurement of free phenytoin in blood with a self-contained fiber-optic immunosensor. *Analytical chemistry* **66**, 1675–1682 (1994).

106. Huang, L.-S. *et al.* Detection of the antiepileptic drug phenytoin using a single free-standing piezoresistive microcantilever for therapeutic drug monitoring. *Biosensors and Bioelectronics* **59**, 233–238 (2014).

107. Medyantseva, E. *et al.* Determination of antidepressants using monoamine oxidase amperometric biosensors based on screen-printed graphite electrodes modified with multi-walled carbon nanotubes. *Pharmaceutical Chemistry Journal* **48**, 478–482 (2014).

108. dos Santos Neto, A. G. *et al.* Electrochemical sensor for detection of imipramine antidepressant at low potential based on oxidized carbon nanotubes, ferrocenecarboxylic acid, and cyclodextrin: application in psychotropic drugs and urine samples. *Journal of Solid State Electrochemistry* **22**, 1385–1394 (2018).

109. Åsberg, M., Cronholm, B., Sjöqvist, F. & Tuck, D. Correlation of subjective side effects with plasma concentrations of nortriptyline. *Br Med J* **4**, 18–21 (1970).

110. Machado-Vieira, R. *et al.* The timing of antidepressant effects: a comparison of diverse pharmacological and somatic treatments. *Pharmaceuticals* **3**, 19–41 (2010).

111. Stassen, H. H. & Angst, J. Delayed onset of action of antidepressants. *CNS drugs* **9**, 177–184 (1998).

112. Peláez, E. C. *et al.* Nanoplasmonic biosensor device for the monitoring of acenocoumarol therapeutic drug in plasma. *Biosensors and Bioelectronics* **119**, 149–155 (2018).

113. Lu, J. *et al.* Immunoassay for detection of infliximab in whole blood using a fiber-optic surface plasmon resonance biosensor. *Analytical chemistry* **89**, 3664–3671 (2017).

114. McKeating, K. S., Aubé, A. & Masson, J.-F. Biosensors and nanobiosensors for therapeutic drug and response monitoring. *Analyst* **141**, 429–449 (2016).

115. Hillhouse, T. M. & Porter, J. H. A brief history of the development of antidepressant drugs: from monoamines to glutamate. *Experimental and clinical psychopharmacology* **23**, 1 (2015).

116. Gillman, P. K. Tricyclic antidepressant pharmacology and therapeutic drug interactions updated. *Br J Pharmacol* **151**, 737–748 (2007).

117. Hackett, L. P., Dusci, L. J. & Ilett, K. F. A comparison of high-performance liquid chromatography and fluorescence polarization immunoassay for therapeutic drug monitoring of tricyclic antidepressants. *Therapeutic drug monitoring* **20**, 30–34 (1998).

118. Müller, M. *et al.* Therapeutic drug monitoring of tricyclic antidepressants: how does it work under clinical conditions? *Pharmacopsychiatry* **36**, 98–104 (2003).

119. Preskorn, S., Dorey, R. C. & Jerkovich, G. Therapeutic drug monitoring of tricyclic antidepressants. *Clinical chemistry* **34**, 822–828 (1988).

120. Rudorfer, M. V. & Potter, W. Z. Metabolism of tricyclic antidepressants. *Cellular and molecular neurobiology* **19**, 373–409 (1999).

121. Knihnicki, P. *et al.* Electrochemical sensor for determination of desipramine in biological materials. *Procedia Engineering* **47**, 1342–1345 (2012).

122. Xu, X.-L., Huang, F., Zhou, G.-L., Zhang, S. & Kong, J.-L. A Novel Electrochemical Sensor for Probing Doxepin Created on a Glassy Carbon Electrode Modified with Poly(4-Amino- benzoic Acid)/Multi-Walled Carbon Nanotubes Composite Film. *Sensors* **10**, (2010).

123. Krieg, A. K. & Gauglitz, G. Ultrasensitive label-free immunoassay for optical determination of amitriptyline and related tricyclic antidepressants in human serum. *Analytical chemistry* **87**, 8845–8850 (2015).

124. Overview - Antidepressants. *nhs.uk* https://www.nhs.uk/mental-health/talking-therapies-medicine-treatments/medicines-and-psychiatry/antidepressants/overview/ (2021).

125. Tsoucalas, G., Karamanou, M., Lymperi, M., Gennimata, V. & Androutsos, G. The "torpedo" effect in medicine. *International maritime health* **65**, 65–67 (2014).

126. AlGhatrif, M. & Lindsay, J. A brief review: history to understand fundamentals of electrocardiography. *Journal of community hospital internal medicine perspectives* **2**, 14383 (2012).

127. Aquilina, O. A brief history of cardiac pacing. *Images Paediatr Cardiol* **8**, 17–81 (2006).

128. Mishra, S. Electroceuticals in medicine – The brave new future. *Indian Heart Journal* **69**, 685–686 (2017).

129. Lau, C.-P., Siu, C.-W. & Tse, H.-F. Future of implantable devices for cardiac rhythm management. *Circulation* **129**, 811–822 (2014).

130. Kavehei, O., Hamilton, T. J., Truong, N. D. & Nikpour, A. Opportunities for Electroceuticals in Epilepsy. *Trends in pharmacological sciences* **40**, 735–746 (2019).

131. Gibney, S. *et al.* Toward nanobioelectronic medicine: Unlocking new applications using nanotechnology. *Wiley Interdisciplinary Reviews: Nanomedicine and Nanobiotechnology* **13**, e1693 (2021).

132. Wilson, B. S. & Dorman, M. F. Cochlear implants: a remarkable past and a brilliant future. *Hearing research* **242**, 3–21 (2008).

133. Dagnelie, G. Retinal implants: emergence of a multidisciplinary field. *Current opinion in neurology* **25**, 67–75 (2012).

134. Weiland, J. D. Bioelectronic retinal prosthesis. in vol. 9836 98360T (International Society for Optics and Photonics, 2016).

135. Rijkhoff, N., Wijkstra, H., Van Kerrebroeck, P. & Debruyne, F. Urinary bladder control by electrical stimulation: review of electrical stimulation techniques in spinal cord injury. *Neurourology and urodynamics* **16**, 39–53 (1997).

136. Koopman, F. A., Schuurman, P. R., Vervoordeldonk, M. J. & Tak, P. P. Vagus nerve stimulation: A new bioelectronics approach to treat rheumatoid arthritis? *Best Practice & Research Clinical Rheumatology* **28**, 625–635 (2014).

137. Levin, M. Reprogramming cells and tissue patterning via bioelectrical pathways: molecular mechanisms and biomedical opportunities. *Wiley Interdisciplinary Reviews: Systems Biology and Medicine* **5**, 657–676 (2013).

138. Tian, B. *et al.* Macroporous nanowire nanoelectronic scaffolds for synthetic tissues. *Nature materials* **11**, 986–994 (2012).

139. Sanjuan-Alberte, P. *et al.* Remotely controlled in situ growth of silver microwires forming bioelectronic interfaces. *ACS applied materials & interfaces* **11**, 8928–8936 (2019).

140. Nuccitelli, R. Application of pulsed electric fields to cancer therapy. *Bioelectricity* **1**, 30–34 (2019).

141. Bonaz, B. *et al.* Chronic vagus nerve stimulation in Crohn's disease: a 6-month follow-up pilot study. *Neurogastroenterology & Motility* **28**, 948–953 (2016).

142. Maul, X. A., Borchard, N. A., Hwang, P. H. & Nayak, J. V. Microcurrent technology for rapid relief of sinus pain: a randomized, placebo-controlled, double-blinded clinical trial. in vol. 9 352–356 (Wiley Online Library, 2019).

143. Anwar-Deen, I. BioElectronics Announces FDA Market Clearance for Over-The-Counter Treatment of Musculoskeletal Pain – ActiPatch® Pain Relief. https://www.actipatch.com/bioelectronics-announces-fda-market-clearance-for-over-the-counter-treatment-of-musculoskeletal-pain/.

144. Son, D. *et al.* Multifunctional wearable devices for diagnosis and therapy of movement disorders. *Nature nanotechnology* **9**, 397–404 (2014).

145. Vettoretti, M. & Facchinetti, A. Combining continuous glucose monitoring and insulin pumps to automatically tune the basal insulin infusion in diabetes therapy: a review. *Biomedical engineering online* **18**, 1–17 (2019).

146. Kim, J., Campbell, A. S., de Ávila, B. E.-F. & Wang, J. Wearable biosensors for healthcare monitoring. *Nature biotechnology* **37**, 389–406 (2019).

147. Park, J. *et al.* Soft, smart contact lenses with integrations of wireless circuits, glucose sensors, and displays. *Science advances* **4**, eaap9841 (2018).

148. Lee, H. *et al.* A graphene-based electrochemical device with thermoresponsive microneedles for diabetes monitoring and therapy. *Nature nanotechnology* **11**, 566–572 (2016).

149. Gao, W. *et al.* Fully integrated wearable sensor arrays for multiplexed in situ perspiration analysis. *Nature* **529**, 509–514 (2016).

150. Bandodkar, A. J. *et al.* Battery-free, skin-interfaced microfluidic/electronic systems for simultaneous electrochemical, colorimetric, and volumetric analysis of sweat. *Science advances* **5**, eaav3294 (2019).

151. Choi, S. *et al.* Highly conductive, stretchable and biocompatible Ag–Au core–sheath nanowire composite for wearable and implantable bioelectronics. *Nature nanotechnology* **13**, 1048–1056 (2018).

152. Nadeau, P. *et al.* Prolonged energy harvesting for ingestible devices. *Nature biomedical engineering* **1**, 1–8 (2017).

153. Theodor, M. *et al.* Subcutaneous blood pressure monitoring with an implantable optical sensor. *Biomedical microdevices* **15**, 811–820 (2013).

154. Dambrosio, N. *et al.* Continuous temperature monitoring for earlier fever detection in neutropenic patients: Patient's acceptance and comparison with standard of care. *Biology of Blood and Marrow Transplantation* **24**, S108–S109 (2018).

155. Commissioner, O. of the. FDA approves pill with sensor that digitally tracks if patients have ingested their medication. *FDA* https://www.fda.gov/news-events/press-announcements/fda-approves-pill-sensor-digitally-tracks-if-patients-have-ingested-their-medication (2020).

156. 'Digital pill' maker Proteus Digital Health files for bankruptcy. *MobiHealthNews* https://www.mobihealthnews.com/news/digital-pill-maker-proteus-digital-health-files-bankruptcy (2020).

157. Yen, H. & Huang, W. The efficacy of commercial smartwatches with a blood pressure-monitoring feature: A pilot randomized controlled trial. *Journal of Nursing Scholarship* (2021).

158. Kropff, J. *et al.* Accuracy and longevity of an implantable continuous glucose sensor in the PRECISE study: a 180-day, prospective, multicenter, pivotal trial. *Diabetes Care* **40**, 63–68 (2017).

159. Barnard, K. D. *et al.* Acceptability of implantable continuous glucose monitoring sensor. *Journal of diabetes science and technology* **12**, 634–638 (2018).

160. [ARCHIVED CONTENT] Exciting opportunities for implants and bioelectronics - Innovate UK. https://webarchive.nationalarchives.gov.uk/ukgwa/20210728212038/https://innovateuk.blog.gov.uk/2017/10/09/exciting-opportunities-for-implants-and-bioelectronics/.

161. Niu, Q. *et al.* Natural polymer-based bioabsorbable conducting wires for implantable bioelectronic devices. *Journal of Materials Chemistry A* **8**, 25323–25335 (2020).

162. Tropp, J. & Rivnay, J. Design of Biodegradable and Biocompatible Conjugated Polymers for Bioelectronics. *Journal of Materials Chemistry C* (2021).

163. Someya, T., Bao, Z. & Malliaras, G. G. The rise of plastic bioelectronics. *Nature* **540**, 379–385 (2016).

164. Sheng, H. *et al.* Recent Advances of Energy Solutions for Implantable Bioelectronics. *Advanced Healthcare Materials* 2100199 (2021).

165. Huang, X. *et al.* Materials strategies and device architectures of emerging power supply devices for implantable bioelectronics. *Small* **16**, 1902827 (2020).

166. Lee, J. H. *et al.* Biocompatible and Biodegradable Neuromorphic Device Based on Hyaluronic Acid for Implantable Bioelectronics. *Advanced Functional Materials* 2107074 (2021).

167. Patil, A. C., Xiong, Z. & Thakor, N. V. Toward nontransient silk bioelectronics: engineering silk fibroin for bionic links. *Small Methods* **4**, 2000274 (2020).

168. Freinkel, S. A brief history of plastic's conquest of the world. *Science American* **1**, 1–7 (2011).

169. Namazi, H. Polymers in our daily life. *BioImpacts: BI* **7**, 73 (2017).

170. Halley, P. & Avérous, L. *Starch polymers: from genetic engineering to green applications*. (Newnes, 2014).

171. Shi, G., Li, F. & Tian, H. Advances and application of polycarbonate in automobile windows and aero glass. *Mater. Rev* **20**, 404–407 (2006).

172. Liechty, W. B., Kryscio, D. R., Slaughter, B. V. & Peppas, N. A. Polymers for drug delivery systems. *Annual review of chemical and biomolecular engineering* **1**, 149–173 (2010).

173. Maitz, M. F. Applications of synthetic polymers in clinical medicine. *Biosurface and Biotribology* **1**, 161–176 (2015).

174. Akamatu, H., Inokuchi, H. & Matsunaga, Y. Electrical conductivity of the perylene–bromine complex. *Nature* **173**, 168–169 (1954).

175. Shirakawa, H., Louis, E. J., MacDiarmid, A. G., Chiang, C. K. & Heeger, A. J. Synthesis of electrically conducting organic polymers: halogen derivatives of polyacetylene,(CH) x. *Journal of the Chemical Society, Chemical Communications* 578–580 (1977).

176. Kuhn, H. H., Child, A. D. & Kimbrell, W. C. Toward real applications of conductive polymers. *Synthetic Metals* **71**, 2139–2142 (1995).

177. Nishio, K. *et al.* Characteristics of a lithium secondary battery using chemically-synthesized conductive polymers. *Journal of power sources* **34**, 153–160 (1991).

178. Kanatzidis, M. G. Conductive polymers. *Chemical and Engineering news* **68**, (1990).

179. Williams, E. L. *et al.* Conducting polymer and hydrogenated amorphous silicon hybrid solar cells. *Applied Physics Letters* **87**, 223504 (2005).

180. Kaur, G., Adhikari, R., Cass, P., Bown, M. & Gunatillake, P. Electrically conductive polymers and composites for biomedical applications. *Rsc Advances* **5**, 37553–37567 (2015).

181. Green, R. A., Baek, S., Poole-Warren, L. A. & Martens, P. J. Conducting polymer-hydrogels for medical electrode applications. *Science and Technology of Advanced Materials* **11**, 014107 (2010).

182. Kumar, D. & Sharma, R. Advances in conductive polymers. *European polymer journal* **34**, 1053–1060 (1998).

183. Bolto, B. A., McNeill, R. & Weiss, D. Electronic conduction in polymers. III. Electronic properties of polypyrrole. *Australian Journal of Chemistry* **16**, 1090–1103 (1963).

184. Kim, J. *et al.* Conductive polymers for next-generation energy storage systems: recent progress and new functions. *Materials Horizons* **3**, 517–535 (2016).

185. Freed, L. E., Engelmayr Jr, G. C., Borenstein, J. T., Moutos, F. T. & Guilak, F. Advanced material strategies for tissue engineering scaffolds. *Advanced Materials* **21**, 3410–3418 (2009).

186. Yao, H. *et al.* Solution processed intrinsically conductive polymer films with high thermoelectric properties and good air stability. *Journal of Materials Chemistry A* **6**, 24496–24502 (2018).

187. Zhao, W., Nugay, I. I., Yalcin, B. & Cakmak, M. Flexible, stretchable, transparent and electrically conductive polymer films via a hybrid electrospinning and solution casting process: In-plane anisotropic conductivity for electro-optical applications. *Displays* **45**, 48–57 (2016).

188. Wang, X.-S., Tang, H.-P., Li, X.-D. & Hua, X. Investigations on the mechanical properties of conducting polymer coating-substrate structures and their influencing factors. *International Journal of Molecular Sciences* **10**, 5257–5284 (2009).

189. Cui, H.-Q. *et al.* Optimization of ethylene glycol doped PEDOT: PSS transparent electrodes for flexible organic solar cells by drop-coating method. *Chinese Journal of Polymer Science* **37**, 760–766 (2019).

190. Liao, G., Li, Q. & Xu, Z. The chemical modification of polyaniline with enhanced properties: A review. *Progress in Organic Coatings* **126**, 35–43 (2019).

191. Tiwari, S. K., Mishra, J., Hatui, G. & Nayak, G. Conductive polymer composites based on carbon nanomaterials. in *Conducting Polymer Hybrids* 117–142 (Springer, 2017).

192. Zeglio, E., Rutz, A. L., Winkler, T. E., Malliaras, G. G. & Herland, A. Conjugated polymers for assessing and controlling biological functions. *Advanced Materials* **31**, 1806712 (2019).

193. Balint, R., Cassidy, N. J. & Cartmell, S. H. Conductive polymers: Towards a smart biomaterial for tissue engineering. *Acta Biomaterialia* **10**, 2341–2353 (2014).

194. Tsukada, S., Nakashima, H. & Torimitsu, K. Conductive polymer combined silk fiber bundle for bioelectrical signal recording. *PloS one* **7**, e33689 (2012).

195. Onoda, M., Abe, Y. & Tada, K. New fabrication technique of conductive polymer/insulating polymer composite films and evaluation of biocompatibility in neuron cultures. *Thin Solid Films* **518**, 743–749 (2009).

196. He, H. *et al.* Biocompatible conductive polymers with high conductivity and high stretchability. *ACS applied materials & interfaces* **11**, 26185–26193 (2019).

197. Widge, A. S., Jeffries-El, M., Cui, X., Lagenaur, C. F. & Matsuoka, Y. Self-assembled monolayers of polythiophene conductive polymers improve biocompatibility and electrical impedance of neural electrodes. *Biosensors and Bioelectronics* **22**, 1723–1732 (2007).

198. Humpolíček, P. *et al.* Polyaniline cryogels: Biocompatibility of novel conducting macroporous material. *Scientific reports* **8**, 1–12 (2018).

199. Inzelt, G., Lewenstam, A. & Scholz, F. *Handbook of reference electrodes*. vol. 541 (Springer, 2013).

200. Langhus, D. L. Analytical Electrochemistry, 2nd Edition (Wang, Joseph). *J. Chem. Educ.* **78**, 457 (2001).

201. Elgrishi, N. *et al.* A practical beginner's guide to cyclic voltammetry. *Journal of chemical education* **95**, 197–206 (2018).

202. Bard, A. J. & Faulkner, L. R. Fundamentals and applications. *Electrochemical methods* **2**, 580–632 (2001).

203. Gosser, D. K. *Cyclic voltammetry: simulation and analysis of reaction mechanisms*. vol. 43 (VCH New York, 1993).

204. Mabbott, G. A. An introduction to cyclic voltammetry. *Journal of Chemical education* **60**, 697 (1983).

205. Mirceski, V., Komorsky-Lovric, S. & Lovric, M. *Square-wave voltammetry: theory and application*. (Springer Science & Business Media, 2007).

206. Osteryoung, J. G. & Osteryoung, R. A. Square wave voltammetry. *Analytical chemistry* **57**, 101–110 (1985).

207. Giessibl, F. J. Advances in atomic force microscopy. *Reviews of modern physics* **75**, 949 (2003).

208. Xu, K. *et al.* Recent development of PeakForce Tapping mode atomic force microscopy and its applications on nanoscience. *Nanotechnology Reviews* **7**, 605–621 (2018).

209. Pittenger, B., Erina, N. & Su, C. Quantitative mechanical property mapping at the nanoscale with PeakForce QNM. *Application Note Veeco Instruments Inc* **1**, 1–11 (2010).

210. Raimondo, M. *et al.* Electrical conductivity of carbon nanofiber reinforced resins: Potentiality of Tunneling Atomic Force Microscopy (TUNA) technique. *Composites Part B: Engineering* **143**, 148–160 (2018).

211. Pai, R. K., Pillai, S. & Ahipa, T. Microscopic analysis of polymer honeycomb thin film studied by PeakForce TUNA for organic solar cell application. *Journal of Renewable and Sustainable Energy* **8**, 023703 (2016).

212. Harniman, R. L. *et al.* Direct observation of electron emission from grain boundaries in CVD diamond by PeakForce-controlled tunnelling atomic force microscopy. *Carbon* **94**, 386–395 (2015).

213. Lader, M. Tricyclic Antidepressants. in *Antidepressants: Past, Present and Future* (eds. Preskorn, S. H., Feighner, J. P., Stanga, C. Y. & Ross, R.) 185–208 (Springer Berlin Heidelberg, 2004). doi:10.1007/978-3-642-18500-7_7.

214. Moore, R. A., Derry, S., Aldington, D., Cole, P. & Wiffen, P. J. Amitriptyline for neuropathic pain in adults. *Cochrane Database Syst Rev* **2015**, CD008242–CD008242 (2015).

215. Lane, R., Baldwin, D. & Preskorn, S. The SSRIs: Advantages, disadvantages and differences. *J Psychopharmacol* **9**, 163–178 (1995).

216. Wang, S.-M. *et al.* Addressing the Side Effects of Contemporary Antidepressant Drugs: A Comprehensive Review. *Chonnam Med J* **54**, 101–112 (2018).

217. Sanghavi, B. J. & Srivastava, A. K. Adsorptive stripping voltammetric determination of imipramine, trimipramine and desipramine employing titanium dioxide nanoparticles and an Amberlite XAD-2 modified glassy carbon paste electrode. *Analyst* **138**, 1395–1404 (2013).

218. Bishop, E. & Hussein, W. Electroanalytical study of tricyclic antidepressants. *Analyst* **109**, 73–80 (1984).

219. Nicholson, R. S. & Shain, I. Theory of stationary electrode polarography. Single scan and cyclic methods applied to reversible, irreversible, and kinetic systems. *Analytical chemistry* **36**, 706–723 (1964).

220. Behan, J. A. *et al.* Influence of carbon nanostructure and oxygen moieties on dopamine adsorption and charge transfer kinetics at glassy carbon surfaces. *Electrochimica Acta* **304**, 221–230 (2019).

221. Beitollah, H. *et al.* Electrochemical behaviors and determination of carbidopa on carbon nanotubes ionic liquid paste electrode. *Journal of Molecular Liquids* **173**, 137–143 (2012).

222. Ivandini, T. *et al.* Electrochemical detection of tricyclic antidepressant drugs by HPLC using highly boron-doped diamond electrodes. *Journal of Electroanalytical Chemistry* **521**, 117–126 (2002).

223. Wang, J., Bonakdar, M. & Morgan, C. Voltammetric measurement of tricyclic antidepressants following interfacial accumulation at carbon electrodes. *Analytical chemistry* **58**, 1024–1028 (1986).

224. Oliveira, S. N. *et al.* Imipramine sensing in pharmaceutical formulations using boron-doped diamond electrode. *Journal of Electroanalytical Chemistry* **788**, 118–124 (2017).

225. Giraudeau, A., Callot, H. & Gross, M. Effects of electron-withdrawing substituents on the electrochemical oxidation of porphyrins. *Inorganic Chemistry* **18**, 201–206 (1979).

226. Jedral, W., Merica, S. G. & Bunce, N. J. Electrochemical oxidation of chlorinated benzenes. *Electrochemistry Communications* **1**, 108–110 (1999).

227. Sandford, C. *et al.* A synthetic chemist's guide to electroanalytical tools for studying reaction mechanisms. *Chemical science* **10**, 6404–6422 (2019).

228. Hou, W., Xiao, Y., Han, G. & Lin, J.-Y. The applications of polymers in solar cells: A review. *Polymers* **11**, 143 (2019).

229. Kinlen, P. & Schuette, W. Aerospace Applications of Conductive Polymers. in 540 (IOP Publishing, 2015).

230. Rathod, V. T., Kumar, J. S. & Jain, A. Polymer and ceramic nanocomposites for aerospace applications. *Applied Nanoscience* **7**, 519–548 (2017).

231. Palza, H., Zapata, P. A. & Angulo-Pineda, C. Electroactive smart polymers for biomedical applications. *Materials* **12**, 277 (2019).

232. Nezakati, T., Seifalian, A., Tan, A. & Seifalian, A. M. Conductive polymers: opportunities and challenges in biomedical applications. *Chemical reviews* **118**, 6766–6843 (2018).

233. Scataglini, S., Moorhead, A. & Feletti, F. A Systematic Review of Smart Clothing in Sports: possible Applications to Extreme Sports. *Muscles, Ligaments & Tendons Journal (MLTJ)* **10**, (2020).

234. Grancarić, A. M. *et al.* Conductive polymers for smart textile applications. *Journal of Industrial Textiles* **48**, 612–642 (2018).

235. Das, T. K. & Prusty, S. Review on conducting polymers and their applications. *Polymer-plastics technology and engineering* **51**, 1487–1500 (2012).

236. Skotheim, T. A. *Handbook of conducting polymers*. (CRC press, 1997).

237. Wang, X.-X. *et al.* Conductive polymer ultrafine fibers via electrospinning: Preparation, physical properties and applications. *Progress in Materials Science* **115**, 100704 (2021).

238. Luo, R., Li, H., Du, B., Zhou, S. & Zhu, Y. A simple strategy for high stretchable, flexible and conductive polymer films based on PEDOT: PSS-PDMS blends. *Organic Electronics* **76**, 105451 (2020).

239. Namsheer, K. & Rout, C. S. Conducting polymers: a comprehensive review on recent advances in synthesis, properties and applications. *RSC Advances* **11**, 5659–5697 (2021).

240. Huang, Y. *et al.* Conductive polymer composites from renewable resources: an overview of preparation, properties, and applications. *Polymers* **11**, 187 (2019).

241. Ravichandran, R., Sundarrajan, S., Venugopal, J. R., Mukherjee, S. & Ramakrishna, S. Applications of conducting polymers and their issues in biomedical engineering. *Journal of the Royal Society Interface* **7**, S559–S579 (2010).

242. Hwang, J. S. *et al.* Effect of solvent on electrical conductivity and gas sensitivity of PEDOT: PSS polymer composite films. *Journal of Applied Polymer Science* **132**, (2015).

243. Xu, S. *et al.* High-performance PEDOT: PSS flexible thermoelectric materials and their devices by triple post-treatments. *Chemistry of Materials* **31**, 5238–5244 (2019).

244. Li, Y., Tanigawa, R. & Okuzaki, H. Soft and flexible PEDOT/PSS films for applications to soft actuators. *Smart Materials and Structures* **23**, 074010 (2014).

245. Tseghai, G. B., Mengistie, D. A., Malengier, B., Fante, K. A. & Van Langenhove, L. PEDOT: PSS-based conductive textiles and their applications. *Sensors* **20**, 1881 (2020).

246. Lo, L.-W. *et al.* An Inkjet-Printed PEDOT: PSS-Based Stretchable Conductor for Wearable Health Monitoring Device Applications. *ACS Applied Materials & Interfaces* **13**, 21693–21702 (2021).

247. Yang, Y., Zhao, G., Cheng, X., Deng, H. & Fu, Q. Stretchable and Healable Conductive Elastomer Based on PEDOT: PSS/Natural Rubber for Self-Powered Temperature and Strain Sensing. *ACS Applied Materials & Interfaces* **13**, 14599–14611 (2021).

248. Manjakkal, L., Szwagierczak, D. & Dahiya, R. Metal oxides based electrochemical pH sensors: Current progress and future perspectives. *Progress in Materials Science* **109**, 100635 (2020).

249. Lu, B. *et al.* Pure pedot: Pss hydrogels. *Nature communications* **10**, 1–10 (2019).

250. Heo, D. N. *et al.* Development of 3D printable conductive hydrogel with crystallized PEDOT: PSS for neural tissue engineering. *Materials Science and Engineering: C* **99**, 582–590 (2019).

251. Abedi, A., Hasanzadeh, M. & Tayebi, L. Conductive nanofibrous Chitosan/PEDOT: PSS tissue engineering scaffolds. *Materials Chemistry and Physics* **237**, 121882 (2019).

252. Marzocchi, M. *et al.* Physical and electrochemical properties of PEDOT: PSS as a tool for controlling cell growth. *ACS applied materials & interfaces* **7**, 17993–18003 (2015).

253. Eaton, P. & West, P. *Atomic force microscopy*. (Oxford university press, 2010).

254. Rugar, D. & Hansma, P. Atomic force microscopy. *Physics today* **43**, 23–30 (1990).

255. Jiang, L. *et al.* Understanding current instabilities in conductive atomic force microscopy. *Materials* **12**, 459 (2019).

256. Oliver, R. A. Advances in AFM for the electrical characterization of semiconductors. *Reports on Progress in Physics* **71**, 076501 (2008).

257. Döbbelin, M. *et al.* Influence of ionic liquids on the electrical conductivity and morphology of PEDOT: PSS films. *Chemistry of materials* **19**, 2147–2149 (2007).

258. Dong, J. & Portale, G. Role of the Processing Solvent on the Electrical Conductivity of PEDOT: PSS. *Advanced Materials Interfaces* **7**, 2000641 (2020).

259. Reza, K. M. *et al.* Tailored PEDOT: PSS hole transport layer for higher performance in perovskite solar cells: Enhancement of electrical and optical properties with improved morphology. *Journal of Energy Chemistry* **44**, 41–50 (2020).

260. Zhu, Z. *et al.* Improving the electrical conductivity of PEDOT: PSS films by binary secondary doping. *Electronic Materials Letters* **12**, 54–58 (2016).

261. Lang, U., Müller, E., Naujoks, N. & Dual, J. Microscopical investigations of PEDOT: PSS thin films. *Advanced Functional Materials* **19**, 1215–1220 (2009).

262. Lang, U., Naujoks, N. & Dual, J. Mechanical characterization of PEDOT: PSS thin films. *Synthetic Metals* **159**, 473–479 (2009).

263. Le, T.-H., Kim, Y. & Yoon, H. Electrical and electrochemical properties of conducting polymers. *Polymers* **9**, 150 (2017).

264. Pingree, L. S., MacLeod, B. A. & Ginger, D. S. The changing face of PEDOT: PSS films: substrate, bias, and processing effects on vertical charge transport. *The Journal of Physical Chemistry C* **112**, 7922–7927 (2008).

265. Kuş, M. & Okur, S. Electrical characterization of PEDOT: PSS beyond humidity saturation. *Sensors and Actuators B: Chemical* **143**, 177–181 (2009).

266. Linseis, V. *et al.* Complete thermoelectric characterization of PEDOT: PSS thin films with a novel ZT test chip platform. *physica status solidi (a)* **215**, 1700930 (2018).

267. Zainal, M. F. & Mohd, Y. Characterization of PEDOT films for electrochromic applications. *Polymer-Plastics Technology and Engineering* **54**, 276–281 (2015).

268. Zubair, N. A., Rahman, N. A., Lim, H. N. & Sulaiman, Y. Production of conductive PEDOT-coated PVA-GO composite nanofibers. *Nanoscale research letters* **12**, 1–13 (2017).

269. Abdah, M. A. A. M., Zubair, N. A., Azman, N. H. N. & Sulaiman, Y. Fabrication of PEDOT coated PVA-GO nanofiber for supercapacitor. *Materials Chemistry and Physics* **192**, 161–169 (2017).

270. Nardes, A. M. *et al.* Microscopic understanding of the anisotropic conductivity of PEDOT: PSS thin films. *Advanced Materials* **19**, 1196–1200 (2007).

271. Takano, T., Masunaga, H., Fujiwara, A., Okuzaki, H. & Sasaki, T. PEDOT nanocrystal in highly conductive PEDOT: PSS polymer films. *Macromolecules* **45**, 3859–3865 (2012).

272. Reza, K. M., Mabrouk, S. & Qiao, Q. A review on tailoring PEDOT: PSS layer for improved performance of perovskite solar cells. *Proc. Nat. Res. Soc* **2**, 02004 (2018).

273. Liu, N. *et al.* Electrospun PEDOT: PSS–PVA nanofiber based ultrahigh-strain sensors with controllable electrical conductivity. *Journal of Materials Chemistry* **21**, 18962–18966 (2011).

274. Strakosas, X. *et al.* A facile biofunctionalisation route for solution processable conducting polymer devices. *Journal of Materials Chemistry B* **2**, 2537–2545 (2014).

275. Tseng, Y.-T. *et al.* Morphology and properties of PEDOT: PSS/soft polymer blends through hydrogen bonding interaction and their pressure sensor application. *Journal of Materials Chemistry C* **8**, 6013–6024 (2020).

276. Jasna, M., Pushkaran, N. K., Manoj, M., Aanandan, C. & Jayaraj, M. Facile preparation of lightweight and flexible PVA/PEDOT: PSS/MWCNT ternary composite for high-performance EMI shielding in the X-band through absorption mechanism. *Journal of Electronic Materials* **49**, 1689–1701 (2020).

277. Chen, C. *et al.* Mechanical characterizations of cast Poly (3, 4-ethylenedioxythiophene): Poly (styrenesulfonate)/Polyvinyl Alcohol thin films. *Synthetic Metals* **161**, 2259–2267 (2011).

278. Carr, O., Gozzi, G., Santos, L. F., Faria, R. M. & Chinaglia, D. L. Analysis of the electrical and optical properties of PEDOT: PSS/PVA blends for low-cost and high-performance organic electronic and optoelectronic devices. *Translational Materials Research* **2**, 015002 (2015).

279. Snaith, H. J., Kenrick, H., Chiesa, M. & Friend, R. H. Morphological and electronic consequences of modifications to the polymer anode 'PEDOT: PSS'. *Polymer* **46**, 2573–2578 (2005).

280. Xia, Y. & Ouyang, J. PEDOT: PSS films with significantly enhanced conductivities induced by preferential solvation with cosolvents and their application in polymer photovoltaic cells. *Journal of Materials Chemistry* **21**, 4927–4936 (2011).

281. Kemerink, M., Timpanaro, S., De Kok, M., Meulenkamp, E. & Touwslager, F. Three-dimensional inhomogeneities in PEDOT: PSS films. *The Journal of Physical Chemistry B* **108**, 18820–18825 (2004).

282. Fan, X. *et al.* PEDOT: PSS for flexible and stretchable electronics: modifications, strategies, and applications. *Advanced Science* **6**, 1900813 (2019).

283. Ritruksa, M. *et al.* Surface modification of PEDOT: PSS film by chemical vapor texturing process for enhanced organic photovoltaics. *Surfaces and Interfaces* **21**, 100716 (2020).

284. Fenoy, G. E., Azzaroni, O., Knoll, W. & Marmisollé, W. A. Functionalization Strategies of PEDOT and PEDOT: PSS Films for Organic Bioelectronics Applications. *Chemosensors* **9**, 212 (2021).

285. Lingstedt, L. V. *et al.* Effect of DMSO solvent treatments on the performance of PEDOT: PSS based organic electrochemical transistors. *Advanced Electronic Materials* **5**, 1800804 (2019).

286. Huang, D. *et al.* Perovskite solar cells with a DMSO-treated PEDOT: PSS hole transport layer exhibit higher photovoltaic performance and enhanced durability. *Nanoscale* **9**, 4236–4243 (2017).

287. Pasha, A., Khasim, S., Al-Hartomy, O. A., Lakshmi, M. & Manjunatha, K. Highly sensitive ethylene glycol-doped PEDOT–PSS organic thin films for LPG sensing. *RSC advances* **8**, 18074–18083 (2018).

288. Mantione, D. *et al.* Low-Temperature Cross-Linking of PEDOT:PSS Films Using Divinylsulfone. *ACS Appl. Mater. Interfaces* **9**, 18254–18262 (2017).

289. Håkansson, A. *et al.* Effect of (3-glycidyloxypropyl)trimethoxysilane (GOPS) on the electrical properties of PEDOT:PSS films. *Journal of Polymer Science Part B: Polymer Physics* **55**, 814–820 (2017).

290. Singh, V., Arora, S., Arora, M., Sharma, V. & Tandon, R. Characterization of doped PEDOT: PSS and its influence on the performance and degradation of organic solar cells. *Semiconductor Science and Technology* **29**, 045020 (2014).

291. Agua, I. del *et al.* DVS-Crosslinked PEDOT:PSS Free-Standing and Textile Electrodes toward Wearable Health Monitoring. *Advanced Materials Technologies* **3**, 1700322 (2018).

292. Ouyang, J. *et al.* On the mechanism of conductivity enhancement in poly (3, 4-ethylenedioxythiophene): poly (styrene sulfonate) film through solvent treatment. *Polymer* **45**, 8443–8450 (2004).

293. Yan, H. & Okuzaki, H. Effect of solvent on PEDOT/PSS nanometer-scaled thin films: XPS and STEM/AFM studies. *Synthetic Metals* **159**, 2225–2228 (2009).

294. Dvir, H. & Gottlieb, M. Effect of silane sizing on polymer-glass adhesion. in 5–9 (2007).

295. Lengvinaite, S., Grazulevicius, J., Grigalevicius, S., Zhang, B. & Xie, Z. Carbazol-3-yl substituted aromatic amines containing crosslinkable groups as materials for multilayer light emitting diodes. *Molecular Crystals and Liquid Crystals* **497**, 164–496 (2008).

296. Ashizawa, S., Horikawa, R. & Okuzaki, H. Effects of solvent on carrier transport in poly (3, 4-ethylenedioxythiophene)/poly (4-styrenesulfonate). *Synthetic Metals* **153**, 5–8 (2005).

297. Zhang, S. *et al.* Solvent-induced changes in PEDOT:PSS films for organic electrochemical transistors. *APL Materials* **3**, 014911 (2014).

298. Wei, T.-C., Chen, S.-H. & Chen, C.-Y. Highly conductive PEDOT: PSS film made with ethylene-glycol addition and heated-stir treatment for enhanced photovoltaic performances. *Materials Chemistry Frontiers* **4**, 3302–3309 (2020).

299. Yildirim, E. *et al.* A theoretical mechanistic study on electrical conductivity enhancement of DMSO treated PEDOT: PSS. *Journal of Materials Chemistry C* **6**, 5122–5131 (2018).

300. Lin, Y.-J., Lee, J.-Y. & Chen, S.-M. Changing electrical properties of PEDOT: PSS by incorporating with dimethyl sulfoxide. *Chemical Physics Letters* **664**, 213–218 (2016).

301. Ahmad, Z., Azman, A. W., Buys, Y. F. & Sarifuddin, N. Mechanisms for doped PEDOT: PSS electrical conductivity improvement. *Materials Advances* **2**, 7118–7138 (2021).

302. Lin, Y.-J., Ni, W.-S. & Lee, J.-Y. Effect of incorporation of ethylene glycol into PEDOT: PSS on electron phonon coupling and conductivity. *Journal of Applied Physics* **117**, 215501 (2015).

303. Nardes, A., Kemerink, M. & Janssen, R. Anisotropic hopping conduction in spin-coated PEDOT: PSS thin films. *Physical review B* **76**, 085208 (2007).

304. Palumbiny, C. M. *et al.* The crystallization of PEDOT: PSS polymeric electrodes probed in situ during printing. *Advanced materials* **27**, 3391–3397 (2015).

305. Ouyang, L., Musumeci, C., Jafari, M. J., Ederth, T. & Inganas, O. Imaging the phase separation between PEDOT and polyelectrolytes during processing of highly conductive PEDOT: PSS films. *ACS applied materials & interfaces* **7**, 19764–19773 (2015).

306. Eshraghi, A. A. *et al.* The cochlear implant: historical aspects and future prospects. *Anat Rec (Hoboken)* **295**, 1967–1980 (2012).

307. Bhatia, N. & El-Chami, M. Leadless pacemakers: a contemporary review. *Journal of geriatric cardiology: JGC* **15**, 249 (2018).

308. Ritter, P. *et al.* The rationale and design of the Micra Transcatheter Pacing Study: safety and efficacy of a novel miniaturized pacemaker. *Ep Europace* **17**, 807–813 (2015).

309. Duray, G. Z. *et al.* Long-term performance of a transcatheter pacing system: 12-month results from the Micra Transcatheter Pacing Study. *Heart rhythm* **14**, 702–709 (2017).

310. Svrakic, M., Roland Jr, J. T., McMenomey, S. O. & Svirsky, M. A. Initial Operative Experience and Short Term Hearing Preservation Results with a Mid-Scala Cochlear Implant Electrode Array. *Otology & neurotology: official publication of the American Otological Society, American Neurotology Society [and] European Academy of Otology and Neurotology* **37**, 1549 (2016).

311. AB Technical Reports | Advanced Bionics. https://www.advancedbionics.com/us/en/home/professionals/document-library/ab-technical-reports.html.

312. Anderson, J. M. 9.19 - Biocompatibility. in *Polymer Science: A Comprehensive Reference* (eds. Matyjaszewski, K. & Möller, M.) 363–383 (Elsevier, 2012). doi:10.1016/B978-0-444-53349-4.00229-6.

313. Gad, S. C. *Safety evaluation of pharmaceuticals and medical devices: international regulatory guidelines*. (Springer Science & Business Media, 2010).

314. Feron, K. *et al.* Organic Bioelectronics: Materials and Biocompatibility. *Int J Mol Sci* **19**, 2382 (2018).

315. Wu, X. & Peng, H. Polymer-based flexible bioelectronics. *Science Bulletin* **64**, 634–640 (2019).

316. Panda, A. K. & Basu, B. Biomaterials-based bioengineering strategies for bioelectronic medicine. *Materials Science and Engineering: R: Reports* **146**, 100630 (2021).

317. Li, Y., Li, N., De Oliveira, N. & Wang, S. Implantable bioelectronics toward long-term stability and sustainability. *Matter* **4**, 1125–1141 (2021).

318. Donahue, M. J. *et al.* Tailoring PEDOT properties for applications in bioelectronics. *Materials Science and Engineering: R: Reports* **140**, 100546 (2020).

319. Pani, D. *et al.* Fully textile, PEDOT: PSS based electrodes for wearable ECG monitoring systems. *IEEE Transactions on Biomedical Engineering* **63**, 540–549 (2015).

320. Lee, S., Eom, T., Kim, M.-K., Yang, S.-G. & Shim, B. S. Durable soft neural micro-electrode coating by an electrochemical synthesis of PEDOT: PSS/graphene oxide composites. *Electrochimica Acta* **313**, 79–90 (2019).

321. Pal, R. K. *et al.* Conducting polymer-silk biocomposites for flexible and biodegradable electrochemical sensors. *Biosensors and Bioelectronics* **81**, 294–302 (2016).

322. Solazzo, M. *et al.* PEDOT: PSS interfaces stabilised using a PEGylated crosslinker yield improved conductivity and biocompatibility. *Journal of Materials Chemistry B* **7**, 4811–4820 (2019).

323. Cellot, G. *et al.* PEDOT: PSS interfaces support the development of neuronal synaptic networks with reduced neuroglia response in vitro. *Frontiers in neuroscience* **9**, 521 (2016).

324. Luo, S.-C. *et al.* Poly (3, 4-ethylenedioxythiophene)(PEDOT) nanobiointerfaces: thin, ultrasmooth, and functionalized PEDOT films with in vitro and in vivo biocompatibility. *Langmuir* **24**, 8071–8077 (2008).

325. Ferlauto, L. *et al.* Development and characterization of PEDOT: PSS/alginate soft microelectrodes for application in neuroprosthetics. *Frontiers in neuroscience* **12**, 648 (2018).

326. Abidian, M. R., Ludwig, K. A., Marzullo, T. C., Martin, D. C. & Kipke, D. R. Interfacing conducting polymer nanotubes with the central nervous system: chronic neural recording using poly (3, 4-ethylenedioxythiophene) nanotubes. *Advanced Materials* **21**, 3764–3770 (2009).

327. Schander, A. *et al.* In-vitro evaluation of the long-term stability of PEDOT: PSS coated microelectrodes for chronic recording and electrical stimulation of neurons. in 6174–6177 (IEEE, 2016).

328. Tadayyon, G. *et al.* In vitro analysis of a physiological strain sensor formulated from a PEDOT: PSS functionalized carbon nanotube-poly (glycerol sebacate urethane) composite. *Materials Science and Engineering: C* **121**, 111857 (2021).

329. Liu, C. *et al.* A wireless, implantable optoelectrochemical probe for optogenetic stimulation and dopamine detection. *Microsystems & Nanoengineering* **6**, 1–12 (2020).

330. Dorati, R. *et al.* Biodegradable scaffolds for bone regeneration combined with drug-delivery systems in osteomyelitis therapy. *Pharmaceuticals* **10**, 96 (2017).

331. Turabee, M. H., Thambi, T., Duong, H. T. T., Jeong, J. H. & Lee, D. S. A pH-and temperature-responsive bioresorbable injectable hydrogel based on polypeptide block copolymers for the sustained delivery of proteins in vivo. *Biomaterials science* **6**, 661–671 (2018).

332. Karlsson, J., Vaughan, H. J. & Green, J. J. Biodegradable polymeric nanoparticles for therapeutic cancer treatments. *Annual review of chemical and biomolecular engineering* **9**, 105–127 (2018).

333. Lu, D. *et al.* Bioresorbable wireless sensors as temporary implants for in vivo measurements of pressure. *Advanced Functional Materials* **30**, 2003754 (2020).

334. Kang, S.-K. *et al.* Bioresorbable silicon electronic sensors for the brain. *Nature* **530**, 71–76 (2016).

335. Kang, S.-K., Koo, J., Lee, Y. K. & Rogers, J. A. Advanced materials and devices for bioresorbable electronics. *Accounts of chemical research* **51**, 988–998 (2018).

336. Boutry, C. M. *et al.* A stretchable and biodegradable strain and pressure sensor for orthopaedic application. *Nature Electronics* **1**, 314–321 (2018).

337. Xue, Y. *et al.* Trigger-Detachable Hydrogel Adhesives for Bioelectronic Interfaces. *Advanced Functional Materials* 2106446 (2021).

338. Daggumati, P., Matharu, Z. & Seker, E. Effect of nanoporous gold thin film morphology on electrochemical DNA sensing. *Analytical chemistry* **87**, 8149–8156 (2015).

339. Hao, J., Xiao, T., Wu, F., Yu, P. & Mao, L. High antifouling property of ion-selective membrane: toward in vivo monitoring of pH change in live brain of rats with membrane-coated carbon fiber electrodes. *Analytical chemistry* **88**, 11238–11243 (2016).

340. Baggerman, J., Smulders, M. M. & Zuilhof, H. Romantic surfaces: a systematic overview of stable, biospecific, and antifouling zwitterionic surfaces. *Langmuir* **35**, 1072–1084 (2019).

341. Heggestad, J. T., Fontes, C. M., Joh, D. Y., Hucknall, A. M. & Chilkoti, A. In Pursuit of Zero 2.0: Recent developments in nonfouling polymer brushes for immunoassays. *Advanced Materials* **32**, 1903285 (2020).

342. Chen, X. & Noy, A. Antifouling strategies for protecting bioelectronic devices. *APL Materials* **9**, 020701 (2021).

343. Carabelli, A. M. *et al.* Single-Cell Tracking on Polymer Microarrays Reveals the Impact of Surface Chemistry on Pseudomonas aeruginosa Twitching Speed and Biofilm Development. *ACS Applied Bio Materials* **3**, 8471–8480 (2020).

344. He, Y. *et al.* Exploiting Generative Design for 3D Printing of Bacterial Biofilm Resistant Composite Devices. *Advanced Science* 2100249 (2021).

345. Feczkó, T. *et al.* Theranostic Sorafenib-Loaded Polymeric Nanocarriers Manufactured by Enhanced Gadolinium Conjugation Techniques. *Pharmaceutics* **11**, 489 (2019).

346. Duvvuri, S., Janoria, K. G. & Mitra, A. K. Effect of polymer blending on the release of ganciclovir from PLGA microspheres. *Pharmaceutical research* **23**, 215–223 (2006).

347. Niekraszewicz, A., Kucharska, M., Kardas, I. & Szadkowski, M. Resorbable tightening of blood vessel protheses prepared from synthetic polymers. *Fibres and Textiles in Eastern Europe* **17**, 77 (2009).

348. Kirsch, M. *et al.* Xeno-free in vitro cultivation and osteogenic differentiation of hAD-MSCs on resorbable 3D printed RESOMER®. *Materials* **13**, 3399 (2020).

349. Vijayavenkataraman, S. *et al.* 3D-printed PCL/PPy conductive scaffolds as three-dimensional porous nerve guide conduits (NGCs) for peripheral nerve injury repair. *Frontiers in bioengineering and biotechnology* 266 (2019).

350. Huang, B. *et al.* In vivo study of conductive 3D printed PCL/MWCNTs scaffolds with electrical stimulation for bone tissue engineering. *Bio-Design and Manufacturing* **4**, 190–202 (2021).

351. Prasopthum, A. *et al.* Three dimensional printed degradable and conductive polymer scaffolds promote chondrogenic differentiation of chondroprogenitor cells. *Biomaterials Science* **8**, 4287–4298 (2020).

352. Guex, A. G. *et al.* Highly porous scaffolds of PEDOT: PSS for bone tissue engineering. *Acta biomaterialia* **62**, 91–101 (2017).

353. Jayaram, A. K. *et al.* 3D hybrid scaffolds based on PEDOT: PSS/MWCNT composites. *Frontiers in chemistry* **7**, 363 (2019).

354. Kotsakou, M. *et al.* Pacemaker insertion. *Annals of translational medicine* **3**, (2015).

355. Chen, Y., Kim, Y.-S., Tillman, B. W., Yeo, W.-H. & Chun, Y. Advances in Materials for Recent Low-Profile Implantable Bioelectronics. *Materials (Basel)* **11**, (2018).

356. Lee, P. M., Xiong, Z. & Ho, J. Methods for powering bioelectronic microdevices. *Bioelectronics in Medicine* **1**, 201–217 (2018).

357. European Commission. Council Directive 90/385/EEC on Active Implantable Medical Devices (AIMDD). *Official Journal of the European Communities* **33**, L–189 (1990).

358. Guo, Y. *et al.* PEDOT: PSS "wires" printed on textile for wearable electronics. *ACS applied materials & interfaces* **8**, 26998–27005 (2016).

359. Lv, D. *et al.* Enhanced flexible room temperature ammonia sensor based on PEDOT: PSS thin film with FeCl3 additives prepared by inkjet printing. *Sensors and Actuators B: Chemical* **298**, 126890 (2019).

360. Lin, C.-Y., Chen, J.-G., Hu, C.-W., Tunney, J. J. & Ho, K.-C. Using a PEDOT: PSS modified electrode for detecting nitric oxide gas. *Sensors and Actuators B: Chemical* **140**, 402–406 (2009).

361. Hu, Z., Zhang, J., Hao, Z. & Zhao, Y. Influence of doped PEDOT: PSS on the performance of polymer solar cells. *Solar Energy Materials and Solar Cells* **95**, 2763–2767 (2011).

362. Mantione, D. *et al.* Low-Temperature Cross-Linking of PEDOT:PSS Films Using Divinylsulfone. https://pubs.acs.org/doi/abs/10.1021/acsami.7b02296 (2017) doi:10.1021/acsami.7b02296.

363. Kamensky, M., Eliseeva, S., Láng, G., Ujvári, M. & Kondratiev, V. Electrochemical Properties of Overoxidized Poly-3, 4-Ethylenedioxythiophene. *Russian Journal of Electrochemistry* **54**, 893–901 (2018).

364. Markoulidis, F., Dawe, A. & Lekakou, C. Electrochemical double-layer capacitors with lithium-ion electrolyte and electrode coatings with PEDOT: PSS binder. *Journal of Applied Electrochemistry* **51**, 373–385 (2021).

365. Multilayer, P. Polymers for Advanced Architectures.

366. Bießmann, L. *et al.* Monitoring the Swelling Behavior of PEDOT: PSS electrodes under high humidity conditions. *ACS applied materials & interfaces* **10**, 9865–9872 (2018).

367. Xia, Y., Zhang, H. & Ouyang, J. Highly conductive PEDOT: PSS films prepared through a treatment with zwitterions and their application in polymer photovoltaic cells. *Journal of Materials Chemistry* **20**, 9740–9747 (2010).

368. Berm, E. J. *et al.* A simple dried blood spot method for therapeutic drug monitoring of the tricyclic antidepressants amitriptyline, nortriptyline, imipramine, clomipramine, and their active metabolites using LC-MS/MS. *Talanta* **134**, 165–172 (2015).

369. Malfará, W. R. *et al.* Reliable HPLC method for therapeutic drug monitoring of frequently prescribed tricyclic and nontricyclic antidepressants. *J Pharm Biomed Anal* **44**, 955–962 (2007).

370. Yamuna, A. *et al.* Selective electrochemical detection of antidepressant drug imipramine in blood serum and urine samples using an antimony telluride-graphite nanofiber electrode. *Microchimica Acta* **188**, 1–12 (2021).

371. Mäder, K. RESOMER@-biodegradable polymer for sutures, medical devices, drug delivery systems and tissue engineering. *Mater. Matters* **6**, 62–66 (2011).

372. Polino, G. *et al.* Synthesis and characterization of PEDOT-PEGDA blends for bioelectronic applications: surface properties and effects on cell morphology. *Flexible and Printed Electronics* **5**, 014012 (2020).

373. Li, P., Du, D., Guo, L., Guo, Y. & Ouyang, J. Stretchable and conductive polymer films for high-performance electromagnetic interference shielding. *Journal of Materials Chemistry C* **4**, 6525–6532 (2016).

374. Kozai, T. D. *et al.* Chronic in vivo evaluation of PEDOT/CNT for stable neural recordings. *IEEE Transactions on Biomedical Engineering* **63**, 111–119 (2015).

375. Dominguez-Alfaro, A. *et al.* Tailored methodology based on vapor phase polymerization to manufacture PEDOT/CNT scaffolds for tissue engineering. *ACS biomaterials science & engineering* **6**, 1269–1278 (2019).

376. Samba, R. *et al.* Application of PEDOT-CNT Microelectrodes for Neurotransmitter Sensing. *Electroanalysis* **26**, 548–555 (2014).

377. Polcari, D., Dauphin-Ducharme, P. & Mauzeroll, J. Scanning electrochemical microscopy: a comprehensive review of experimental parameters from 1989 to 2015. *Chemical reviews* **116**, 13234–13278 (2016).

378. Huang, Z. *et al.* PeakForce scanning electrochemical microscopy with nanoelectrode probes. *Microscopy Today* **24**, 18–25 (2016).

379. Arrigan, D. W. Nanoelectrodes, nanoelectrode arrays and their applications. *Analyst* **129**, 1157–1165 (2004).

380. Chang, B.-Y. & Park, S.-M. Electrochemical impedance spectroscopy. *Annual Review of Analytical Chemistry* **3**, 207–229 (2010).

381. Hui, Y., Bian, C., Wang, J., Tong, J. & Xia, S. Comparison of two types of overoxidized PEDOT films and their application in sensor fabrication. *Sensors* **17**, 628 (2017).

382. Ruiz, S. A. & Chen, C. S. Microcontact printing: A tool to pattern. *Soft Matter* **3**, 168–177 (2007).

383. Barbulovic-Nad, I. *et al.* Bio-microarray fabrication techniques—a review. *Critical reviews in biotechnology* **26**, 237–259 (2006).

384. Celiz, A. D. *et al.* ToF-SIMS imaging of a polymer microarray prepared using ink-jet printing of acrylate monomers. *Surface and interface analysis* **45**, 202–205 (2013).

385. Hook, A. L. *et al.* Polymer microarrays for high throughput discovery of biomaterials. *Journal of visualized experiments: JoVE* (2012).

386. Hao, H. *et al.* Rapid build-up of high-throughput screening microarrays with biochemistry gradients via light-induced thiol–ene "click" chemistry. *Journal of Materials Chemistry B* **9**, 3032–3037 (2021).

387. Babos, G., Biró, E., Meiczinger, M. & Feczkó, T. Dual drug delivery of sorafenib and doxorubicin from PLGA and PEG-PLGA polymeric nanoparticles. *Polymers* **10**, 895 (2018).

388. Lommen, J. *et al.* Release kinetics of the model protein FITC-BSA from different polymer-coated bovine bone substitutes. *Head & face medicine* **15**, 1–13 (2019).

389. RESOMER® bioresorbable polymers for medical devices. https://healthcare.evonik.com/en/medical-devices/biodegradable-materials/resomer-portfolio/standard-polymers.

390. Shahhoseini, F., Langille, E. A., Azizi, A. & Bottaro, C. S. Thin film molecularly imprinted polymer (TF-MIP), a selective and single-use extraction device for high-throughput analysis of biological samples. *Analyst* **146**, 3157–3168 (2021).

391. Neuss, S. *et al.* Transcriptome analysis of MSC and MSC-derived osteoblasts on resomer® Lt706 and Pcl: impact of biomaterial substrate on osteogenic differentiation. *PloS one* **6**, e23195 (2011).

392. Neuss, S. *et al.* Assessment of stem cell/biomaterial combinations for stem cell-based tissue engineering. *Biomaterials* **29**, 302–313 (2008).

393. Boehler, C., Aqrawe, Z. & Asplund, M. Applications of PEDOT in bioelectronic medicine. *Bioelectronics in Medicine* **2**, 89–99 (2019).

394. Alva, S. *et al.* Accuracy of a 14-day factory-calibrated continuous glucose monitoring system with advanced algorithm in pediatric and adult population with diabetes. *Journal of Diabetes Science and Technology* 1932296820958754 (2020).

395. Ofori, A. A., Song, K. D. & Guo, H. Near-field communication for battery-free in vivo sensors. in vol. 11590 115900X (International Society for Optics and Photonics, 2021).

396. Kim, B., Yu, J. & Kim, H. In-vivo nfc: Remote monitoring of implanted medical devices with improved privacy. in 327–328 (2012).